Classical and Quantum Chaos

Part II: Semiclassical Chaos

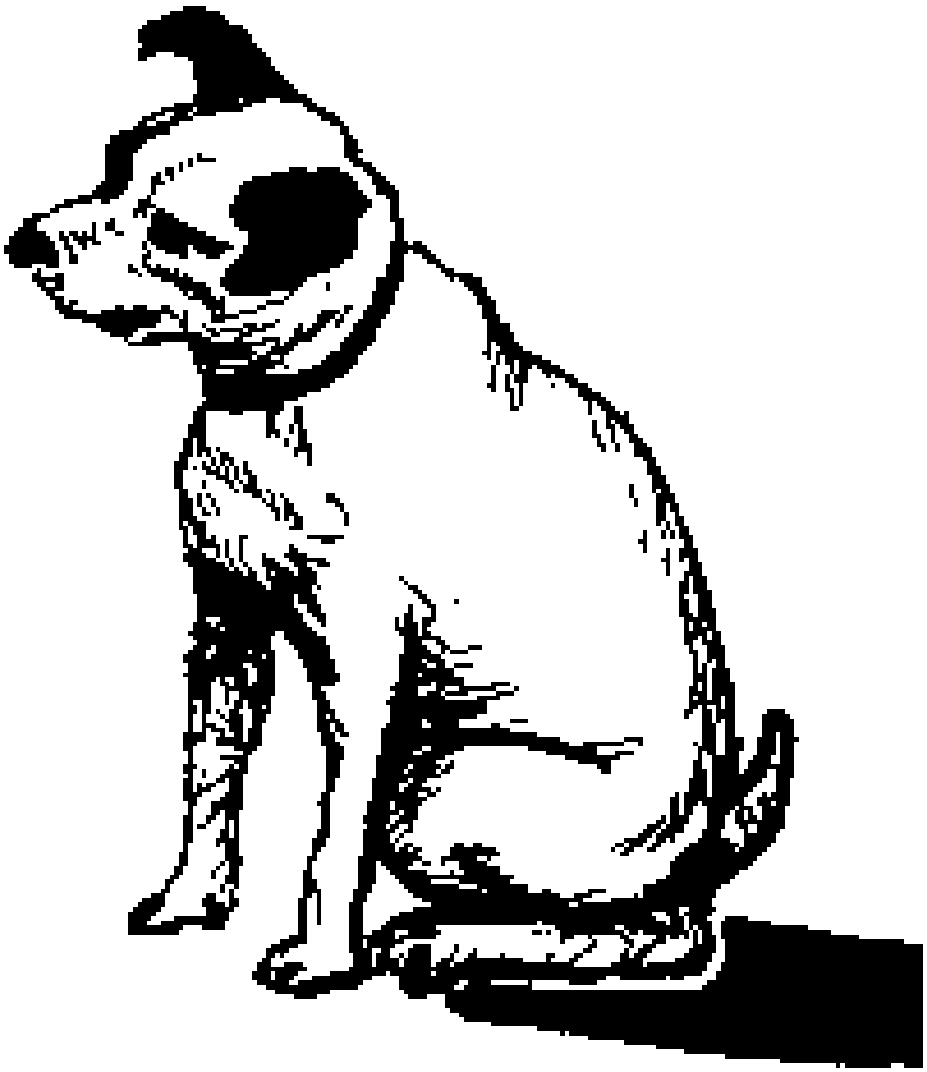

Predrag Cvitanović – Roberto Artuso – Per Dahlqvist – Ronnie Mainieri – Gregor Tanner – Gábor Vattay – Niall Whelan – Andreas Wirzba

---

version 10, Aug 26 2003 printed August 27, 2003
www.nbi.dk/ChaosBook/ChaosBook comments to: predrag@nbi.dk

Chapter 22

Prologue

> Anyone who uses words "quantum" and "chaos" in the same sentence should be hung by his thumbs on a tree in the park behind the Niels Bohr Institute.
> Joseph Ford

(G. Vattay, G. Tanner and P. Cvitanović)

You have read the first volume of this book. So far, so good – anyone can play a game of classical pinball, and a skilled neuroscientist can poke rat brains. Information about the chaotic dynamics was obtained by calculating spectra of linear operators such as the evolution operator of sect. 8.2 or the associated partial differential equations such as the Liouville equation (7.37). The spectra of these operators could then again be described in terms of the periodic orbits of the deterministic dynamics by means of trace formulas and cycle expansions.

But what happens quantum mechanically, that is, if we scatter waves rather than point-like pinballs? Can we turn the problem round and study linear PDE's in terms of the underlying deterministic dynamics? And, is there a link between structures in the spectrum or the eigenfunctions of a PDE and the dynamical properties of the underlying classical flow? The answer is yes, but ... things are becoming somewhat more complicated when studying 2nd or higher order linear PDE's. We can find classical dynamics associated with a linear PDE, just take geometric optics as a familiar example. Propagation of light follows a second order wave equation but may in certain limits be well described in terms of geometric rays. A theory in terms of properties of the classical dynamics alone, referred to here as the *semiclassical theory*, will not be exact, in contrast to the classical periodic orbit formulas obtained so far. Waves exhibit new phenomena, such as interference, diffraction, and the higher $\hbar$ corrections which will here be only partially incorporated into the periodic orbit theory.

22.1 Quantum pinball

We will restrict the discussion in what follows to a the non-relativistic Schrödinger equation. The approach will be very much in the spirit of the early days of quantum mechanics, before its wave character has been fully uncovered by Schrödinger in the mid 1920's. Indeed, were physicists of the period as familiar with classical chaos as we are today, this theory could have been developed 80 years ago. It was the discrete nature of the hydrogen spectrum which inspired the Bohr - de Broglie picture of the old quantum theory: one places a wave instead of a particle on a Keplerian orbit around the hydrogen nucleus. The quantization condition is that only those orbits contribute for which this wave is stationary; from this followed the Balmer spectrum and the Bohr-Sommerfeld quantization which eventually led to the more sophisticated theory of Heisenberg, Schrödinger and others. Today we are very aware of the fact that elliptic orbits are an idiosyncracy of the Kepler problem, and that chaos is the rule; so can the Bohr quantization be generalized to chaotic systems?

The question was answered affirmatively by Gutzwiller, as late as 1971: a chaotic system can indeed be quantized by placing a wave on each of the *infinity* of unstable periodic orbits. Due to the instability of the orbits the wave does not stay localized but leaks into neighborhoods of other periodic orbits. Contributions of different periodic orbits interfere and the quantization condition can no longer be attributed to a single periodic orbit: A coherent summation over the infinity of periodic orbit contributions gives the desired spectrum.

The pleasant surprise is that the zeros of the dynamical zeta function (1.9)

$$1/\zeta(z) = \prod_p (1 - t_p)$$

also yield excellent estimates of *quantum* resonances, with the quantum amplitude associated with a given cycle approximated semiclassically by the weight

$$t_p = \frac{1}{|\Lambda_p|^{\frac{1}{2}}} e^{\frac{i}{\hbar} S_p - i\pi m_p/2} \ , \tag{22.1}$$

whose magnitude is the square root of the classical weight (12.10)

$$t_p = \frac{1}{|\Lambda_p|} e^{\beta \cdot A_p - s T_p} \, ,$$

and the phase is given by the Bohr-Sommerfeld action integral S_p, together with an additional topological phase m_p, the number of caustics along the periodic trajectory, points where the naive semiclassical approximation fails.

☞ chapter 26

In this approach, the quantal spectra of classically chaotic dynamical systems are determined from the zeros of dynamical zeta functions, defined by cycle expansions of infinite products of form

$$1/\zeta = \prod_p (1 - t_p) = 1 - \sum_f t_f - \sum_p c_p \tag{22.2}$$

with weight t_p associated to every prime (non-repeating) periodic orbit (or *cycle*) p.

The key observation is that the chaotic dynamics is often organized around a few *fundamental* cycles. These short cycles capture the skeletal topology of the motion in the sense that any long orbit can approximately be pieced together from the fundamental cycles. In chapter 15 it was shown that for this reason the cycle expansion (22.2) is a highly convergent expansion dominated by short cycles grouped into *fundamental* contributions, with longer cycles contributing rapidly decreasing *curvature* corrections. Computations with dynamical zeta functions are rather straightforward; typically one determines lengths and stabilities of a finite number of shortest periodic orbits, substitutes them into (22.2), and estimates the zeros of $1/\zeta$ from such polynomial approximations.

From the vantage point of the dynamical systems theory, the trace formulas (both the exact Selberg and the semiclassical Gutzwiller trace formula) fit into a general framework of replacing phase space averages by sums over periodic orbits. For classical hyperbolic systems this is possible since the invariant density can be represented by sum over all periodic orbits, with weights related to their instability. The semiclassical periodic orbit sums differ from the classical ones only in phase factors and stability weights; such differences may be traced back to the fact that in quantum mechanics the amplitudes rather than the probabilities are added.

However, we should note that the type of the dynamics has a strong influence on the convergence of cycle expansions and thus also on the spectra; this necessitates development of different approaches for different types of dynamical behavior such as, on one hand, the strongly hyperbolic and, on the other hand, the intermittent dynamics of chapters 15 and 18. For generic nonhyperbolic systems (which we shall not discuss here), with mixed phase space and marginally stable orbits, periodic orbit summations are hard to control, and it is still not clear that the periodic orbit sums should necessarily be the computational method of choice.

Where is all this taking us? The goal of this part of the book is to demonstrate that the cycle expansions, developped so far in classical settings are also a powerful tool for evaluation of *quantum* resonances of classically chaotic systems.

First we shall warm up playing our game of pinball, this time in a quantum version. Were the game of pinball a closed system, quantum mechanically one would determine its stationary eigenfunctions and eigenenergies. For open systems one seeks instead complex resonances, where the imaginary part of the eigenenergy describes the rate at which the quantum wave function leaks out of the central scattering region. This will turn out to work well, except who truly wants to know accurately the resonaces of a quantum pinball?

22.2 Quantization of helium

However, given (22.1) we are finally in position to accomplish something altogether remarkable; we put together all ingredients that made the pinball unpredictable, and compute a "chaotic" part of the helium spectrum to shocking accuracy. From the classical dynamics point of view, helium is an example of Poincaré's dreaded and intractable 3-body problem. Undaunted, we forge ahead and consider the *collinear* helium, with zero total angular momentum, and the two electrons on the opposite sides of the nucleus.

We set the electron mass to 1, the nucleus mass to ∞, the helium nucleus charge to 2, the electron charges to -1. The Hamiltonian is

$$H = \frac{1}{2}p_1^2 + \frac{1}{2}p_2^2 - \frac{2}{r_1} - \frac{2}{r_2} + \frac{1}{r_1 + r_2}\,. \tag{22.3}$$

Due to the energy conservation, only three of the phase space coordinates (r_1, r_2, p_1, p_2) are independent. The dynamics can be visualized as a motion in the (r_1, r_2), $r_i \geq 0$ quadrant, fig. 22.1, or, better still, by a well chosen 2-d Poincaré section.

The motion in the (r_1, r_2) plane is topologically similar to the pinball motion in a 3-disk system, except that the motion is not free, but in the Coulomb potential. The classical collinear helium is also a repeller; almost all of the classical trajectories escape. Miraculously, the symbolic dynamics for the survivors again turns out to be binary, just as in the 3-disk game

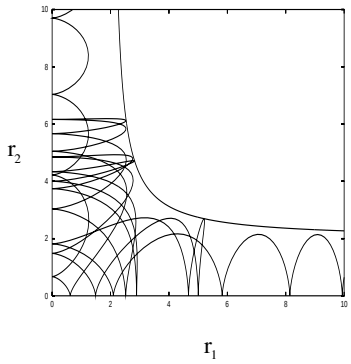

Figure 22.1: A typical collinear helium trajectory in the $r_1 - r_2$ plane; the trajectory enters along the r_1 axis and escapes to infinity along the r_2 axis.

of pinball, so we know what cycles need to be computed for the cycle expansion (1.10). A set of shortest cycles up to a given symbol string length then yields an estimate of the helium spectrum. This simple calculation yields surprisingly accurate eigenvalues; even though the cycle expansion was based on the *semiclassical approximation* (22.1) which is expected to be good only in the classical large energy limit, the eigenenergies are good to 1% all the way down to the ground state.

chapter 29

Before we can get to this point, we first have to recapitulate some basic notions of quantum mechanics; after having defined the main quantum objects of interest, the quantum propagator and the Green's function, we will relate the quantum propagation to the classical flow of the underlying dynamical system. We will then proceed to construct semiclassical approximations to the quantum propagator and the Green's function. A rederivation of classical Hamiltonian dynamics starting from the Hamilton-Jacobi equation will be offered along the way. The derivation of the Gutzwiller trace formula and the semiclassical zeta function as a sum and as a product over periodic orbits will be given in chapter 27. In subsequent chapters we buttress our case by applying and extending the theory: a cycle expansion calculation of scattering resonances in a 3-disk billiard in chapter 28, the spectrum of helium in chapter 29, and the incorporation of diffraction effects in chapter 30.

Guide to literature

A key prerequisite to developing any theory of "quantum chaos" is solid understanding of Hamiltonian mechanics. For that, Arnol'd monograph [1.24] is the essential reference. Ozorio de Almeida's monograph [6.11] offers a compact introduction to the aspects of Hamiltonian dynamics required for the quantization of integrable and nearly integrable systems, with emphasis on periodic orbits, normal forms, catastrophy theory and torus quantization. The book by Brack and Bhaduri [22.1] is an excellent introduction to

the semiclassical methods. Gutzwiller's monograph [22.2] is an advanced introduction focusing on chaotic dynamics both in classical Hamiltonian settings and in the semiclassical quantization. This book is worth browsing through for its many insights and erudite comments on quantum and celestial mechanics even if one is not working on problems of quantum chaology. More suitable as a graduate course text is Reichl's presentation [22.3].

This book does not discuss the random matrix theory approach to chaos in quantal spectra; no randomness assumptions are made here, rather the goal is to milk the deterministic chaotic dynamics for its full worth. The book concentrates on the periodic orbit theory. For an introduction to "quantum chaos" that focuses on the random matrix theory the reader is referred to the excellent monograph by Haake [22.4], among others.

References

[22.1] M. Brack and R.K. Bhaduri, *Semiclassical Physics* (Addison-Wesley, New York 1997).

[22.2] M.C. Gutzwiller, *Chaos in Classical and Quantum Mechanics* (Springer, New York 1990).

[22.3] L.E. Reichl, *The Transition to Chaos in Conservative Classical Systems: Quantum Manifestations* (Springer-Verlag, New York, 1992).

[22.4] F. Haake, *Quantum Signatures of Chaos* (Springer-Verlag, New York, 1991).

Chapter 23

Quantum mechanics, briefly

We start with a review of standard quantum mechanical concepts prerequisite to the derivation of the semiclassical trace formula.

In coordinate representation the time evolution of a quantum mechanical wave function is governed by the Schrödinger equation

$$i\hbar\frac{\partial}{\partial t}\psi(q,t) = \hat{H}(q, \frac{\hbar}{i}\frac{\partial}{\partial q})\psi(q,t), \tag{23.1}$$

where the Hamilton operator $\hat{H}(q, -i\hbar\partial_q)$ is obtained from the classical Hamiltonian by substitution $p \to -i\hbar\partial_q$. Most of the Hamiltonians we shall consider here are of form

$$H(q,p) = T(p) + V(q)\,, \qquad T(p) = p^2/2m\,, \tag{23.2}$$

describing dynamics of a particle in a d-dimensional potential $V(q)$. For time independent Hamiltonians we are interested in finding stationary solutions of the Schrödinger equation of the form

$$\psi_n(q,t) = e^{-iE_n t/\hbar}\phi_n(q), \tag{23.3}$$

where E_n are the eigenenergies of the time-independent Schrödinger equation

$$\hat{H}\phi(q) = E\phi(q)\,. \tag{23.4}$$

If the kinetic term can be separated out as in (23.2), the time-independent Schrödinger equation

$$-\frac{\hbar^2}{2m}\partial^2\phi(q) + V(q)\phi(q) = E\phi(q) \tag{23.5}$$

can be rewritten in terms of a local wavenumber

$$(\partial^2 + k^2(q))\phi = 0\,, \qquad \hbar^2 k(q) = \sqrt{2m(E - V(q))}\,. \tag{23.6}$$

For bound systems the spectrum is discrete and the eigenfunctions form an orthonormal

$$\int d^d q\, \phi_n(q)\phi_m^*(q) = \delta_{nm} \tag{23.7}$$

and complete

$$\sum_n \phi_n(q)\phi_n^*(q') = \delta(q - q')\,. \tag{23.8}$$

set of functions in a Hilbert space. For simplicity we will assume that the system is bound, although most of the results will be applicable to open systems, where one has complex resonances instead of real energies, and the spectrum has continuous components.

☞ chapter 28

A given wave function can be expanded in the energy eigenbasis

$$\psi(q,t) = \sum_n c_n e^{-iE_n t/\hbar}\phi_n(q)\,, \tag{23.9}$$

where the expansion coefficient c_n is given by the projection of the initial wave function $\psi(q,0)$ onto the nth eigenstate

$$c_n = \int d^d q\, \phi_n^*(q)\psi(q,0). \tag{23.10}$$

By substituting (23.10) into (23.9), we can cast the evolution of a wave function into a multiplicative form

$$\psi(q,t) = \int d^d q' K(q,q',t)\psi(q',0)\,,$$

with the kernel

$$K(q,q',t) = \sum_n \phi_n(q)\, e^{-iE_n t/\hbar} \phi_n^*(q') \tag{23.11}$$

called the quantum evolution operator, or the *propagator*. Applied twice, first for time t_1 and then for time t_2, it propagates the initial wave function from q' to q'', and then from q'' to q

$$K(q,q',t_1+t_2) = \int dq''\, K(q,q'',t_2) K(q'',q',t_1) \tag{23.12}$$

forward in time, hence the name "propagator". In non-relativistic quantum mechanics the range of q'' is infinite, meaning that the wave can propagate at any speed; in relativistic quantum mechanics this is rectified by restricting the propagation to the forward light cone.

Since the propagator is a linear combination of the eigenfunctions of the Schrödinger equation, it also satisfies the Schrödinger equation

$$i\hbar \frac{\partial}{\partial t} K(q,q',t) = \hat{H}(q, \frac{i}{\hbar}\frac{\partial}{\partial q}) K(q,q',t)\,, \tag{23.13}$$

and is thus a wave function defined for $t \geq 0$; from the completeness relation (23.8) we obtain the boundary condition at $t = 0$:

$$\lim_{t \to 0_+} K(q,q',t) = \delta(q-q')\,. \tag{23.14}$$

The propagator thus represents the time evolution of a wave packet which starts out as a configuration space delta-function localized in the point q' at the initial time $t = 0$.

For time independent Hamiltonians the time dependence of the wave functions is known as soon as the eigenenergies E_n and eigenfunctions ϕ_n have been determined. With time dependence rendered "trivial", it makes sense to focus on the *Green's function*, the Laplace transformation of the propagator

$$G(q,q',E+i\epsilon) = \frac{1}{i\hbar}\int_0^\infty dt\, e^{\frac{i}{\hbar}Et - \frac{\epsilon}{\hbar}t} K(q,q',t) = \sum_n \frac{\phi_n(q)\phi_n^*(q')}{E - E_n + i\epsilon}\,. \tag{23.15}$$

Here ϵ is a small positive number, ensuring the existence of the integral. The eigenenergies show up as poles in the Green's function with residues corresponding to the wave function amplitudes. If one is only interested in the spectrum, one may restrict the considerations to the (formal) trace of the Green's function,

$$\mathrm{tr}\, G(q,q',E) = \int d^d q\, G(q,q,E) = \sum_n \frac{1}{E-E_n}\,, \tag{23.16}$$

where E is complex, with a positive imaginary part, and we have used the eigenfunction orthonormality (23.7). This trace is formal, since as it stands, the sum in (23.16) is often divergent. We shall return to this point in sects. 27.1.1 and 27.1.2.

A a useful characterization of the set of eigenvalues is given in terms of the *density of states*, with a delta function peak at each eigenenergy, fig. 23.1(a),

$$d(E) = \sum_n \delta(E-E_n). \tag{23.17}$$

26.1
page 504

Using the identity

$$\delta(E-E_n) = -\lim_{\epsilon\to+0}\frac{1}{\pi}\mathrm{Im}\,\frac{1}{E-E_n+i\epsilon} \tag{23.18}$$

we can express the density of states in terms of the trace of the Green's function, that is

$$d(E) = \sum_n \delta(E-E_n) = -\lim_{\epsilon\to 0}\frac{1}{\pi}\mathrm{Im}\,\mathrm{tr}\, G(q,q',E+i\epsilon). \tag{23.19}$$

sect. 27.1.1

This relation is the reason why we chose to describe the quantum spectrum in terms of the density of states. As we shall see, a semiclassical formula for right hand side of this relation will yield the quantum spectrum in terms of periodic orbits.

The density of states can be written as the derivative $d(E) = \mathrm{d}N(E)/\mathrm{d}E$ of another useful quantity, the *spectral staircase* function

$$N(E) = \sum_n \Theta(E-E_n) \tag{23.20}$$

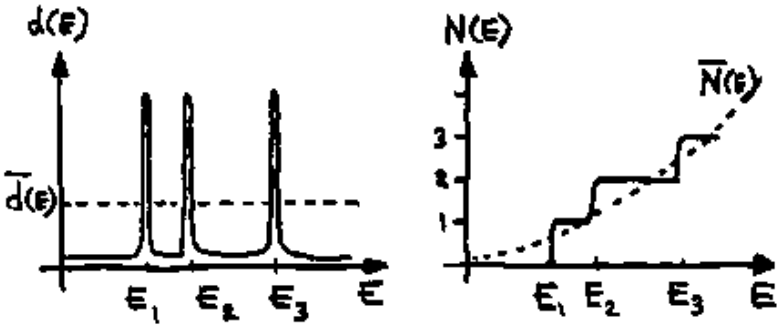

Figure 23.1: Schematic picture of **a)** the density of states $d(E)$, and **b)** the spectral staircase function $N(E)$. The dashed lines denote the mean density of states $\bar{d}(E)$ and the average number of states $\bar{N}(E)$ discussed in more detail in sect. 17.1.

which counts the number of eigenenergies below E, fig. 23.1(b). Here Θ is the Heaviside function

$$\Theta(x) = 1 \quad \text{if } x > 0; \quad \Theta(x) = 0 \quad \text{if } x < 0\,. \tag{23.21}$$

This completes our lightning review of quantum mechanics.

Chapter 24

WKB quantization

Consider a time-independent Schrödinger equation in 1 spatial dimension:

$$-\frac{\hbar^2}{2m}\psi''(q) + V(q)\psi(q) = E\psi(q)\,. \tag{24.1}$$

with potential $V(q)$ growing sufficiently fast as $q \to \pm\infty$ so that the particle motion is confined for any E. Define the local momentum, wavenumber

$$p(q) = \sqrt{2m(E - V(q))}, \quad p(q) = \hbar k(q)\,. \tag{24.2}$$

Then

$$\psi'' + k^2(q)\psi = 0\,. \tag{24.3}$$

Substitution $\psi = Ae^{\frac{i}{\hbar}S}$, A, S real functions of q, yields

$$(S')^2 = p^2 + \hbar^2\frac{A''}{A} \tag{24.4}$$

$$S''A + 2S'A' = \frac{1}{A}\frac{d}{dq}(S'A^2) = 0\,. \tag{24.5}$$

(D-dimensional version of these equations will be given below, in (26.3) and (26.4).) The Wentzel-Kramers-Brillouin *(WKB)* or *semiclassical* approximation consists in dropping the $\hbar^2$ term in (24.4). Recalling that $p = \hbar k$, dropping this term amounts to claiming that $k^2 \gg \frac{A''}{A}$ which in turn implies that the phase of the wavefunction is changing much faster than its overall

amplitude. This justifies the standard interpretation as a short wavelength approximation. This approximation is also consistent with saying $\hbar \ll 1$.

Integrating (24.4) we obtain the phase increment of a wave function initially at q, at energy E

$$S(q,q',E) = \int_{q'}^{q} dq" \cdot p(q") \,. \tag{24.6}$$

Integration of (24.5) is even easier

$$A(q) = \frac{C}{|p(q)|^{\frac{1}{2}}}, \qquad C = |p(q')|^{\frac{1}{2}} \psi(q') \,, \tag{24.7}$$

where C is the integration constant, fixed by requiring that the wave function is single-valued everywhere, including the initial point q'. The WKB ansatz, or the semi-classical wave function is given by

$$\psi_{sc}(q) = \frac{C}{|p(q)|^{\frac{1}{2}}} e^{\frac{i}{\hbar} S(qq'E)} \,. \tag{24.8}$$

This is fine, except at the turning points, where all energy is potential, and

$$p(q) \to 0 \quad \text{as} \quad q \to q_T \,, \tag{24.9}$$

so that the assumption that $k^2 \gg \frac{A''}{A}$ fails. What to do? The answer is given in every quantum mechanics textbook, usually by expanding the potential close to the turning point

$$V(q) = V(q_T) + (q - q_T) V'(q_T) + \cdots \,,$$

solving the Airy equation and matching the oscillatory and the exponentially decaying "forbidden" region wave function pieces by means of the *WKB connection formulas*. That requires staring at Airy functions and learning about their asymptotics - a challenge that we will have to eventually face up to, in order to incorporate diffraction phenomena into semiclassical quantization. However, for the task at hand a simple physical picture, due to Maslov, does the job. In the q coordinate, the turning points are defined by the zero kinetic energy condition, and the motion appears singular. Not so in the full phase space: the trajectory in a smooth confining 1-d potential is always a smooth loop, with the "special" role of the turning

points q_L, q_R seen to be an artifact of the particular choice of the (q,p) coordinate frame. Maslov's idea was to proceed from (q',p') to (q_A,p_A) in the $\psi(q)$ representation, then switch by means of a Fourier transform to the momentum representation

$$\widetilde{\psi}(p) = \frac{1}{\sqrt{2\pi\hbar}} \int dq\, e^{-\frac{i}{\hbar}qp} \psi(q)\,, \tag{24.10}$$

continue from (q_A,p_A) to (q_B,p_B), switch back to the coordinate representation,

$$\psi(q) = \frac{1}{\sqrt{2\pi\hbar}} \int dp\, e^{\frac{i}{\hbar}qp}\, \widetilde{\psi}(p)\,, \tag{24.11}$$

and so on.

The only rub is that we do not know how to evaluate these transforms exactly. As the WKB wave function (24.8) is anyhow approximate, it suffices to estimate these transforms with leading order in $\hbar$ accuracy. This we do by the stationary phase method.

24.1 Method of stationary phase

Semiclassical approximations are based on saddlepoint evaluations of integrals of the type

$$I = \int d^d x\, A(x)\, e^{is\Phi(x)}\,, \qquad x, \Phi(x) \in \mathbb{R}, \tag{24.12}$$

where s is assumed to be a large, real parameter, and $\Phi(x)$ is a real-valued function. In our applications $s = 1/\hbar$ will always be assumed large.

For large s the phase oscillates rapidly and "averages to zero" everywhere except at the *extremal points* $\Phi'(x_0) = 0$, where $\Phi''(x_0) \neq 0$ but can have either sign. The method of approximating an integral by its values at extremal points is called the *method of stationary phase*. Consider first the case of a one-dimensional integral, and expand $\Phi(x_0 + \delta x)$ around x_0 to second order in δx,

$$I = \int dx\, A(x)\, e^{is(\Phi(x_0) + \frac{1}{2}\Phi''(x_0)\delta x^2 + \ldots)}\,.$$

If $A(x)$ varies slowly around x_0 compared to the exponential function, we may retain the leading term in the Taylor expansion of the amplitude, and approximate the integral up to quadratic terms in the phase by

$$I \approx A(x_0) e^{is\Phi(x_0)} \int_{-\infty}^{\infty} dx\, e^{is\Phi''(x_0)\frac{x^2}{2}} .$$

24.6
page 460

Using the *Fresnel integral* formula

$$\frac{1}{\sqrt{2\pi}} \int_{-\infty}^{\infty} dx\, e^{-\frac{x^2}{2ia}} = \sqrt{ia} = |a|^{1/2}\, e^{i\frac{\pi}{4}\frac{a}{|a|}} \tag{24.13}$$

we obtain

$$I \approx A(x_0) \left| \frac{2\pi}{s\Phi''(x_0)} \right|^{1/2} e^{is\Phi(x_0)\pm i\frac{\pi}{4}} , \tag{24.14}$$

where $\pm$ corresponds to the positive/negative sign of $s\Phi''(x_0)$.

24.2 WKB quantization

We can now evaluate the Fourier transforms (24.10), (24.11) to the same order in $\hbar$ as the WKB wave function by means of the stationary phase method

$$\begin{aligned} \widetilde{\psi}_{sc}(p) &= \frac{C}{\sqrt{2\pi\hbar}} \int \frac{dq}{|p(q)|^{\frac{1}{2}}}\, e^{\frac{i}{\hbar}(S(q)-qp)} \\ &\approx \frac{C}{\sqrt{2\pi\hbar}} \frac{e^{\frac{i}{\hbar}(S(q^*)-q^*p)}}{|p(q^*)|^{\frac{1}{2}}} \int dq\, e^{\frac{i}{2\hbar}S''(q^*)(q-q^*)^2} , \end{aligned} \tag{24.15}$$

where q^* is given implicitly by the stationary phase condition

$$0 = S'(q^*) - p = p(q^*) - p$$

and the sign of $S''(q^*) = p'(q^*)$ determines the phase of the Fresnel integral (24.13)

$$\widetilde{\psi}_{sc}(p) = \frac{C}{|p(q^*)p'(q^*)|^{\frac{1}{2}}} e^{\frac{i}{\hbar}[S(q^*)-q^*p]+\frac{i\pi}{4}sgn(S''(q^*)} . \tag{24.16}$$

As we continue from (q_A, p_A) to (q_B, p_B), nothing problematic happens - $p(q^*)$ is finite, and so is the acceleration $p'(q^*)$, otherwise the trajectory would take infinite time to get across. We recognize the exponent as the Legendre transform

$$\tilde{S}(p) = S(q(p)) - q(p)p$$

which re-expresses everything in terms of the p variable

$$q^* = q(p), \quad \frac{d}{dq}q = 1 = \frac{dp}{dq}\frac{dq(p)}{dp} = q'(p)p'(q^*)\,. \tag{24.17}$$

As it crosses q_L, the weight in (24.16)

$$\frac{d}{dq}p^2(q_L) = 2p(q_L)p'(q_L) = -2mV'(q) \tag{24.18}$$

is finite, and $S''(q^*) = p'(q^*) < 0$ for any point in the lower left quadrant, including (q_A, p_A), hence the phase loss in (24.16) is $-\frac{\pi}{4}$. To go back from p to q representation, just turn the phase space loop a quarter turn anticlockwise. Everything is the same if you replace $(q, p) \to (-p, q)$; so, without much ado we get at the point (q_B, p_B)

$$\psi_{sc}(q) = \frac{e^{\frac{i}{\hbar}(\tilde{S}(p^*)+qp^*)-\frac{i\pi}{4}}}{|q^*(p^*)|^{\frac{1}{2}}}\,\widetilde{\psi}_{sc}(p^*) = \frac{e^{\frac{i}{\hbar}S(q)-\frac{i\pi}{2}}}{|p(q)|^{\frac{1}{2}}}C\,. \tag{24.19}$$

The extra $|p'(q^*)|^{1/2}$ weight in (24.16) is cancelled by the $|q'(p^*)|^{1/2}$ term, by the Legendre relation (24.17).

We note in passing that the Fresnel integral phase slip requires a potential with finite slope $V'(q)$. In case of infinite wall (billiards) a different argument applies: the wave function must vanish at the wall, and the phase slip due to a specular reflection is $-\pi$, not $-\pi/2$.

The main message is that going through a smooth potential turn-back the WKB wave function phase slips by $-\frac{\pi}{2}$. This is equally true for the right and the left turn-backs, as can be seen by turning the phase space loop by $\frac{1}{2}$ turn, and flipping coordinates $(q, p) \to (-q, -p)$. While a turn-back is not an invariant concept (for a short trajectory segment, it can be undone by a 45^o turn), for a complete period $(q(T), p(T)) = (q', p')$ the total phase slip is always by $2 \cdot \pi/2$, as a loop always has $m = 2$ turn-backs.

The *WKB quantization condition* follows by demanding that the wave function computed after a complete period be single-valued. With normalization (24.7) we obtain

$$\psi(q') = \psi(q(T)) = \left|\frac{p(q')}{p(q(T))}\right|^{\frac{1}{2}} e^{i(\frac{1}{\hbar}\oint p(q)dq - \pi)}\psi(q')\,.$$

The prefactor equals 1 by the periodic orbit condition $q(T) = q'$, hence the phase must be a multiple of 2π

$$\frac{1}{\hbar}\oint p(q)dq = 2\pi\left(n + \frac{m}{4}\right)\,. \tag{24.20}$$

By definition, the action integral in (24.20) is the area enclosed by the phase space loop, and the quantization condition says that eigenenergies correspond to loops whose action is an integer multiple of the basis quantum of action, the Planck constant $\hbar$. Plus the extra topological phase, which, even though it had been discovered many times in centuries past, had to wait for its quantum mechanical (re)birth until 1970's. This result involves only canonically invariant classical quantities (action and phase) despite its derivation in terms of noninvariant coordinates.

24.2.1 Harmonic oscillator quantization

Let us check the WKB quantization for one case whose quantum mechanics we fully understand: the harmonic oscillator

$$E = \frac{1}{2m}\left(p^2 + (mwq)^2\right)\,.$$

The phase space loop is now a circle in the (mwq, p) plane, action is its area $S = 2\pi E/w$, and the WKB spectrum

$$E_n = \hbar w(n + 1/2) \tag{24.21}$$

turns out to be the *exact* harmonic oscillator spectrum. Morally, stationary phase condition (24.15) keeps $V(q)$ accurate to order q^2, which in this case is the whole answer (but we were plain lucky, really). Nevertheless, for many 1-d problems WKB spectrum turns out to be very accurate. Surprisingly so, if one interprets dropping the $\hbar^2$ term in (24.4) as a short wavelength approximation.

Commentary

Remark 24.1 Airy function. The stationary phase approximation is all that is needed for the semiclassical approximation, with the proviso that D in (26.35) has no zero eigenvalues. The zero eigenvalue case would require going beyond the Gaussian saddle-point approximation, which typically leads to approximations of the integrals in terms of Airy functions [27.12].

24.9
page 461

Exercises

Exercise 24.1 WKB ansatz. *Try to show that no other ansatz other than the (26.1) gives a meaningful definition of the momentum in the $\hbar \to 0$ limit.*

Exercise 24.2 1-dimensional harmonic oscillator. *Take a 1-dimensional harmonic oscillator $U(q) = \frac{1}{2}kq^2$. Take a WKB wave function of form $A(q,t) = a(t)$ and $R(q,t) = r(t)+b(t)q+c(t)q^2$, where $r(t), a(t), b(t)$ and $c(t)$ are time dependent coefficients. Derive ordinary differential equations by using (26.3) and (26.4) and solve them. Continuation: (24.5).*

Exercise 24.3 1-dimensional linear potential. *Take a 1-dimensional linear potential $U(q) = -Fq$. Take a WKB wave function of form $A(q,t) = a(t)$ and $R(q,t) = r(t)+b(t)q+c(t)q^2$, where $r(t), a(t), b(t)$ and $c(t)$ are time dependent coefficients. Derive and solve the ordinary differential equations from (26.3) and (26.4).*

Exercise 24.4 d-dimensional quadratic potentials. *Generalize the above method to general d-dimensional quadratic potentials.*

Exercise 24.5 Time evolution of R. *(Continuation of (24.2)). Calculate the time evolution of $R(q,0) = a + bq + cq^2$ for a 1-dimensional harmonic oscillator using (26.12) and (26.13).*

Exercise 24.6 Fresnel integral. *Show that*

$$\int_{-\infty}^{\infty} dx\, e^{iax^2/2} = \left(\frac{2\pi}{|a|}\right)^{1/2} e^{\frac{i\pi m}{4}} \tag{24.22}$$

where $m = a/|a|$ is the sign of a.

Exercise 24.7 Stationary phase approximation. *All semiclassical approximations are based on saddlepoint evaluations of integrals of type*

$$I = \int d^d x A(x) e^{i\Phi(x)/\hbar} \tag{24.23}$$

for small values of $\hbar$. Obtain the stationary phase estimate

$$I \approx \sum_n A(x_n) e^{i\Phi(x_n)/\hbar} \frac{(2\pi i\hbar)^{d/2}}{\sqrt{\det \mathbf{D}^2\Phi(x_n)}},$$

where $\mathbf{D}^2\Phi(x_n)$ denotes the second derivative matrix.

Exercise 24.8 Sterling formula for $n!$. *Compute an approximate value of $n!$ for large n with the help of stationary phase approximation. Hint: $n! = \int_0^\infty dt\, t^n e^{-t}$.*

Exercise 24.9 Airy function for large arguments. *Important contributions as stationary phase points may arise from extremal points where the first non-zero term in a Taylor expansion of the phase is of third or higher order. Such situations occur, for example, at bifurcation points or in diffraction effects, (such as waves near sharp corners, waves creeping around obstacles). In such calculations one meets Airy functions integrals of the form*

$$Ai(x) = \frac{1}{2\pi} \int_{-\infty}^{+\infty} dy\, e^{i(x\,y - \frac{y^3}{3})}\,. \tag{24.24}$$

Calculate the Airy function $Ai(x)$ by stationary phase approximation. What happens when considering the limit $x \to 0$. Estimate for which value of x the stationary phase approximation breaks down. Give it a go.

Chapter 25

Relaxation for cyclists

Cycles, that is, solutions of the periodic orbit condition (14.1)

$$f^{t+T}(x) = f^t(x)\,, \qquad T > 0 \tag{25.1}$$

are prerequisite to chapters 11 and 12 evaluation of spectra of classical evolution operators, and, as we shall see in chapter 27, the semiclassical approximations to quantum evolution operators. Chapter 14 offered an introductory, hands-on guide to extraction of periodic orbits by means of the Newton-Raphson method. Here we take a very different tack, drawing inspiration from variational principles of classical mechanics, and path integrals of quantum mechanics.

In sect. 14.2.1 we converted orbits unstable forward in time into orbits stable backwards in time. Indeed, all methods for finding unstable cycles are based on the idea of constructing a new dynamical system such that (i) the position of the cycle is the same for the original system and the transformed one, (ii) the unstable cycle in the original system is a stable cycle of the transformed system.

The Newton-Raphson method for determining a fixed point x_* for a map $x' = f(x)$ is an example. The method replaces iteration of $f(x)$ by iteration of the Newton-Raphson map (14.5)

$$x'_i = g_i(x) = x_i - \left(\frac{1}{\mathbf{J}(x) - \mathbf{1}}\right)_{ij} (f(x) - x)_j\,. \tag{25.2}$$

A fixed point x_* for a map $f(x)$ is also a fixed point of $g(x)$, indeed a super-stable fixed point since $\partial g_i(x_*)/\partial x_j = 0$. This makes the convergence to the fixed point super-exponential.

We also learned in chapter 14 that methods that start with initial guesses for a number of points along a cycle are considerably more robust and safer than searches based on direct solution of the fixed-point condition (25.1). The relaxation (or variational) methods that we shall now describe take this multipoint approach to its logical extreme, and start by a guess of not a few points along a periodic orbit, but a guess of the entire orbit.

The idea is to make an informed rough guess of what the desired periodic orbit looks like globally, and then use variational methods to drive the initial guess toward the exact solution. Sacrificing computer memory for robustness of the method, we replace a guess that a *point* is on the periodic orbit by a guess of the *entire orbit*. And, sacrificing speed for safety, in sect. 25.1 we replace the Newton-Raphson *iteration* by a fictitious time *flow* that minimizes a cost function computed as deviation of the approximate flow from the true flow along a loop approximation to a periodic orbit.

If you have some insight into the topology of the flow and its symbolic dynamics, or have already found a set of short cycles, you might be able to construct an initial approximation to a longer cycle p as a sequence of N points $(\tilde{x}_1^{(0)}, \tilde{x}_2^{(0)}, \cdots, \tilde{x}_N^{(0)})$ with the periodic boundary condition $\tilde{x}_{N+1} = \tilde{x}_1$. Suppose you have an iterative method for improving your guess; after k iterations the cost function

$$F^2(\tilde{x}^{(k)}) = \sum_i^N \left(\tilde{x}_{i+1}^{(k)} - f(\tilde{x}_i^{(k)})\right)^2 \tag{25.3}$$

or some other more cleverly constructed function (for classical mechanics - action) is a measure of the deviation of the kth approximate cycle from the true cycle. This observation motivates variational approaches to determining cycles.

We give here three examples of such methods, two for maps, and one for billiards. In sect. 25.1 we start out by converting a problem of finding an unstable fixed point of a map into a problem of constructing a differential flow for which the desired fixed point is an attracting equilibrium point. Solving differential equations can be time intensive, so in sect. 25.2 we replace such flows by discrete iterations. In sect. 25.3 we show that for $2D$-dimensional billiard flows variation of D coordinates (where D is the number of Hamiltonian degrees of freedom) suffices to determine cycles in the full $2D$-dimensional phase space.

25.1 Fictitious time relaxation

(O. Biham, C. Chandre and P. Cvitanović)

The relaxation (or gradient) algorithm for finding cycles is based on the observation that a trajectory of a map such as the Hénon map (3.10),

$$\begin{aligned} x_{i+1} &= 1 - ax_i^2 + by_i \\ y_{i+1} &= x_i \,, \end{aligned} \tag{25.4}$$

is a stationary solution of the relaxation dynamics defined by the flow

$$\frac{dx_i}{d\tau} = v_i, \quad i = 1, \ldots, n \tag{25.5}$$

for any vector field $v_i = v_i(x)$ which vanishes on the trajectory. Here τ is a "fictitious time" variable, unrelated to the dynamical time (in this example, the discrete time of map iteration). As the simplest example, take v_i to be the deviation of an approximate trajectory from the exact 2-step recurrence form of the Hénon map (3.11)

$$v_i = x_{i+1} - 1 + ax_i^2 - bx_{i-1}. \tag{25.6}$$

For fixed x_{i-1}, x_{i+1} there are two values of x_i satisfying $v_i = 0$. These solutions are the two extremal points of a local "potential" function (no sum on i)

$$v_i = \frac{\partial}{\partial x_i} V_i(x) \,, \qquad V_i(x) = x_i(x_{i+1} - bx_{i-1} - 1) + \frac{a}{3} x_i^3 \,. \tag{25.7}$$

Assuming that the two extremal points are real, one is a local minimum of $V_i(x)$ and the other is a local maximum. Now here is the idea; replace (25.5) by

$$\frac{dx_i}{d\tau} = \sigma_i v_i, \quad i = 1, \ldots, n, \tag{25.8}$$

where $\sigma_i = \pm 1$.

The modified flow will be in the direction of the extremal point given by the local maximum of $V_i(x)$ if $\sigma_i = +1$ is chosen, or in the direction of the one corresponding to the local minimum if we take $\sigma_i = -1$. This is not quite what happens in solving (25.8) - all x_i and $V_i(x)$ change at each integration step - but this is the observation that motivates the method. The differential equations (25.8) then drive an approximate initial guess toward the exact trajectory. A sketch of the landscape in which x_i converges

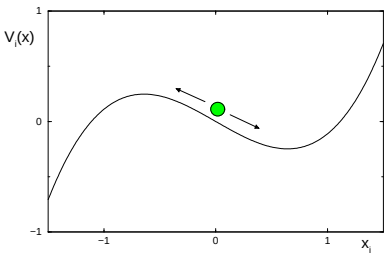

Figure 25.1: "Potential" $V_i(x)$ (25.7) for a typical point along an inital guess trajectory. For $\sigma_i = +1$ the flow is toward the local maximum of $V_i(x)$, and for $\sigma_i = -1$ toward the local minimum. A large deviation of x_i's is needed to destabilize a trajectory passing through such local extremum of $V_i(x)$, hence the basin of attraction is expected to be large.

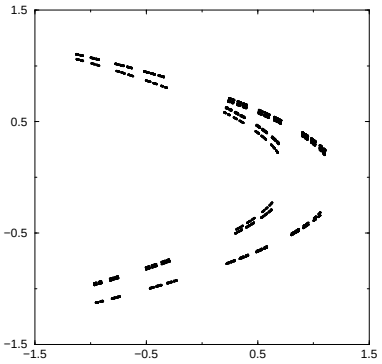

Figure 25.2: The repeller for the Hénon map at $a = 1.8$, $b = 0.3$.

towards the proper fixed point is given in fig. 25.1. As the "potential" function (25.7) is not bounded for a large $|x_i|$, the flow diverges for initial guesses which are too distant from the true trajectory. However, the basin of attraction of initial guesses that converge to a given cycle is nevertheless very large, with the spread in acceptable initial guesses for fig. 25.1 of order 1, in contrast to the exponential precision required of initial guesses by the Newton-Raphson method.

Example 25.1 Hénon map cycles. *Our aim in this calculation is to find all periodic orbits of period n for the Hénon map (25.4), in principle at most 2^n orbits. We start by choosing an initial guess trajectory $(x_1, x_2, \cdots, x_n)$ and impose the periodic boundary condition $x_{n+1} = x_1$. The simplest and a rather crude choice of the initial condition in the Hénon map example is $x_i = 0$ for all i. In order to find a given orbit one sets $\sigma_i = -1$ for all iterates i which are local minima of $V_i(x)$, and $\sigma_i = 1$ for iterates which are local maxima. In practice one runs through a complete list of prime cycles, such as the table 9.2. The real issue for all searches for periodic orbits, this one included, is how large is the basin of attraction of the desired periodic orbit? There is no easy answer to this question, but empirically it turns out that for the Hénon map such initial guess almost always converges to the desired trajectory as long as the initial $|x|$ is not too large compared to $1/\sqrt{a}$. Fig. 25.1 gives some indication of a typical basin of attraction of the method (see also fig. 25.3).*

The calculation is carried out by solving the set of n ordinary differential equations (25.8) using a simple Runge-Kutta method with a relatively large step size ($h = 0.1$) until $|v|$ becomes smaller than a given value ε (in a typical calculation $\varepsilon \sim 10^{-7}$). Empirically, in the case that an orbit corresponding to the desired itinerary does not exist, the initial guess escapes to infinity since the "potential" $V_i(x)$ grows without bound.

25.3
page 479

n	p	(y_p , x_p)	λ_p
1	0	(-1.13135447 , -1.13135447)	1.18167262
	1	(0.63135447 , 0.63135447)	0.65427061
2	01	(0.97580005 , -0.47580005)	0.55098676
4	0111	(-0.70676677 , 0.63819399)	0.53908457
6	010111	(-0.41515894 , 1.07011813)	0.55610982
	011111	(-0.80421990 , 0.44190995)	0.55245341
7	0011101	(-1.04667757 , -0.17877958)	0.40998559
	0011111	(-1.08728604 , -0.28539206)	0.46539757
	0101111	(-0.34267842 , 1.14123046)	0.41283650
	0111111	(-0.88050537 , 0.26827759)	0.51090634
8	00011101	(-1.25487963 , -0.82745422)	0.43876727
	00011111	(-1.25872451 , -0.83714168)	0.43942101
	00111101	(-1.14931330 , -0.48368863)	0.47834615
	00111111	(-1.14078564 , -0.44837319)	0.49353764
	01010111	(-0.52309999 , 0.93830866)	0.54805453
	01011111	(-0.38817041 , 1.09945313)	0.55972495
	01111111	(-0.83680827 , 0.36978609)	0.56236493
9	000111101	(-1.27793296 , -0.90626780)	0.38732115
	000111111	(-1.27771933 , -0.90378859)	0.39621864
	001111101	(-1.10392601 , -0.34524675)	0.51112950
	001111111	(-1.11352304 , -0.36427104)	0.51757012
	010111111	(-0.36894919 , 1.11803210)	0.54264571
	011111111	(-0.85789748 , 0.32147653)	0.56016658
10	0001111101	(-1.26640530 , -0.86684837)	0.47738235
	0001111111	(-1.26782752 , -0.86878943)	0.47745508
	0011111101	(-1.12796804 , -0.41787432)	0.52544529
	0011111111	(-1.12760083 , -0.40742737)	0.53063973
	0101010111	(-0.48815908 , 0.98458725)	0.54989554
	0101011111	(-0.53496022 , 0.92336925)	0.54960607
	0101110111	(-0.42726915 , 1.05695851)	0.54836764
	0101111111	(-0.37947780 , 1.10801373)	0.56915950
	0111011111	(-0.69555680 , 0.66088560)	0.54443884
	0111111111	(-0.84660200 , 0.34750875)	0.57591048
13	1110011101000	(-1.2085766485 , -0.6729999948)	0.19882434
	1110011101001	(-1.0598110494 , -0.2056310390)	0.21072511

Table 25.1: All prime cycles up to period 10 for the Hénon map, $a = 1.4$ and $b = 0.3$. The columns list the period n_p, the itinerary (defined in remark 25.4), a cycle point (y_p, x_p), and the cycle Lyapunov exponent $\lambda_p = \ln|\Lambda_p|/n_p$. While most of the cycles have $\lambda_p \approx 0.5$, several significantly do not. The $\overline{0}$ cycle point is very unstable, isolated and transient fixed point, with no other cycles returning close to it. At period 13 one finds a pair of cycles with exceptionally low Lyapunov exponents. The cycles are close for most of the trajectory, differing only in the one symbol corresponding to two cycle points straddle the (partition) fold of the attractor. As the system is not hyperbolic, there is no known lower bound on cycle Lyapunov exponents, and the Hénon's strange "attractor" might some day turn out to be nothing but a transient on the way to a periodic attractor of some long period.

n	M_n	N_n	n	M_n	N_n	n	M_n	N_n
11	14	156	17	166	2824	23	1930	44392
12	19	248	18	233	4264	24	2902	69952
13	32	418	19	364	6918	25	4498	112452
14	44	648	20	535	10808	26	6806	177376
15	72	1082	21	834	17544	27	10518	284042
16	102	1696	22	1225	27108	28	16031	449520

Table 25.2: The number of unstable periodic orbits of the Hénon map for $a = 1.4$, $b = 0.3$, of all periods $n \leq 28$. M_n is the number of prime cycles of length n, and N_n is the total number of periodic points of period n (including repeats of shorter prime cycles).

Applied to the Hénon map at the Hénon's parameters choice $a = 1.4$, $b = 0.3$, the method has yielded all periodic orbits to periods as long as $n = 28$, as well as selected orbits up to period $n = 1000$. All prime cycles up to period 10 for the Hénon map, $a = 1.4$ and $b = 0.3$, are listed in table 25.1. The number of unstable periodic orbits for periods $n \leq 28$ is given in table 25.2. Comparing this with the list of all possible 2-symbol alphabet prime cycles, table 9.2, we see that the pruning is quite extensive, with the number of cycle points of period n growing as $e^{0.4645 \cdot n} = (1.592)^n$ rather than as 2^n.

As another example we plot all unstable periodic points up to period $n = 14$ for $a = 1.8$, $b = 0.3$ in fig. 25.2. Comparing this repelling set with the strange attractor for the Hénon's parameters fig. 3.4, we note the existence of gaps in the set, cut out by the preimages of the escaping regions.

☞ remark 25.2

In practice, the relaxation flow (25.8) finds (almost) all periodic orbits which exist and indicates which ones do not. For the Hénon map the method enables us to calculate almost all unstable cycles of essentially any desired length and accuracy.

The idea of the relaxation algorithm illustrated by the above Hénon map example is that instead of searching for an unstable periodic orbit of a map, one searches for a stable attractor of a vector field. More generally, consider a d-dimensional map $x' = f(x)$ with a hyperbolic fixed point x_*. Any fixed point x_* is by construction an equilibrium point of the fictitious time flow

$$\frac{dx}{d\tau} = f(x) - x. \tag{25.9}$$

If all eigenvalues of the Jacobian matrix $J(x_*) = Df(x_*)$ have real parts smaller than unity, then x_* is a stable equilibrium point of the flow.

If some of the eigenvalues have real parts larger than unity, then one needs to modify the vector field so that the corresponding directions of the flow are turned into stable directions in a neighborhood of the fixed point. In the spirit of (25.8), modify the flow by

$$\frac{dx}{d\tau} = \mathbf{C}\left(f(x) - x\right), \tag{25.10}$$

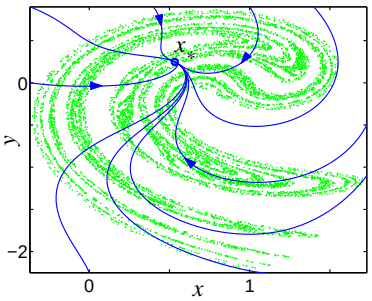

Figure 25.3: Typical trajectories of the vector field (25.9) for the stabilization of a hyperbolic fixed point of the Ikeda map (25.11) located at $(x, y) \approx (0.53275, 0.24689)$. The circle indicates the position of the fixed point. Note that the basin of attraction of this fixed point is large, larger than the entire Ikeda attractor.

where $\mathbf{C}$ is a $[d \times d]$ invertible matrix. The aim is to turn x_* into a stable equilibrium point of the flow by an appropriate choice of $\mathbf{C}$. It can be shown that a set of permutation / reflection matrices with one and only one non-vanishing entry ± 1 per row or column (for d-dimensional systems, there are $d!2^d$ such matrices) suffices to stabilize any fixed point. In practice, one chooses a particular matrix $\mathbf{C}$, and the flow is integrated. For each choice of $\mathbf{C}$, one or more hyperbolic fixed points of the map may turn into stable equilibria of the flow.

appendix G.2

Example 25.2 Ikeda map. *We illustrate the method with the determination of the periodic orbits of the Ikeda map:*

$$\begin{aligned} x' &= 1 + a(x\cos w - y\sin w) \\ y' &= a(x\sin w + y\cos w) \\ \text{where}\quad w &= b - \frac{c}{1+x^2+y^2}\,, \end{aligned} \tag{25.11}$$

with $a = 0.9$, $b = 0.4$, $c = 6$. The fixed point x_* is located at $(x, y) \approx (0.53275, 0.24689)$, with eigenvalues of the Jacobian matrix $(\Lambda_1, \Lambda_2) \approx (-2.3897, -0.3389)$, so the flow is already stabilized with $\mathbf{C} = \mathbf{1}$. Fig. 25.3 depicts the flow of the vector field around the fixed point x_*.

In order to determine x_*, one needs to integrate the vector field (25.9) forward in time (the convergence is exponential in time), using a fourth order Runge-Kutta or any other integration routine.

In contrast, determination of the 3-cycles of the Ikeda map requires nontrivial $\mathbf{C}$ matrices, different from the identity. Consider for example the hyperbolic fixed point $(x, y) \approx (-0.13529, -0.37559)$ of the third iterate f^3 of the Ikeda map. The flow of the vector field for $\mathbf{C} = \mathbf{1}$, Fig. 25.4(a), indicates a hyperbolic equilibrium point, while for $\mathbf{C} = \left(\begin{smallmatrix} 1 & 0 \\ 0 & -1 \end{smallmatrix}\right)$ the flow of the vector field, fig. 25.4(b) indicates that x_* is an attracting equilibrium point, reached at exponential speed by integration forward in time.

The generalization from searches for fixed points to searches for cycles is straightforward. In order to determine a prime cycle $x = (x_1, x_2, \ldots, x_n)$ of a d-dimensional map $x' = f(x)$, we modify the multipoint shooting method of sect. 14.4.1, and consider the nd-dimensional vector field

$$\frac{dx}{d\tau} = \mathbf{C}\,(f(x) - x)\,, \tag{25.12}$$

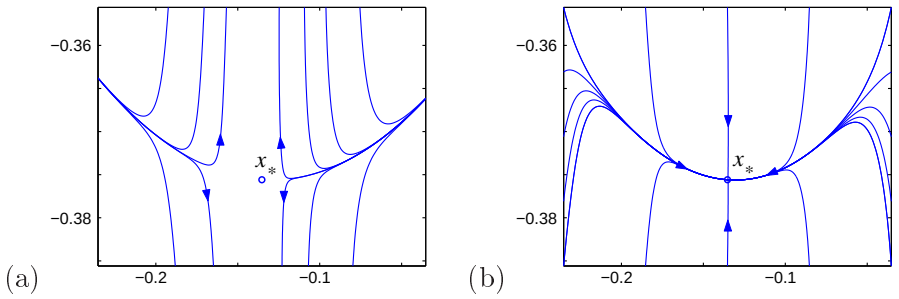

Figure 25.4: Typical trajectories of the vector field (25.10) for a hyperbolic fixed point $(x, y) \approx (-0.13529, -0.37559)$ of f^3, where f is the Ikeda map (25.11). The circle indicates the position of the fixed point. For the vector field corresponding to (*a*) $\mathbf{C} = \mathbf{1}$, x_* is a hyperbolic equilibrium point of the flow, while for (*b*) $\mathbf{C} = \left(\begin{smallmatrix} 1 & 0 \\ 0 & -1 \end{smallmatrix}\right)$, x_* is an attracting equilibrium point.

where $f(x) = (f(x_n), f(x_1), f(x_2), \ldots, f(x_{n-1}))$, and $\mathbf{C}$ is an invertible $[nd \times nd]$ matrix. For the Hénon map, it is sufficient to consider a set of 2^n diagonal matrices with eigenvalues ± 1. Risking a bit of confusion, we denote by x, $f(x)$ both the d-dimensional vectors in (25.10), and nd-dimensional vectors in (25.12), as the structure of the equations is the same.

25.2 Discrete iteration relaxation method

(C. Chandre, F.K. Diakonos and P. Schmelcher)

The problem with the Newton-Raphson iteration (25.2) is that it requires very precise initial guesses. For example, the nth iterate of a unimodal map has as many as 2^n periodic points crammed into the unit interval, so determination of all cycles of length n requires that the initial guess for each one of them has to be accurate to roughly 2^{-n}. This is not much of a problem for 1-dimensional maps, but making a good initial guess for where a cycle might lie in a d-dimensional phase space can be a challenge.

Emboldened by the success of the cyclist relaxation trick (25.8) of manually turning instability into stability by a sign change, we now (*i*) abandon the Newton-Raphson method altogether, (*ii*) abandon the continuous fictitious time flow (25.9) with its time-consuming integration, replacing it by a map g with a larger basin of attraction (not restricted to a linear neighborhood of the fixed point). The idea is to construct a very simple map g, a linear transformation of the original f, for which the fixed point is stable. We replace the Jacobian matrix prefactor in (25.2) (whose inversion can be time-consuming) by a constant matrix prefactor

$$x' = g(x) = x + \Delta\tau \mathbf{C}(f(x) - x), \tag{25.13}$$

where $\Delta\tau$ is a positive real number, and $\mathbf{C}$ is a $[d\times d]$ permutation and reflection matrix with one and only one non-vanishing entry ± 1 per row or column. A fixed point of f is also a fixed point of g. Since $\mathbf{C}$ is invertible, the inverse is also true.

This construction is motivated by the observation that for small $\Delta\tau \to d\tau$ the map (25.13) is the Euler method for integrating the modified flow (25.10), with the integration step $\Delta\tau$.

The argument why a suitable choice of matrix $\mathbf{C}$ can lead to the stabilization of an unstable periodic orbit is similar to the one used to motivate the construction of the modified vector field in sect. 25.1. Indeed, the flow (25.8) is the simplest example of this method, with the infinitesimal fictitious time increment $\Delta\tau \to d\tau$, the infinitesimal coordinate correction $(x - x') \to dx_i$, and the $[n\times n]$ diagonal matrix $\mathbf{C} \to \sigma_i = \pm 1$.

For a given fixed point of $f(x)$ we again chose a $\mathbf{C}$ such that the flow in the expanding directions of $\mathbf{J}(x_*)$ is turned into a contracting flow. The aim is to stabilize x_* by a suitable choice of $\mathbf{C}$. In the case where the map has multiple fixed points, the set of fixed points is obtained by changing the matrix $\mathbf{C}$ (in general different for each unstable fixed point) and varying initial conditions for the map g. For example, for 2-dimensional dissipative maps it can be shown that the 3 matrices

☞ remark 25.3

$$\mathbf{C} \in \left\{ \begin{pmatrix} 1 & 0 \\ 0 & 1 \end{pmatrix}, \begin{pmatrix} -1 & 0 \\ 0 & 1 \end{pmatrix}, \begin{pmatrix} 1 & 0 \\ 0 & -1 \end{pmatrix} \right\}$$

☞ appendix G.2

suffice to stabilize all kinds of possible hyperbolic fixed points.

If $\Delta\tau$ is chosen sufficiently small, the magnitude of the eigenvalues of the fixed point x_* in the transformed system are smaller than one, and one has a stable fixed point. However, $\Delta\tau$ should not be chosen too small: Since the convergence is geometrical with a ratio $1 - \alpha\Delta\tau$ (where the value of constant α depends on the stability of the fixed point in the original system), small $\Delta\tau$ can slow down the speed of convergence. The critical value of $\Delta\tau$, which just suffices to make the fixed point stable, can be read off from the quadratic equations relating the stability coefficients of the original system and those of the transformed system. In practice, one can find the optimal $\Delta\tau$ by iterating the dynamical system stabilized with a given $\mathbf{C}$ and $\Delta\tau$. In general, all starting points converge on the attractor provided $\Delta\tau$ is small enough. If this is not the case, the trajectory either diverges (if $\Delta\tau$ is far too large) or it oscillates in a small section of the phase space (if $\Delta\tau$ is close to its stabilizing value).

The search for the fixed points is now straightforward: A starting point chosen in the global neighborhood of the fixed point iterated with the transformed dynamical system g converges to the fixed point due to its stability.

Numerical investigations show that the domain of attraction of a stabilized fixed point is a rather extended connected area, by no means confined to a linear neighborhood. At times the basin of attraction encompasses the complete phase space of the attractor, so one can be sure to be within the attracting basin of a fixed point regardless of where on the on the attractor on picks the initial condition.

The step size $|g(x) - x|$ decreases exponentially when the trajectory approaches the fixed point. To get the coordinates of the fixed points with a high precision, one therefore needs a large number of iterations for the trajectory which is already in the linear neighborhood of the fixed point. To speed up the convergence of the final part of the approach to a fixed point we recommend a combination of the above approach with the Newton-Raphson method (25.2).

The fixed points of the nth iterate f^n are cycle points of a cycle of period n. If we consider the map

$$x' = g(x) = x + \Delta\tau \mathbf{C}(f^n(x) - x)\,, \tag{25.14}$$

the iterates of g converge to a fixed point provided that $\Delta\tau$ is sufficiently small and $\mathbf{C}$ is a $[d\times d]$ constant matrix chosen such that it stabilizes the flow. As n grows, $\Delta\tau$ has to be chosen smaller and smaller. In the case of the Ikeda map example 25.2 the method works well for $n \leq 20$. As in (25.12), the multipoint shooting method is the method of preference for determining longer cycles. Consider $x = (x_1, x_2, \ldots, x_n)$ and the nd-dimensional map

$$x' = f(x) = (f(x_n), f(x_1), \ldots, f(x_{n-1}))\,.$$

Determining cycles with period n for the d-dimensional f is equivalent to determining fixed points of the multipoint dn-dimensional f. The idea is to construct a matrix $\mathbf{C}$ such that the fixed point of f becomes stable for the map:

$$x' = x + \Delta\tau \mathbf{C}(f(x) - x),$$

where $\mathbf{C}$ is now a $[nd\times nd]$ permutation/reflection matrix with only one non-zero matrix element ± 1 per row or column. For any given matrix $\mathbf{C}$, a certain fraction of the cycles becomes stable and can be found by iterating the transformed map which is now a nd dimensional map.

From a practical point of view, the main advantage of this method compared to the Newton-Raphson method is twofold: (i) the stability matrix

of the flow need not be computed, so there is no large matrix to invert, simplifying considerably the implementation, and (*ii*) empirical basins of attractions for individual **C** are much larger than for the Newton-Raphson method. The price is a reduction in the speed of convergence.

25.3 Least action method

(P. Dahlqvist)

The methods of sects. 25.1 and 25.2 are somewhat *ad hoc*, as for general flows and iterated maps there is no fundamental principle to guide us in chosing the cost function, such as (25.3), to vary.

For Hamiltonian dynamics, we are on much firmer ground; Maupertuis least action principle. You yawn your way through it in every mechanics course - Maupertuis believed that the principle provided a proof of the existence of God - but as we shall now see, it is a very hands-on numerical method for finding cycles.

Indeed, the simplest and numerically most robust method for determining cycles of planar billiards is given by the principle of least action, or equivalently, by extremizing the length of an approximate orbit that visits a given sequence of disks. In contrast to the multipoint shooting method of sect. 14.4.1 which requires variation of $2N$ phase-space points, extremization of a cycle length requires variation of only N bounce positions s_i.

The problem is to find the extremum values of cycle length $L(s)$ where $s = (s_1, \ldots, s_N)$, that is find the roots of $\partial_i L(s) = 0$. Expand to first order

$$\partial_i L(s_0 + \delta s) = \partial_i L(s_0) + \sum_j \partial_i \partial_j L(s_0) \delta s_j + \ldots$$

and use $\mathbf{J}_{ij}(s_0) = \partial_i \partial_j L(s_0)$ in the N-dimensional Newton-Raphson iteration scheme of sect. 14.2.2

25.1 page 479

$$s_i \mapsto s_i - \sum_j \left(\frac{1}{\mathbf{J}(s)} \right)_{ij} \partial_j L(s) \tag{25.15}$$

The extremization is achieved by recursive implementation of the above algorithm, with proviso that if the dynamics is pruned, one also has to check that the final extremal length orbit does not penetrate a billiard wall.

25.2 page 479

As an example, the short periods and stabilities of 3-disk cycles computed this way are listed table 25.3.

14.10 page 277

p	Λ_p	T_p
0	9.898979485566	4.000000000000
1	-1.177145519638$\times 10^{1}$	4.267949192431
01	-1.240948019921$\times 10^{2}$	8.316529485168
001	-1.240542557041$\times 10^{3}$	12.321746616182
011	1.449545074956$\times 10^{3}$	12.580807741032
0001	-1.229570686196$\times 10^{4}$	16.322276474382
0011	1.445997591902$\times 10^{4}$	16.585242906081
0111	-1.707901900894$\times 10^{4}$	16.849071859224
00001	-1.217338387051$\times 10^{5}$	20.322330025739
00011	1.432820951544$\times 10^{5}$	20.585689671758
00101	1.539257907420$\times 10^{5}$	20.638238386018
00111	-1.704107155425$\times 10^{5}$	20.853571517227
01011	-1.799019479426$\times 10^{5}$	20.897369388186
01111	2.010247347433$\times 10^{5}$	21.116994322373
000001	-1.205062923819$\times 10^{6}$	24.322335435738
000011	1.418521622814$\times 10^{6}$	24.585734788507
000101	1.525597448217$\times 10^{6}$	24.638760250323
000111	-1.688624934257$\times 10^{6}$	24.854025100071
001011	-1.796354939785$\times 10^{6}$	24.902167001066
001101	-1.796354939785$\times 10^{6}$	24.902167001066
001111	2.005733106218$\times 10^{6}$	25.121488488111
010111	2.119615015369$\times 10^{6}$	25.165628236279
011111	-2.366378254801$\times 10^{6}$	25.384945785676

Table 25.3: All prime cycles up to 6 bounces for the three-disk fundamental domain, center-to-center separation $R = 6$, disk radius $a = 1$. The columns list the cycle itinerary, its expanding eigenvalue Λ_p, and the length of the orbit (if the velocity=1 this is the same as its period or the action). Note that the two 6 cycles $\overline{001011}$ and $\overline{001101}$ are degenerate due to the time reversal symmetry, but are not related by any discrete spatial symmetry. (Computed by P.E. Rosenqvist.)

Commentary

Remark 25.1 Piece-wise linear maps. The Lozi map (3.12) is linear, and 100,000's of cycles can be easily computed by [2x2] matrix multiplication and inversion.

Remark 25.2 Relaxation method. The relaxation (or gradient) algorithm is one of the methods for solving extremal problems [25.10]. The method described above was introduced by Biham and Wenzel [25.1], who have also generalized it (in the case of the Hénon map) to determination of *all* 2^n cycles of period n, real or complex [25.2]. The applicability and reliability of the method is discussed in detail by Grassberger, Kantz and Moening [25.4], who give examples of the ways in which the method fails: (a) it might reach a limit cycle rather than a equilibrium saddlepoint (that can be remedied by the complex Biham-Wenzel algorithm [25.2]) (b) different symbol sequences can converge to the same cycle (that is, more refined initial conditions might be needed). Furthermore, Hansen (ref. [25.5] and chapter 4. of ref. [1.3]) has pointed out that the method cannot find certain cycles for specific values of the Hénon map parameters.

In practice, the relaxation method for determining periodic orbits of maps appears to be effective almost always, but not always. It is much slower than the multipoint shooting method of sect. 14.4.1, but also much quicker to program, as it does not require evaluation of stability matrices and their inversion. If the complete set of cycles is required, the method has to be supplemented by other methods.

Remark 25.3 Hybrid Newton-Raphson/relaxation methods. The method discussed in sect. 25.2 was introduced by Schmelcher *et al* [25.6]. The method was extended to flows by means of the Poincaré surface of section technique in ref. [25.7]. It is also possible to combine the Newton-Raphson method and (25.13) in the construction of a transformed map [25.11]. In this approach, each step of the iteration scheme is a linear superposition of a step of the stability transformed system and a step of the Newton-Raphson algorithm. Far from the linear neighborhood the weight is dominantly on the globally acting stability transformation algorithm. Close to the fixed point, the steps of the iteration are dominated by the Newton-Raphson procedure.

Remark 25.4 Relation to the Smale horseshoe symbolic dynamics. For a complete horseshoe Hénon repeller (a sufficiently large), such as the one given in fig. 25.2, the signs $\sigma_i \in \{1, -1\}$ are in a 1-to-1 correspondence with the Smale horsheshoe symbolic dynamics $s_i \in \{0, 1\}$:

$$s_i = \begin{cases} 0 & \text{if } \sigma_i = -1\,, \quad x_i < 0 \\ 1 & \text{if } \sigma_i = +1\,, \quad x_i > 0 \end{cases} \quad . \tag{25.16}$$

For arbitrary parameter values with a finite subshift symbolic dynamics or with arbitrarily complicated pruning, the relation of sign sequences $\{\sigma_1, \sigma_2, \cdots, \sigma_n\}$ to the itineraries $\{s_1, s_2, \cdots, s_n\}$ can be much subtler; this is discussed in ref. [25.4].

Remark 25.5 Ikeda map. Ikeda map (25.11) was introduced in ref. [25.9] is a model which exhibits complex dynamics observed in nonlinear optical ring cavities.

Remark 25.6 Relaxation for continuous time flows. For a d-dimensional flow $\dot{x} = v(x)$, the method described above can be extended by considering a Poincaré surface of section. The Poincaré section yields a map f with dimension d-1, and the above discrete iterative maps procedures can be carried out. A method that keeps the trial orbit continuous throughout the calculation is the Newton descent, a variational method for finding periodic orbits of continuous time flows, is described in refs. [25.12, 25.13].

Remark 25.7 Stability ordering. The parameter $\Delta\tau$ in (25.13) is a key quantity here. It is related to the stability of the desired cycle in the transformed system: The more unstable a fixed point is, the smaller $\Delta\tau$ has to be to stabilize it. With increasing cycle periods, the unstable eigenvalue of the stability matrix increases and therefore $\Delta\tau$ has to be reduced to achieve stabilization of all fixed points. In many cases the least unstable cycles of a given period n are of physically most important [25.8]. In this context $\Delta\tau$ operates as a stability filter. It allows the selective stabilization of only those cycles which posses Lyapunov exponents smaller than a cut-off value. If one starts the search for cycles within a given period n with a value $\Delta\tau \approx O(10^{-1})$, and gradually lowers $\Delta\tau$ one obtains the sequence of all unstable orbits of order n sorted with increasing values of their Lyapunov exponents. For the specific choice of $\mathbf{C}$ the relation between $\Delta\tau$ and the stability coefficients of the fixed points of the original system is strictly monotonous. Transformed dynamical systems with other $\mathbf{C}$'s do not obey such a strict behavior but show a rough ordering of the sequence of stability eigenvalues of the fixed points stabilized in the course of decreasing values for $\Delta\tau$. As explained in sect. 15.4, stability ordered cycles are needed to order cycle expansions of dynamical quantities of chaotic systems for which a symbolic dynamics is not known. For such systems, an ordering of cycles with respect to their stability has been proposed [15.13, 15.14, 15.12], and shown to yield good results in practical applications.

☞ sect. 15.4

Remark 25.8 Action extremization method. The action extremization (sect. 25.3) as a numerical method for finding cycles has been

introduced independently by many people. We have learned it from G. Russberg, and from M. Sieber's and F. Steiner's hyperbola billiard computations [25.14, 25.15]. The convergence rate is really impressive, for the Sinai billiard some 5000 cycles are computed within CPU seconds with rather bad initial guesses.

Variational methods are the key ingredient of the Aubry-Mather theory of area-preserving twist maps (known in the condensed matter literature as the Frenkel-Kontorova models of 1-dimensional crystals), discrete-time Hamiltonian dynamical systems particularly suited to explorations of the K.A.M. theorem. Proofs of the Aubry-Mather theorem [25.17] on existence of quasi-periodic solutions are variational. It was quickly realized that the variational methods can also yield reliable, high precision computations of long periodic orbits of twist map models in 2 or more dimensions, needed for K.A.M. renormalization studies [25.16].

A fictitious time gradient flow similar to the one discussed here in sect. 25.1 was introduced by Anegent [25.18] for twist maps, and used by Gole [25.19] in his proof of the Aubry-Mather theorem. Mathematical bounds on the regions of stability of K.A.M. tori are notoriously restrictive compared to the numerical indications, and de la Llave, Falcolini and Tompaidis [25.20, 25.21] have found the gradient flow formulation advantageous both in studies of the analyticity domains of the K.A.M. stability, as well as proving the Aubry-Mather theorem for extended systems (for a pedagogical introduction, see the lattice dynamics section of ref. [25.22]).

All of the twist-maps work is based on extremizing the discrete dynamics version of the action S (in this context sometimes called a "generating function"). However, in their investigations in the complex plane, Falcolini and de la Llave [25.20] do find it useful to minimize instead $S\bar{S}$, analogous to our cost function (25.3).

Résumé

Unlike the Newton-Raphson method, variational methods are very robust. As each step around a cycle is short, they do not suffer from exponential instabilities, and with rather coarse initial guesses one can determine cycles of arbitrary length.

References

[25.1] O. Biham and W. Wenzel, *Phys. Rev. Lett.* **63**, 819 (1989).

[25.2] O. Biham and W. Wenzel, *Phys. Rev.* **A 42**, 4639 (1990).

[25.3] P. Grassberger and H. Kantz, *Phys. Lett. A* **113**, 235 (1985).

[25.4] P. Grassberger, H. Kantz and U. Moening, *J. Phys.* **A 43**, 5217 (1989).

[25.5] K.T. Hansen, *Phys. Lett.* **A 165**, 100 (1992).

[25.6] P. Schmelcher and F.K. Diakonos, *Phys. Rev. Lett.* **78**, 4733 (1997); *Phys. Rev. E* **57**, 2739 (1998).

[25.7] D. Pingel, P. Schmelcher and F.K. Diakonos, O. Biham, *Phys. Rev. E* **64**, 026214 (2001).

[25.8] F. K. Diakonos, P. Schmelcher, O. Biham, *Phys. Rev. Lett.* **81**, 4349 (1998).

[25.9] K. Ikeda, *Opt. Commun.* **30**, 257 (1979).

[25.10] F. Stummel and K. Hainer, *Praktische Mathematik* (Teubner, Stuttgart 1982).

[25.11] R.L. Davidchack and Y.C. Lai, *Phys. Rev. E* **60**, 6172 (1999).

[25.12] P. Cvitanović and Y. Lan, "Turbulent fields and their recurrences", in N. Antoniou, ed., *Proceed. of 10. Intern. Workshop on Multiparticle Production: Correlations and Fluctuations in QCD* (World Scientific, Singapore 2003). `nlin.CD/0308006`

[25.13] Y. Lan and P. Cvitanović, "Variational method for finding periodic orbits in a general flow", submitted to *Phys. Rev.* **E** (August 2003). `nlin.CD/0305008`

[25.14] M. Sieber and F. Steiner, " Quantum Chaos in the Hyperbola Billiard", *Phys. Lett.* **A 148**, 415 (1990).

[25.15] M. Sieber, *The Hyperbola Billiard: A Model for the Semiclassical Quantization of Chaotic Systems*, Ph.D. thesis (Hamburg 1991); DESY report 91-030.

[25.16] H. T. Kook and J. D. Meiss, "Periodic orbits for reversible symplectic mappings", *Physica D* **35**, 65 (1989).

[25.17] J.N. Mather, "Variational construction of orbits of twist difeomorphisms", J. Amer. Math. Soc. **4** 207 (1991).

[25.18] S. B. Angenent, "The periodic orbits of an area preserving twist-map", *Comm. Math. Phys.* **115**, 353 (1988).

[25.19] C. Golé, "A new proof of the Aubry-Mather's theorem", *Math. Z.* **210**, 441 (1992).

[25.20] C. Falcolini and R. de la Llave, "Numerical calculation of domains of analyticity for perturbation theories in the presence of small divisors", *J. Stat. Phys.* **67**, 645 (1992).

[25.21] S. Tompaidis, "Numerical Study of Invariant Sets of a Quasi-periodic Perturbation of a Symplectic Map", *Experimental Mathematics* **5**, 211 (1996).

[25.22] R. de la Llave, *Variational methods for quasiperiodic solutions of partial differential equations*, `mp_arc 00-56`.

Exercises

Exercise 25.1 Evaluation of cycles by minimization*. *Given a symbol sequence, you can construct a guess trajectory by taking a point on the boundary of each disk in the sequence, and connecting them by straight lines. If this were a rubber band wrapped through 3 rings, it would shrink into the physical trajectory, which minimizes the action (in this case, the length) of the trajectory.*

Write a program to find the periodic orbits for your billiard simulator. Use the least action principle to extremize the length of the periodic orbit, and reproduce the periods and stabilities of 3-disk cycles, table 25.3. After that check the accuracy of the computed orbits by iterating them forward with your simulator. What is $|f^{T_p}(x) - x|$*?*

Exercise 25.2 Tracking cycles adiabatically*. *Once a cycle has been found, orbits for different system parameters values may be obtained by varying slowly (adiabatically) the parameters, and using the old orbit points as starting guesses in the Newton method. Try this method out on the 3-disk system. It works well for* $R : a$ *sufficiently large. For smaller values, some orbits change rather quickly and require very small step sizes. In addition, for ratios below* $R : a = 2.04821419\ldots$ *families of cycles are pruned, that is some of the minimal length trajectories are blocked by intervening disks.*

Exercise 25.3 Find cycles of the Hénon map. *Apply the method of sect. 25.1 to the Hénon map at the Hénon's parameters choice* $a = 1.4$, $b = 0.3$*, and compute all prime cycles for at least* $n \leq 6$*. Estimate the topological entropy, either from the definition (10.1), or as the zero of a truncated topological zeta function (10.21). Do your cycles agree with the cycles listed in table 25.1?*

Chapter 26

Semiclassical evolution

> William Rowan Hamilton was born in 1805. At three he could read English; by four he began to read Latin, Greek and Hebrew, by ten he read Sanskrit, Persian, Arabic, Chaldee, Syrian and sundry Indian dialects. At age seventeen he began to think about optics, and worked out his great principle of "Characteristic Function".
>
> Turnbull, *Lives of Mathematicians*

(G. Vattay, G. Tanner and P. Cvitanović)

Semiclassical approximations to quantum mechanics are valid in the regime where the de Broglie wavelength $\lambda \sim \hbar/p$ of a particle with momentum p is much *shorter* than the length scales across which the potential of the system changes significantly. In the short wavelength approximation the particle is a point-like object bouncing off potential walls the same way it does in the classical mechanics. The real novelty of quantum mechanics is the interference of the point-like particle with other versions of itself travelling along different classical trajectories, a feat impossible in classical mechanics. The short wavelength – or semiclassical – formalism is developed by formally taking the limit $\hbar \to 0$ in quantum mechanics in such a way that quantum quantities go to their classical counterparts.

☞ remark 26.1

26.1 Hamilton-Jacobi theory

The mathematical formulation of the semiclassical approximation starts out with a rewrite of the wave function

$$\psi(q,t) = A(q,t)e^{iR(q,t)/\hbar}\,, \tag{26.1}$$

in terms of a pair of real functions $R(q,t)$ and $A(q,t)$, its phase and magnitude. The time evolution of the phase and the magnitude of ψ follows from the Schrödinger equation (23.1)

24.1 page 460

$$\left(i\hbar\frac{\partial}{\partial t}+\frac{\hbar^2}{2m}\frac{\partial^2}{\partial q^2}-V(q)\right)\psi(q,t)=0\,. \tag{26.2}$$

Take for concreteness a Hamiltonian $\hat{H}$ of form (23.2), assume $A\neq 0$, and separate out the real and the imaginary parts. We get two equations: The real part governs the time evolution of the phase

$$\frac{\partial R}{\partial t}+\frac{1}{2m}\left(\frac{\partial R}{\partial q}\right)^2+V(q)-\frac{\hbar^2}{2m}\frac{1}{A}\frac{\partial^2}{\partial q^2}A=0\,, \tag{26.3}$$

and the imaginary part the time evolution of the amplitude

24.2 page 460
24.3 page 460

$$\frac{\partial A}{\partial t}+\frac{1}{m}\sum_{i=1}^{d}\frac{\partial A}{\partial q_i}\frac{\partial R}{\partial q_i}+\frac{1}{2m}A\frac{\partial^2 R}{\partial q^2}=0\,. \tag{26.4}$$

24.4 page 460

In this way a linear PDE for a complex wave function is converted into a set of coupled non-linear PDE's for real-valued functions R and A. The coupling term in (26.3) is, however, of order $\hbar^2$ and thus small in the semiclassical limit $\hbar\to 0$. Now we make the *Wentzel-Kramers--Brillouin* (WKB) *ansatz*: we assume the magnitude $A(q,t)$ varies slowly compared to the phase $R(q,t)/\hbar$, so we drop the $\hbar$-dependent term. In this approximation the phase $R(q,t)$ and the corresponding "momentum field" $\frac{\partial R}{\partial q}(q,t)$ can be determined from the amplitude independent equation

$$\frac{\partial R}{\partial t}+H\left(q,\frac{\partial R}{\partial q}\right)=0\,. \tag{26.5}$$

In classical mechanics this equation is known as the *Hamilton-Jacobi equation*. We will refer to this step as the *semiclassical approximation* to wave mechanics, and from now on work only within this approximation.

26.1.1 Hamilton's equations

If you already understand the Hamilton-Jacobi theory, you can safely skip this section.

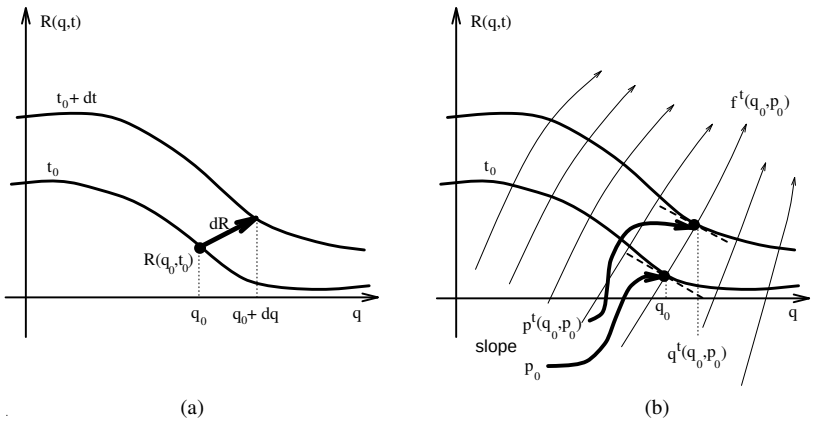

Figure 26.1: (a) A phase $R(q,t)$ plotted as a function of the position q for two infinitesimally close times. (b) The phase $R(q,t)$ transported by a swarm of "particles"; The Hamilton's equations (26.10) construct $R(q,t)$ by transporting $q_0 \to q(t)$ and the slope of $R(q_0,t_0)$, that is $p_0 \to p(t)$.

fast track:
sect. 26.1.3, p. 487

The wave equation (23.1) describes how the wave function ψ evolves with time, and if you think of ψ as an (infinite dimensional) vector, position q plays a role of an index. In one spatial dimension the phase R plotted as a function of the position q for two different times looks something like fig. 26.1(a): The phase $R(q,t_0)$ deforms smoothly with time into the phase $R(q,t)$ at time t. Hamilton's idea was to let a swarm of particles transport R and its slope $\partial R/\partial q$ at q at initial time $t=t_0$ to a corresponding $R(q,t)$ and its slope at time t, fig. 26.1(b). For notational convenience, define

$$p_i = p_i(q,t) := \frac{\partial R}{\partial q_i}\,, \quad i = 1,2,\ldots,d\,. \tag{26.6}$$

We saw earlier that (26.3) reduces in the semiclassical approximation to the Hamilton-Jacobi equation (26.5). To make life simple, we shall assume throughout this chapter that the Hamilton's function $H(q,p)$ does not depend explicitly on time t, that is the energy is conserved.

To start with, we also assume that the function $R(q,t)$ is smooth and well defined for every q at the initial time t. This is true for sufficiently short times; as we will see later R develops folds and becomes multi-valued as t progresses. Consider now the variation of the function $R(q,t)$ with respect to independent infinitesimal variations of the time and space coordinates dt and dq, fig. 26.1(a)

$$dR = \frac{\partial R}{\partial t}dt + \frac{\partial R}{\partial q}dq\,. \tag{26.7}$$

Dividing through by dt and substituting (26.5) we obtain the total derivative of $R(q,t)$ with respect to time *along as yet arbitrary direction* $\dot{q}$, that is,

$$\frac{dR}{dt}(q,\dot{q},t) = -H(q,p) + \dot{q}\cdot p\,. \tag{26.8}$$

Note that the "momentum" $p = \partial R/\partial q$ is a well defined function of q and t. In order to integrate $R(q,t)$ with the help of (26.8) we also need to know how $p = \partial R/\partial q$ changes along $\dot{q}$. Varying p with respect to independent infinitesimal variations dt and dq and substituting the Hamilton-Jacobi equation (26.5) yields

$$d\frac{\partial R}{\partial q} = \frac{\partial^2 R}{\partial q \partial t}dt + \frac{\partial^2 R}{\partial q^2}dq = -\left(\frac{\partial H}{\partial q} + \frac{\partial H}{\partial p}\frac{\partial p}{\partial q}\right)dt + \frac{\partial p}{\partial q}dq\,.$$

Note that $H(q,p)$ depends on q also through $p(q,t) = \partial R/\partial q$, hence the $\frac{\partial H}{\partial p}$ term in the above equation. Dividing again through by dt we get the time derivative of $\partial R/\partial q$, that is,

$$\dot{p}(q,\dot{q},t) + \frac{\partial H}{\partial q} = \left(\dot{q} - \frac{\partial H}{\partial p}\right)\frac{\partial p}{\partial q}\,. \tag{26.9}$$

Time variation of p depends not only on the yet unknown $\dot{q}$, but also on the second derivatives of R with respect to q with yet unknown time dependence. However, if we *choose* $\dot{q}$ (which was arbitrary, so far) such that the right hand side of the above equation vanishes, we can calculate the function $R(q,t)$ along a specific trajectory $(q(t),p(t))$ given by integrating the ordinary differential equations

$$\dot{q} = \frac{\partial H(q,p)}{\partial p}, \qquad \dot{p} = -\frac{\partial H(q,p)}{\partial q} \tag{26.10}$$

with initial conditions

$$q(t_0) = q', \qquad p(t_0) = p' = \frac{\partial R}{\partial q}(q',t_0). \tag{26.11}$$

☞ sect. 5.1

We recognize (26.10) as the Hamilton's equations of motion of classical mechanics.

$\dot{q}$ is no longer an independent function, and the phase $R(q,t)$ can now be computed by integrating equation (26.8) along the trajectory $(q(t),p(t))$

$$\begin{aligned} R(q,t) &= R(q',t_0) + R(q,t;q',t_0) \\ R(q,t;q',t_0) &= \int_{t_0}^{t} d\tau \left[\dot{q}(\tau)\cdot p(\tau) - H(q(\tau),p(\tau))\right] , \end{aligned} \tag{26.12}$$

with the initial conditions (26.11). In this way the Hamilton-Jacobi *partial* differential equation (26.3) is solved by integrating a set of *ordinary* differential equations, the Hamilton's equations. In order to determine $R(q,t)$ for arbitrary q and t we have to find a q' such that the trajectory starting in $(q', p' = \partial_q R(q',t_0))$ reaches q in time t and then compute R along this trajectory, see fig. 26.1(b). Erudite reader has already noticed that the integrand of (26.12) is known as the Lagrangian, and that a variational principle lurks somewhere, but we shall not make much fuss about that here.

Throughout this chapter we assume that the energy is conserved, and that the only time dependence of $H(q,p)$ is through $(q(\tau),p(\tau))$, so the value of $R(q,t;q',t_0)$ does not depend on t_0, but only on the elapsed time $t-t_0$. To simplify notation we will set $t_0 = 0$ and write

$$R(q,q',t) = R(q,t;q',0)\,.$$

The initial momentum of the particle must coincide with the initial momentum of the trajectory connecting q' and q:

$$p' = \frac{\partial}{\partial q'} R(q',0) = -\frac{\partial}{\partial q'} R(q,q',t). \tag{26.13}$$

26.3
page 504

Function $R(q,q',t)$ is known as the *Hamilton's principal function*.

24.5
page 460

To summarize: Hamilton's achievement was to trade in the Hamilton-Jacobi *partial* differential equation (26.5) describing the evolution of a wave front for a finite number of *ordinary* differential equations of motion, with the initial phase $R(q,0)$ incremented by the integral (26.12) evaluated along the phase space trajectory $(q(\tau),p(\tau))$.

26.1.2 Action

Before proceeding, we note in passing a few facts about Hamiltonian dynamics that will be needed for the construction of semiclassical Green's

functions. If the energy is conserved, the $\int H(q,p)d\tau$ integral in (26.12) is simply Et. The first term, or the *action*

$$S(q,q',E) = \int_0^t d\tau\, \dot{q}(\tau)\cdot p(\tau) = \int_{q'}^{q} dq\cdot p \tag{26.14}$$

is integrated along a trajectory from q' to q with a fixed energy E. By (26.12) the action is the Legendre transform of Hamilton's principal function

$$S(q,q',E) = R(q,q',t) + Et\,. \tag{26.15}$$

The time of flight t along the trajectory connecting $q' \to q$ with fixed energy E is given by

$$\frac{\partial}{\partial E} S(q,q',E) = t\,. \tag{26.16}$$

The way to think about the formula (26.15) for action is that the time of flight is a function of the energy, $t = t(q,q',E)$. The left hand side is explicitly a function of E; the right hand side is an implicit function of E through energy dependence of the flight time t.

Going in the opposite direction, the energy of a trajectory $E = E(q,q',t)$ connecting $q' \to q$ with a given time of flight t is given by the derivative of Hamilton's principal function

$$\frac{\partial}{\partial t} R(q,q',t) = -E\,, \tag{26.17}$$

and the second variations of R and S are related in the standard way of Legendre transforms:

$$\frac{\partial^2}{\partial t^2} R(q,q',t) \frac{\partial^2}{\partial E^2} S(q,q',E) = -1\,. \tag{26.18}$$

A geometric visualization of what the phase evolution looks like is very helpful in understanding the origin of topological indices to be introduced in what follows. Given an initial phase $R(q,t_0)$, the gradient $\partial_q R$ defines a d-dimensional *Lagrangian manifold* $(q,\, p = \partial_q R(q))$ in the full $2d$ dimensional phase space (q,p). The defining property of this manifold is that any contractable loop γ in it has zero action,

☞ sect. 26.1.4

$$0 = \oint_\gamma dq\cdot p,$$

a fact that follows from the definition of p as a gradient, and the Stokes theorem. Hamilton's equations of motion preserve this property and map a Lagrangian manifold into a Lagrangian manifold time t later.

Returning back to the main line of our argument: we show next that the velocity field given by the Hamilton's equations together with the continuity equation determines the amplitude of the wave function.

26.1.3 Density evolution

To obtain the full solution of the Schrödinger equation (23.1), we also have to integrate (26.4). Already Schrödinger noted that

$$\rho = \rho(q,t) := A^2 = \psi^*\psi$$

plays the role of a density, and that the gradient of R may be interpreted as a local semiclassical momentum, as the momentum density is

$$\psi(q,t)^*(-i\hbar\frac{\partial}{\partial q})\psi(q,t) \;=\; -i\hbar A\frac{\partial A}{\partial q} + \rho\frac{\partial R}{\partial q}\,.$$

Evaluated along the trajectory $(q(t),p(t))$, the amplitude equation (26.4) is equivalent to the continuity equation (7.36) after multiplying (26.4) by $2A$, that is

$$\frac{\partial\rho}{\partial t} + \frac{\partial}{\partial q_i}(\rho v_i) = 0\,. \tag{26.19}$$

Here, $v_i = \dot{q}_i = p_i/m$ denotes a velocity field, which is in turn determined by the phase $R(q,t)$ or equivalently by the Lagrangian manifold $(q(t), p(t) = \partial_q R(q,t))$,

$$v = \frac{1}{m}\frac{\partial}{\partial q}R(q,t).$$

As we already know how to solve the Hamilton-Jacobi equation (26.5), we can also solve for the density evolution as follows:

The density $\rho(q)$ can be visualized as the density of a configuration space flow $q(t)$ of a swarm of hypothetical particles; the trajectories $q(t)$ are solutions of Hamilton's equations with initial conditions given by $(q(0) = q', p(0) = p' = \partial_q R(q',0))$.

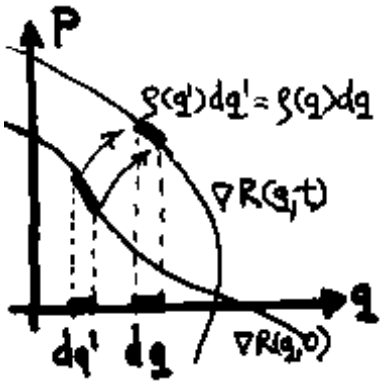

Figure 26.2: Density evolution of an initial surface $(q', p' = \partial_q R(q', 0)$ into $(q(t), p(t))$ surface time t later, sketched in 1 dimension. While the number of trajectories and the phase space Liouville volume are conserved, the density of trajectories projected on the q coordinate varies; trajectories which started in dq' at time zero end up in the interval dq.

If we take a small configuration space volume $d^d q$ around some point q at time t, then the number of particles in it is $\rho(q,t)d^d q$. They started initially in a small volume $d^d q'$ around the point q' of the configuration space. For the moment, we assume that there is only one solution, the case of several paths will be considered below. The number of particles at time t in the volume is the same as the number of particles in the initial volume at $t = 0$,

$$\rho(q(t), t)d^d q = \rho(q', 0)d^d q' \,,$$

see fig. 26.2. The ratio of the initial and the final volumes can be expressed as

$$\rho(q(t), t) = \left| \det \frac{\partial q'}{\partial q} \right| \rho(q', 0) \,. \tag{26.20}$$

☞ sect. 7.2

As we know how to compute trajectories $(q(t), p(t))$, we know how to compute this jacobian and, by (26.20), the density $\rho(q(t), t)$ at time t.

26.1.4 Semiclassical wave function

Now we have all ingredients to write down the semiclassical wave function at time t. Consider first the case when our initial wave function can be written in terms of single-valued functions $A(q', 0)$ and $R(q', 0)$. For sufficiently short times, $R(q, t)$ will remain a single-valued function of q, and every $d^d q$ configuration space volume element keeps its orientation. The evolved wave function is in the semiclassical approximation then given by

$$\psi_{sc}(q, t) \quad = \quad A(q, t)e^{iR(q,t)/\hbar} = \sqrt{\det \frac{\partial q'}{\partial q}}\, A(q', 0)e^{i(R(q',0)+R(q,q',t))/\hbar}$$

$$= \sqrt{\det \frac{\partial q'}{\partial q}}\, e^{iR(q,q',t)/\hbar}\, \psi(q',0)\,.$$

As the time progresses the Lagrangian manifold $\partial_q R(q,t)$ can develop folds, so for longer times the value of the phase $R(q,t)$ is not necessarily unique; in general more than one trajectory will connect points q and q' with different phases $R(q,q',t)$ accumulated along these paths, see fig. 26.3.

Whenever the Lagrangian manifold develops a fold, the density of the phase space trajectories in the fold projected on the configuration coordinates diverges. As illustrated in fig. 26.3, when the Lagrangian manifold develops a fold at $q = q_1$; the volume element dq_1 in the neighborhood of the folding point which steams from some inital volume element dq' is proportional to $\sqrt{dq'}$ instead of dq' at the fold. The Jacobian $\partial q'/\partial q$ diverges like $1/\sqrt{q_1 - q(t)}$ when computed along the trajectory going trough the folding point at q_1. After the folding the orientation of the interval dq' has changed when being mapped into dq_2; in addition the function R, as well as its derivative which defines the Lagrangian manifold, becomes multi-valued. Distinct trajectories starting from different initial points q' can now reach the same final point q_2. (That is, the point q' may have more than one pre-image.) The presence of a fold is signaled by the divergence of an eigenvalue of the Jacobian $\partial q'/\partial q$. The projection of a simple fold, or of an envelope of a family of phase space trajectories, is called a *caustic*; this expression comes from the Greek word for "capable of burning", evoking the luminous patterns that one observes swirling across the bottom of a swimming pool.

We thus expect in general a collection of different trajectories from q' to q which we will index by j, with different phase increments $R_j(q,q',t)$. The hypothetical particles of the density flow at a given configuration space point can move with different momenta $p = \partial_q R_j(q,t)$. This is not an ambiguity, since in the full (q,p) phase space each particle follows its own trajectory with a unique momentum.

The folding also changes the orientation of the pieces of the Lagrangian manifold $(q, \partial_q R(q,t))$ with respect to the initial manifold, so the eigenvalues of the Jacobian determinant change sign at each fold crossing. We can keep track of the signs by writing the Jacobian determinant as

$$\det \left.\frac{\partial q'}{\partial q}\right|_j = e^{-i\pi m_j(q,q',t)} \left|\det \left.\frac{\partial q'}{\partial q}\right|_j\right| ,$$

where $m_j(q,q',t)$ counts the number of sign changes of the Jacobian determinant on the way from q' to q along the trajectory indexed with j, see

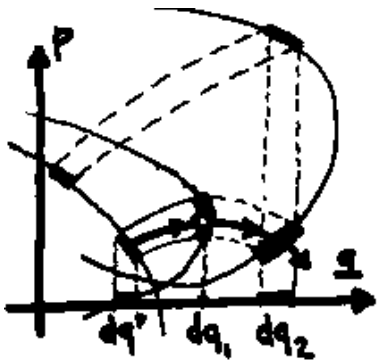

Figure 26.3: Folding of the Lagrangian surface $(q, \partial_q R(q,t))$.

fig. 26.3. We shall refer to the integer $m_j(q,q',t)$ as the *topological or Morse index* of the trajectory. So in general the semiclassical approximation to the wave function is thus a sum over possible trajectories that start in q' and end in q in time t

$$\psi_{sc}(q,t) = \sum_j \left| \det \frac{\partial q'}{\partial q} \right|_j^{1/2} e^{iR_j(q,q',t)/\hbar - i\pi m_j(q,q',t)/2} \psi(q'_j, 0)\,, \qquad (26.21)$$

each contribution weighted by corresponding density, phase increment and the topological index.

That the correct topological index is obtained by simply counting the number of eigenvalue sign changes and taking the square root is not obvious - the careful argument requires that quantum wave functions evaluated across the folds remain single valued.

26.2 Semiclassical propagator

We saw in chapter 23 that the evolution of an initial wave function $\psi(q,0)$ is completely determined by the propagator (23.11). As $K(q,q',t)$ itself satisfies the Schrödinger equation (23.13), we can treat it as a wave function parameterized by the configuration point q'. In order to obtain a semiclassical approximation to the propagator we follow now the ideas developed in the last section. There is, however, one small complication: the initial condition (23.14) demands that the propagator at $t = 0$ is a δ-function at $q = q'$, that is, the amplitude is infinite at q' and the phase is not well defined. Our hypothetical cloud of particles is thus initially localized at $q = q'$ with *any* initial velocity. This is in contrast to the situation in the previous section where we assumed that the particles at a given point q have well defined velocity (or a discrete set of velocities) given by $\dot{q} = \partial_p H(q,p)$.

We will now derive at a semiclassical expression for $K(q,q',t)$ by considering the propagator for short times first, and extrapolating from there to arbitrary times t.

26.2.1 Short time propagator

For infinitesimally short times δt away from the singular point $t=0$ we assume that it is again possible to write the propagator in terms of a well defined phase and amplitude, that is

$$K(q,q',\delta t) = A(q,q',\delta t)e^{\frac{i}{\hbar}R(q,q',\delta t)}\,.$$

As all particles start at $q=q'$, $R(q,q',\delta t)$ will be of the form (26.12), that is

$$R(q,q',\delta t) = p\dot{q}\delta t - H(q,p)\delta t\,, \tag{26.22}$$

with $\dot{q}\approx(q-q')/\delta t$. For Hamiltonians of the form (23.2) we have $\dot{q}=p/m$, which leads to

$$R(q,q',\delta t) = \frac{m(q-q')^2}{2\delta t} - V(q)\delta t\,.$$

Here V can be evaluated any place along the trajectory from q to q', for example at the midway point $V((q+a')/2)$. Inserting this into our ansatz for the propagator we obtain

$$K_{sc}(q,q',\delta t) \approx A(q,q',\delta t)e^{\frac{i}{\hbar}\left(\frac{m}{2\delta t}(q-q')^2 - V(q)\delta t\right)}\,. \tag{26.23}$$

For infinitesimal times we can neglect the term $V(q)\delta t$, so $K_{sc}(q,q',\delta t)$ is a d-dimensional gaussian with width $\sigma^2 = i\hbar\delta t/m$. This gaussian is a finite width approximation to the Dirac delta function

$$\delta_\sigma(z) = \lim_{\sigma\to 0}\frac{1}{\sqrt{2\pi\sigma^2}}e^{-z^2/2\sigma^2} \tag{26.24}$$

if $A=(m/2\pi i\hbar\delta t)^{d/2}$, with $A(q,q',\delta t)$ fixed by the Dirac delta function normalization condition. The correctly normalized propagator for infinitesimal times δt is therefore

26.4 page 504

$$K_{sc}(q,q',\delta t) \approx \left(\frac{m}{2\pi i\hbar\delta t}\right)^{d/2} e^{\frac{i}{\hbar}\left(\frac{m(q-q')^2}{2\delta t} - V(q)\delta t\right)}\,. \tag{26.25}$$

The short time dynamics of the Lagrangian manifold $(q, \partial_q R)$ which corresponds to the quantum propagator can now be deduced from (26.22); one obtains

$$\frac{\partial R}{\partial q} = p \approx \frac{m}{\delta t}(q - q')\,,$$

that is, is the particles start for short times on a Lagrangian manifold which is a plane in phase space, see fig. 26.4. Note, that for $\delta t \to 0$, this plane is given by the condition $q = q'$, that is, particles start on a plane parallel to the momentum axis. As we have already noted, all particles start at $q = q'$ but with different velocities for $t = 0$. The inital surface $(q', p' = \partial_q R(q', 0))$ is mapped into the surface $(q(t), p(t))$ some time t later. The slope of the Lagrangian plane for a short finite time is given as

$$\frac{\partial p_i}{\partial q_j} = -\frac{\partial^2 R}{\partial q_j \partial q_i'} = -\frac{\partial p_i'}{\partial q_j} = \frac{m}{\delta t}\delta_{ij}\,.$$

The prefactor $(m/\delta t)^{d/2}$ in (26.25) can therefore be interpreted as the determinant of the Jacobian of the transformation from final position coordinates q to initial momentum coordinates p', that is

$$K_{sc}(q, q', \delta t) = \frac{1}{(2\pi i\hbar)^{d/2}} \left\| \frac{\partial p'}{\partial q} \right\|^{1/2} e^{iR(q,q',\delta t)/\hbar}, \tag{26.26}$$

where

$$C(q, q', \delta t)_{ji} = -\left.\frac{\partial p_i'}{\partial q_j}\right|_{t,q'} = -\frac{\partial^2 R(q, q', \delta t)}{\partial q_j \partial q_i'} \tag{26.27}$$

The subscript $\cdots|_t$ indicates that the partial derivatives are to be evaluated with t, q' fixed.

The propagator in (26.26) that has been obtained for short times is, however, already more or less in its final form. We only have to evolve our short time approximation of the propagator according to (26.21)

$$K_{sc}(q'', q', t' + \delta t) = \sum_j \left| \det \left.\frac{\partial q}{\partial q"}\right|_j \right|^{1/2} e^{iR_j(q'',q,t')/\hbar - i\pi m_j(q'',q,t')/2} K(q_j, q_j', \delta t)\,,$$

and we included here already the possibility that the phase becomes multivalued, that is, that there is more than one path from q' to q''. The topological index $m_j = m_j(q'', q', t)$ is the number of singularities in the Jacobian

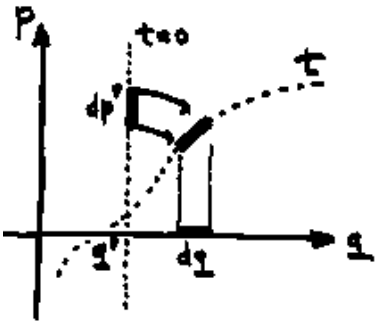

Figure 26.4: Evolution of the semiclassical propagator. The configuration which corresponds to the initial conditions of the propagator is a Lagrangian manifold $q = q'$, that is, a plane parallel to the p axis. The hypothetical particles are thus initially all placed at q' but take on all possible momenta p'. The Jacobian matrix C (26.28) relates an initial volume element in momentum space dp' to a final configuration space volume dq.

along the trajectory j from q' to q''. We can write $K_{sc}(q'', q', t' + \delta t)$ in closed form using the fact that $R(q'', q, t') + R(q, q', \delta t) = R(q'', q', t' + \delta t)$ and the multiplicativity of Jacobian determinants, that is

$$\begin{aligned} \det \frac{\partial q}{\partial qi"} \det C(q, q', t) &= \det \left.\frac{\partial q}{\partial q''}\right|_t \det \left.\frac{\partial p'}{\partial q}\right|_{q',\delta t} \qquad (26.28) \\ &= \det \left.\frac{\partial p'}{\partial q''}\right|_{q',t'+\delta t} = \det C(q'', q', t' + \delta t)\,. \end{aligned}$$

The final form of the semiclassical or *Van Vleck propagator*, is thus

$$K_{sc}(q, q', t) = \sum_j \frac{1}{(2\pi i\hbar)^{d/2}} |\det C_j(q, q', t)|^{1/2} e^{iR_j(q,q',t)/\hbar - im_j\pi/2}\,. \qquad (26.29)$$

This Van Vleck propagator is the essential ingredient of the semiclassical quantization to follow.

The apparent simplicity of the semiclassical propagator is deceptive. The wave function is not evolved simply by multiplying by a complex number of magnitude $\sqrt{\det \partial p'/\partial q}$ and phase $R(q, q', t)$; the more difficult task in general is to find the trajectories connecting q' and q in a given time t.

In addition, we have to treat the approximate propagator (26.29) with some care. Unlike the full quantum propagator which satisfies the group property (23.12) exactly the semiclassical propagator performs this only approximately, that is

$$K_{sc}(q, q', t_1 + t_2) \approx \int dq''\, K_{sc}(q, q'', t_2) K_{sc}(q'', q', t_1)\,. \qquad (26.30)$$

The connection can be made explicit by the stationary phase approximation, sect. 24.1. Approximating the integral in (26.30) by integrating only

over regions near points q'' at which the phase is stationary, leads to the stationary phase condition

$$\frac{\partial R(q,q'',t_2)}{\partial q_i''} + \frac{\partial R(q'',q',t_1)}{\partial q_i''} = 0. \tag{26.31}$$

Classical trajectories contribute whenever the final momentum for a path from q' to q'' and the initial momentum for a path from q'' to q coincide. Unlike the classical evolution of sect. 8.2, the semiclassical evolution is not an evolution by linear operator multiplication, but evolution supplemented by a stationary phase condition $p_{out} = p_{in}$ that matches up the classical momenta at each evolution step.

26.2.2 Free particle propagator

To develop some intuition about the above formalism, consider the case of a free particle. For a free particle the potential energy vanishes, the kinetic energy is $\frac{m}{2}\dot{q}^2$, and the Hamilton's principal function (26.12) is

$$R(q,q',t) = \frac{m(q-q')^2}{2t}\,. \tag{26.32}$$

The matrix $C(q,q',t)$ from (26.27) can be evaluated explicitly, and the Van Vleck propagator is

$$K_{sc}(q,q',t) = \Big(\frac{m}{2\pi i\hbar t}\Big)^{d/2} e^{im(q-q')^2/2\hbar t}\,, \tag{26.33}$$

identical to the short times propagator (26.25), with $V(q) = 0$. This case is rather exceptional: for a free particle the semiclassical propagator turns out to be the exact quantum propagator $K(q,q',t)$, as can be checked by substitution in the Schrödinger equation (26.2). The Feynman path integral formalism uses this fact to construct an exact quantum propagator by integrating the free particle propagator (with $V(q)$ treated as constant for short times) along all possible (not necessary classical) paths from q' to q.

☞ remark 26.3

26.5 page 504
26.6 page 504
26.7 page 504

26.3 Semiclassical Green's function

So far we have derived semiclassical formulas for the time evolution of wave functions, that is, we obtained approximate solutions to the time dependent

Schrödinger equation (23.1). Even though we assumed in the calculation a time independent Hamiltonian of the special form (23.2), the derivation leads to the same final result (26.29) were one to consider more complicated or explicitly time dependent Hamiltonians. The propagator is thus important when we are interested in finite time quantum mechanical effects. For time independent Hamiltonians, the time dependence of the propagator as well as of wave functions is, however, essentially given in terms of the energy eigen-spectrum of the system, as in (23.9). It is therefore advantageous to switch from a time representation to an energy representation, that is from the propagator (23.11) to the energy dependent Green's function (23.15). A semiclassical approximation of the Green's function $G_{sc}(q,q',E)$ is given by the Laplace transform (23.15) of the Van Vleck propagator $K_{sc}(q,q',t)$:

$$G_{sc}(q,q',E) = \frac{1}{i\hbar}\int_0^\infty \delta t\, e^{iEt/\hbar} K_{sc}(q,q',t)\,. \tag{26.34}$$

The expression as it stands is not very useful; in order to evaluate the integral at least approximately we need to again turn to the method of stationary phase.

26.3.1 Stationary phase in higher dimensions

24.6 page 460

Generalizing the method of sect. 24.1 to d dimensions, consider stationary phase points fulfilling

$$\frac{d}{dx_i}\Phi(x)\Big|_{x=x_0} = 0 \quad \forall i = 1,\dots d\,.$$

An expansion of the phase up to second order involves now the symmetric matrix of second derivatives of $\Phi(x)$, that is

$$D_{ij}(x_0) = \frac{\partial^2}{\partial x_i \partial x_j}\Phi(x)\Big|_{x=x_0}\,.$$

After choosing a suitable coordinate system which diagonalizes D, we can approximate the d-dimensional integral by d one-dimensional Fresnel integrals; the stationary phase estimate of (24.12) is then

$$I \approx \sum_{x_0} (2\pi i/s)^{d/2}\, |\det D(x_0)|^{-1/2} A(x_0)\, e^{is\Phi(x_0) - \frac{i\pi}{2}m(x_0)}\,, \tag{26.35}$$

where the sum runs over all stationary phase points x_0 of $\Phi(x)$ and $m(x_0)$ counts the number of negative eigenvalues of $\mathbf{D}(x_0)$.

26.8 page 505
24.7 page 460
24.8 page 461

The stationary phase approximation is all that is needed for the semiclassical approximation, with the proviso that D in (26.35) has no zero eigenvalues.

26.3.2 Long trajectories

When evaluating the integral (26.34) approximately we have to distinguish between two types of contributions: those coming from stationary points of the phase and those coming from infinitesimally short times. The first type of contributions can be obtained by stationary phase approximation and will be treated in this section. The latter originate from the singular behavior of the propagator for $t \to 0$ where the assumption that the amplitude changes slowly compared to the phase is no longer valid. The short time contributions therefore have to be treated separately, which we will do in sect. 26.3.3.

The stationary phase points t^* of the integrand in (26.34) are given by the condition

$$\frac{\partial}{\partial t} R(q, q', t^*) + E = 0\,. \tag{26.36}$$

We recognize this condition as the solution of (26.17), the time $t^* = t^*(q, q', E)$ in which a particle of energy E starting out in q' reaches q. Taking into account the second derivative of the phase evaluated at the stationary phase point,

$$R(q, q', t) + Et = R(q, q', t^*) + Et^* + \frac{1}{2}(t - t^*)^2 \frac{\partial^2}{\partial t^2} R(q, q', t^*) + \cdots$$

the stationary phase approximation of the integral corresponding to a specific branch j of the Van Vleck propagator (26.29) yields

$$G_j(q, q', E) = \frac{1}{i\hbar(2i\pi\hbar)^{(d-1)/2}} \left| \det C_j \left(\frac{\partial^2 R_j}{\partial t^2} \right)^{-1} \right|^{1/2} e^{\frac{i}{\hbar} S_j - \frac{i\pi}{2} m_j}\,, \tag{26.37}$$

where $m_j = m_j(q, q', E)$ now includes a possible additional phase arising from the time stationary phase integration (24.13), and $C_j = C_j(q, q', t^*)$,

$R_j = R_j(q, q', t^*)$ are evaluated at the transit time t^*. We re-express the phase in terms of the energy dependent action (26.15)

$$S(q, q', E) = R(q, q', t^*) + Et^*, \qquad \text{with} \quad t^* = t^*(q, q', E), \tag{26.38}$$

the Legendre transform of the Hamilton's principal function. Note that the partial derivative of the action (26.38) with respect to q_i

$$\frac{\partial S(q, q', E)}{\partial q_i} = \frac{\partial R(q, q', t^*)}{\partial q_i} + \left(\frac{\partial R(q, q', t)}{\partial t^*} + E \right) \frac{\partial t}{\partial q_i}.$$

is equal to

$$\frac{\partial S(q, q', E)}{\partial q_i} = \frac{\partial R(q, q', t^*)}{\partial q_i}, \tag{26.39}$$

due to the stationary phase condition (26.36), so the definition of momentum as a partial derivative with respect to q remains unaltered by the Legendre transform from time to energy domain.

26.9 page 505

Next we will simplify the amplitude term in (26.37) and rewrite it as an explicit function of the energy. Consider the $[(d+1)\times(d+1)]$ matrix

$$D(q, q', E) = \begin{pmatrix} \frac{\partial^2 S}{\partial q' \partial q} & \frac{\partial^2 S}{\partial q' \partial E} \\ \frac{\partial^2 S}{\partial q \partial E} & \frac{\partial^2 S}{\partial E^2} \end{pmatrix} = \begin{pmatrix} -\frac{\partial p'}{\partial q} & -\frac{\partial p'}{\partial E} \\ \frac{\partial t}{\partial q} & \frac{\partial t}{\partial E} \end{pmatrix}, \tag{26.40}$$

where $S = S(q, q', E)$ and we used (26.13–26.16) here to obtain the left hand side of (26.40). The minus signs follow from observing from the definition of (26.14) that $S(q, q', E) = -S(q', q, E)$. Note that D is nothing but the Jacobian matrix of the coordinate transformation $(q, E) \to (p', t)$ for fixed q'. We can therefore use the multiplication rules of determinants of Jacobians, which are just ratios of volume elements, to obtain

26.11 page 505

$$\begin{aligned} \det D &= (-1)^{d+1} \left\| \frac{\partial(p', t)}{\partial(q, E)} \right\|_{q'} = (-1)^{d+1} \left\| \frac{\partial(p', t)}{\partial(q, t)} \frac{\partial(q, t)}{\partial(q, E)} \right\|_{q'} \\ &= (-1)^{d+1} \left\| \frac{\partial p'}{\partial q} \right\|_{t, q'} \left\| \frac{\partial t}{\partial E} \right\|_{q', q} = \det C \left(\frac{\partial^2 R}{\partial t^2} \right)^{-1}. \end{aligned}$$

We use here the notation $\|.\|_{q',t}$ for a Jacobian determinant with partial derivatives evaluated at t, q' fixed, and likewise for other subscripts. Using

the relation (26.18) which relates the term $\frac{\partial t}{\partial E}$ to $\partial_t^2 R$ we can write the determinant of D as a product of the Van Vleck determinant (26.27) and the amplitude factor arising from the stationary phase approximation. The amplitude in (26.37) can thus be interpreted as the determinant of a Jacobian of a coordinate transformation which includes time and energy as independent coordinates. This causes the increase in the dimensionality of the matrix D relative to the Van Vleck determinant (26.27).

We can now write down the semiclassical approximation of the contribution of the jth trajectory to the Green's function (26.37) in explicitly energy dependent form:

$$G_j(q,q',E) = \frac{1}{i\hbar(2i\pi\hbar)^{(d-1)/2}} \left|\det D^j\right|^{1/2} e^{\frac{i}{\hbar}S_j - \frac{i\pi}{2}m_j} \,. \tag{26.41}$$

However, this is still not the most convenient form of the Green's function.

The trajectory contributing to $G_j(q,q',E)$ is constrained to a given energy E, and will therefore be on a phase space manifold of constant energy, that is $H(q,p) = E$. Writing this condition as partial differential equation for $S(q,q',E)$, that is

$$H(q, \frac{\partial S}{\partial q}) = E \,,$$

one obtains

$$\begin{aligned} \frac{\partial}{\partial q_i'} H(q,p) &= 0 = \frac{\partial H}{\partial p_j}\frac{\partial p_j}{\partial q_i'} = \dot{q}_j \frac{\partial^2 S}{\partial q_j \partial q_i'} \\ \frac{\partial}{\partial q_i} H(q',p') &= 0 = \frac{\partial^2 S}{\partial q_i \partial q_j'}\dot{q}_j' \,, \end{aligned} \tag{26.42}$$

that is the sub-matrix $\partial^2 S/\partial q_i \partial q_j'$ has (left- and right-) eigenvectors corresponding to an eigenvalue 0. In the local coordinate system

$$\mathbf{q} = (q_{\|}, q_{\perp 1}, q_{\perp 2}, \cdots, q_{\perp(d-1)}) \,, \qquad \text{with} \quad \dot{\mathbf{q}} = (\dot{q}, 0, 0, \cdots, 0)$$

in which the longitudinal coordinate axis $q_{\|}$ points along the velocity vector $\dot{q}$, the matrix of variations of $S(q,q',E)$ has a column and a row of zeros as (26.42) takes form

$$\dot{q}\frac{\partial^2 S}{\partial q_{\|}\partial q_i'} = \frac{\partial^2 S}{\partial q_i \partial q_{\|}'}\dot{q}' = 0 \,.$$

The initial and final velocities are non-vanishing except for points $|\dot{q}| = 0$. These are the turning points (where all energy is potential), and we assume that neither q nor q' is a turning point (in our application - periodic orbits - we can always chose $q = q'$ not a turning point). In the local coordinate system with one axis along the trajectory and all other perpendicular to it the determinant of (26.40) is of the form

$$\det D(q,q',E) = (-1)^{d+1} \begin{Vmatrix} 0 & 0 & \frac{\partial^2 S}{\partial E \partial q'_{\|}} \\ 0 & \frac{\partial^2\ S}{\partial q_\perp \partial q'_\perp} & * \\ \frac{\partial^2 S}{\partial q_{\|} \partial E} & * & * \end{Vmatrix} . \tag{26.43}$$

The corner entries can be evaluated using (26.16)

$$\frac{\partial^2 S}{\partial q_{\|} \partial E} = \frac{\partial}{\partial q_{\|}} t = \frac{1}{\dot{q}} , \qquad \frac{\partial^2 S}{\partial E \partial q'_{\|}} = \frac{1}{\dot{q}'} .$$

As the $q_{\|}$ axis points along the velocity direction, velocities $\dot{q}$, $\dot{q}'$ are by construction almost always positive non-vanishing numbers. In this way the determinant of the $[(d+1)\times(d+1)]$ dimensional matrix $D(q,q',E)$ can essentially be reduced to the determinant of a $[(d-1)\times(d-1)]$ dimensional *transverse* matrix $D_\perp(q,q',E)$

$$\begin{aligned} \det D(q,q',E) &= \frac{1}{\dot{q}\dot{q}'} \det D_\perp(q,q',E) \\ D_\perp(q,q',E)_{ik} &= -\frac{\partial^2 S(q,q',E)}{\partial q_{\perp i} \partial q'_{\perp k}} . \end{aligned} \tag{26.44}$$

Putting everything together we obtain the jth trajectory contribution to the semiclassical Green's function

26.12
page 505

$$G_j(q,q',E) = \frac{1}{i\hbar (2\pi\hbar)^{(d-1)/2}} \frac{1}{|\dot{q}\dot{q}'|^{1/2}} \left|\det D_\perp^j\right|^{1/2} e^{\frac{i}{\hbar} S_j - \frac{i\pi}{2} m_j} , \tag{26.45}$$

where the topological index $m_j = m_j(q,q',E)$ now counts the number of changes of sign of $\det D_\perp^j$ along the trajectory j which connects q' to q at energy E. The velocities $\dot{q}$, $\dot{q}'$ also depend on (q,q',E) and the trajectory j. While in the case of the propagator the initial momentum variations $\delta p'$ are unrestricted, for the Green's function the $(\delta q', \delta p')$ variations are restricted to the constant energy shell; the appearance of the $1/\dot{q}\dot{q}'$ weights in the Green's function can be traced to this constraint.

26.3.3 Short trajectories

The stationary phase method cannot be used when t^* is small, both because we cannot extend the integration in (24.13) to $-\infty$, and because the amplitude of $K(q,q',t)$ is divergent. In this case we have to evaluate the integral involving the short time form of the exact quantum mechanical propagator (26.25)

$$G_0(q,q',E) = \frac{1}{i\hbar}\int_0^\infty dt \left(\frac{m}{2\pi i\hbar t}\right)^{d/2} e^{\frac{i}{\hbar}(\frac{m(q-q')^2}{2t} - V(q)t + Et)}\,. \qquad (26.46)$$

By introducing a dimensionless variable $\tau = t\sqrt{2m(E-V(q))}/m|q-q'|$, the integral can be rewritten as

$$G_0(q,q',E) = \frac{m}{i\hbar^2(2\pi i)^{d/2}}\left(\frac{\sqrt{2m(E-V)}}{\hbar|q-q'|}\right)^{\frac{d}{2}-1}\int_0^\infty \frac{d\tau}{\tau^{d/2}} e^{\frac{i}{2\hbar}S_0(q,q',E)(\tau+1/\tau)},$$

where $S_0(q,q',E) = \sqrt{2m(E-V)}|q-q'|$ is the short distance form of the action. Using the integral representation of the Hankel function of first kind

$$H_\nu^+(z) = -\frac{i}{\pi}e^{-i\nu\pi/2}\int_0^\infty e^{\frac{1}{2}iz(\tau+1/\tau)}\tau^{-\nu-1}d\tau$$

we can write the short distance form of the Green's function as

$$G_0(q,q',E) \approx -\frac{im}{2\hbar^2}\left(\frac{\sqrt{2m(E-V)}}{2\pi\hbar|q-q'|}\right)^{\frac{d-2}{2}} H^+_{\frac{d-2}{2}}(S_0(q,q',E)/\hbar). \qquad (26.47)$$

There is nothing scary about the Hankel function - it is merely a useful observation, as for special functions the short wavelength asymptotics comes for free and can be found in standard reference books. The short distance Green's function approximation is valid when $S_0(q,q',E) \leq \hbar$.

Commentary

Remark 26.1 Limit $\hbar \to 0$. The semiclassical limit "$\hbar \to 0$" discussed in sect. 26 is a shorthand notation for the limit in which typical quantities like the actions R or S in semiclassical expressions for the propagator or the Green's function become large compared to $\hbar$. In the world that we live in the quantity $\hbar$ is a fixed physical constant whose value [26.6] is $1.054571596(82)\,10^{-34}$ Js.

Remark 26.2 Madelung's fluid dynamics. A very different interpretation of (26.3–26.4) has been given by Madelung [26.2], and then built upon by Bohm [26.4] and others [26.3, 26.5]. Keeping the $\hbar$ dependent term in (26.3), the ordinary differential equations driving the flow (26.10) have to be altered; if the Hamiltonian can be written as kinetic plus potential term $V(q)$ as in (23.2), the $\hbar^2$ term modifies the p equation of motion as

$$\dot{p_i} = -\frac{\partial}{\partial q_i}\left(V(q) + Q(q,t)\right) , \tag{26.48}$$

where, for the example at hand,

$$Q(q,t) = -\frac{\hbar^2}{2m}\frac{1}{\sqrt{\rho}}\frac{\partial^2}{\partial q^2}\sqrt{\rho} \tag{26.49}$$

interpreted by Bohm [26.4] as the "quantum potential". Madelung observed that Hamilton's equation for the momentum (26.48) can be rewritten as

$$\frac{\partial v_i}{\partial t} + \left(v\cdot\frac{\partial}{\partial q}\right)v_i = -\frac{1}{m}\frac{\partial V}{\partial q_i} - \frac{1}{m\rho}\frac{\partial}{\partial q_j}\sigma_{ij} , \tag{26.50}$$

where $\sigma_{ij} = \frac{\hbar^2\rho}{4m}\frac{\partial^2 \ln\rho}{\partial q_i \partial q_j}$ is the "pressure" stress tensor, $v_i = p_i/m$, and $\rho = A^2$ as defined [26.3] in sect. 26.1.3. We recall that the Eulerian $\frac{\partial}{\partial t} + \frac{\partial q_i}{\partial t}\frac{\partial}{\partial q_i}$ is the ordinary derivative of Lagrangian mechanics, that is $\frac{d}{dt}$. For comparison, the Euler equation for classical hydrodynamics is

$$\frac{\partial v_i}{\partial t} + \left(v\cdot\frac{\partial}{\partial q}\right)v_i = -\frac{1}{m}\frac{\partial V}{\partial q_i} - \frac{1}{m\rho}\frac{\partial}{\partial q_j}(p\delta_{ij}) ,$$

where $p\delta_{ij}$ is the pressure tensor.

The classical dynamics corresponding to quantum evolution is thus that of an "hypothetical fluid" experiencing $\hbar$ and ρ dependent stresses. The "hydrodynamic" interpretation of quantum mechanics has, however, not been very fruitful in practice.

Remark 26.3 Path integrals. The semiclassical propagator (26.29) can also be derived from Feynman's path integral formalism. Dirac was the first to discover that in the short-time limit the quantum propagator (26.33) is exact. Feynman noted in 1946 that one can construct the exact propagator of the quantum Schrödinger equation by formally summing over all possible (and emphatically not classical) paths from q' to q.

Gutzwiller started from the path integral to rederive Van Vleck's semiclassical expression for the propagator; Van Vleck's original derivation is very much in the spirit of what has presented in this chapter. He did, however, not consider the possibility of the formation of caustics or folds of Lagrangian manifolds and thus did not include the topological phases in his semiclassical expression for the propagator. Some 40 years later Gutzwiller [27.16] added the topological indices when deriving the semiclassical propagator from Feynman's path integral by stationary phase conditions.

Résumé

The aim of the semiclassical or short-wavelength methods is to approximate a solution of the Schrödinger equation with a semi-classical wave function

$$\psi_{sc}(q,t) = \sum_j A_j(q,t) e^{iR_j(q,t)/\hbar} ,$$

accurate to the leading order in $\hbar$. Here the sum is over all classical trajectories that connect the initial point q' to the final point q in time t. "Semi–" refers to $\hbar$, the quantum unit of phase in the exponent. The quantum mechanics enters only through this atomic scale, in units of which the variation of the phase across the classical potential is assumed to be large. "–classical" refers to the rest - both the amplitudes $A_j(q,t)$ and the phases $R_j(q,t)$ - which are determined by the classical Hamilton-Jacobi equations.

In the semiclassical approximation the quantum time evolution operator is given by the *semiclassical propagator*

$$K_{sc}(q,q',t) = \frac{1}{(2\pi i\hbar)^{d/2}} \sum_j \left\|\partial p'/\partial q\right\|_j^{1/2} e^{\frac{i}{\hbar}R_j - \frac{i\pi}{2}m_j} ,$$

where the topological index $m_j(q,q',t)$ counts the number of the direction reversal along the jth classical trajectory that connects $q' \to q$ in time t. Until very recently it was not possible to resolve quantum evolution on quantum time scales (such as one revolution of electron around a nucleus) - physical measurements are almost always done at time scales asymptotically large compared to the intrinsic quantum time scale. Formally this information is extracted by means of a Laplace transform of the propagator which yields the energy dependent *semiclassical Green's function*

$$G_{sc}(q,q',E) = G_0(q,q',E) + \frac{1}{i\hbar(2\pi i\hbar)^{\frac{(d-1)}{2}}} \sum_j \left|\frac{1}{\dot{q}\dot{q}'}\right| \left\|\frac{\partial p'_\perp}{\partial q_\perp}\right\|_j^{1/2} e^{\frac{i}{\hbar}S_j - \frac{i\pi}{2}m_j} \quad (26.51)$$

where $G_0(q,q',E)$ is the contribution of short trajectories with $S_0(q,q',E) \leq \hbar$, while the sum is over the contributions of long trajectories (26.45) going from q' to q with fixed energy E, with $S_j(q,q',E) \gg \hbar$.

References

[26.1] A. Einstein, "On the Quantum Theorem of Sommerfeld and Epstein," p. 443, English translation of "Zum Quantensatz von Sommerfeld und Epstein",

Verh. Deutsch. Phys. Ges. **19**, 82 (1917), in *The Collected Papers of Albert Einstein*, Volume **6**: *The Berlin Years: Writings, 1914-1917*, A. Engel, transl. and E. Schucking, (Princeton University Press, Princeton, New Jersey 1997).

[26.2] E. Madelung, *Zeitschr. fr Physik* **40**, 332 (1926).

[26.3] E. Schrödinger, *Annalen der Physik* **79**, 361, 489; **80**, 437, **81**, 109 (1926).

[26.4] D. Bohm, *Phys. Rev.* **85**, 166 (1952).

[26.5] P.R. Holland, *The quantum theory of motion - An account of the de Broglie-Bohm casual interpretation of quantum mechanics* (Cambridge Univ. Press, Cambridge 1993).

[26.6] `physics.nist.gov/cgi-bin/cuu`

Exercises

Exercise 26.1 **Dirac delta function, Lorentzian representation.** *Derive (23.18).*

Exercise 26.2 **Transport equations.** *Write the wave-function in the asymptotic form*

$$\psi(q,t) = e^{\frac{i}{\hbar}R(x,t)+\frac{i}{\hbar}\varepsilon t}\sum_{n\geq 0}(i\hbar)^n A_n(x,t)\,.$$

Derive the transport equations for the A_n by substituting this into the Schrödinger equation and then collecting terms by orders of $\hbar$. Notice that equation for $\dot{A}_n$ only requires knowledge of A_{n-1} and R.

Exercise 26.3 **Easy examples of the Hamilton's principal function.** *Calculate $R(q,q',t)$ for*

a) a d-dimensional free particle

b) a 3-dimensional particle in constant magnetic field

c) a 1-dimensional harmonic oscillator.

Continuation: (26.9).

Exercise 26.4 **Dirac delta function, gaussian representation.** *Consider the gaussian distribution function*

$$\delta_\sigma(z) = \frac{1}{\sqrt{2\pi\sigma^2}}e^{-z^2/2\sigma^2}\,.$$

Show that in $\sigma \to 0$ limit this is the Dirac delta function (26.24).

Exercise 26.5 **d-dimensional free particle propagator.** *Verify the results in sect. 26.2.2; show explicitely that (26.33), the semiclassical Van Vleck propagator in d dimensions, solves the Schrödinger's equation.*

Exercise 26.6 **Charged particle in constant magnetic field.** *Calculate the semiclassical propagator for a charged particle in constant magnetic field in 3 dimensions. Verify that the semiclassical expression coincides with the exact solution.*

Exercise 26.7 **1-dimensional harmonic oscillator propagator.** *Calculate the semiclassical propagator for a 1-dimensional harmonic oscillator and verify that it is identical to the exact quantum propagator.*

Exercise 26.8 d**-dimensional gaussian integrals.** *Show that the gaussian integral in d-dimensions is given by*

$$\frac{1}{(2\pi)^{d/2}}\int d^d x e^{-\frac{1}{2}x^T\cdot M^{-1}\cdot x + x\cdot J} \;=\; |\det M|^{\frac{1}{2}}\, e^{\frac{1}{2}J^T\cdot M\cdot J}\,, \qquad (26.52)$$

where M is a real positive definite $[d\times d]$ matrix, that is a matrix with strictly positive eigenvalues. x, J are d-dimensional vectors, on x^T is the transpose of x.

Exercise 26.9 **Free particle action.** *Calculate the energy dependent action for a free particle, a charged particle in a constant magnetic field and for the harmonic oscillator.*

Exercise 26.10 **Zero length orbits.** *Derive the classical trace (11.1) rigorously and either add the $t\to 0_+$ zero length contribution to the trace formula, or show that it vanishes. Send us a reprint of* Phys. Rev. Lett. *with the correct derivation.*

Exercise 26.11 **A usefull determinant identity.** *Show that the following two determinants equal each other:*
$A[(n+1)\times(n+?)]determinant$

$$\det\left(M'_n\right) \;=\; \overset{\overset{n+1}{\downarrow}}{\begin{bmatrix} x_{1,1} & \dots & x_{1,n} & y_1 \\ \vdots & \ddots & \vdots & \vdots \\ x_{n,1} & \dots & x_{n,n} & y_n \\ z_1 & \dots & z_n & E \end{bmatrix}}\; n+1 \qquad (26.53)$$

and the $[n\times n]$ determinant:

$$E\det\left(M_n\right) = E\; \overset{\overset{n}{\downarrow}}{\begin{bmatrix} x_{1,1}-y_1z_1E^{-1} & \dots & x_{1,n}-y_1z_nE^{-1} \\ \vdots & \ddots & \vdots \\ x_{n,1}-y_nz_1E^{-1} & \dots & x_{n,n}-y_nz_nE^{-1} \end{bmatrix}}\; n \qquad (26.54)$$

Exercise 26.12 **Free particle semiclassical Green's functions.** *Calculate the semiclassical Green's functions for the systems of exercise 26.9.*

Chapter 27

Semiclassical quantization

> If there exist fewer than ℓ integrals of type (14), as is the case, for example, according to POINCARÉ in the three-body problem, then the p_i are not expressible by the q_i and the quantum condition of SOMMERFELD-EPSTEIN fails also in the slightly generalized form that has been given here.
> A. Einstein, *Zum Quantensatz von Sommerfeld und Epstein* (1917)

(G. Vattay, G. Tanner and P. Cvitanović)

We derive here the Gutzwiller trace formula and the semiclassical zeta function, the central results of the semiclassical quantization of classically chaotic systems. In chapter 28 we will rederive these formulas for the case of scattering in open systems. Quintessential wave mechanics effects such as creeping, diffraction and tunneling will be taken up in chapter 30.

27.1 Trace formula

Our next task is to evaluate the Green's function trace (23.16) in the semiclassical approximation. The trace

$$\operatorname{tr} G_{sc}(E) = \int d^d q\, G_{sc}(q,q,E) = \operatorname{tr} G_0(E) + \sum_j \int d^d q\, G_j(q,q,E)$$

receives contributions from "long" classical trajectories labelled by j which start and end in q after finite time, and the "zero length" trajectories whose lengths approach zero as $q' \to q$.

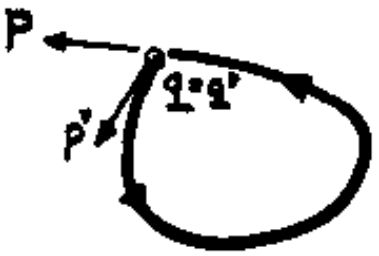

Figure 27.1: A returning trajectory in the configuration space. The orbit is periodic in the full phase space only if the initial and the final momenta of a returning trajectory coincide as well.

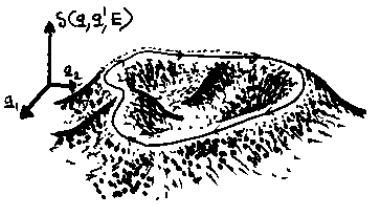

Figure 27.2: A romanticized sketch of $S_p(E) = S(q,q,E) = \oint p(q,E)dq$ landscape orbit. Unstable periodic orbits traverse isolated ridges and saddles of the mountainous landscape of the action $S(q_\parallel, q_\perp, E)$. Along a periodic orbit $S_p(E)$ is constant; in the transverse directions it generically changes quadratically.

First we work out the contributions coming from the finite time *returning* classical orbits, that is trajectories that originate and end at a given configuration point q. As we are identifying q with q', taking of a trace involves (still another!) stationary phase condition in the $q' \to q$ limit,

$$\left.\frac{\partial S_j(q,q',E)}{\partial q_i}\right|_{q'=q} + \left.\frac{\partial S_j(q,q',E)}{\partial q'_i}\right|_{q'=q} = 0\,,$$

meaning that the initial and final momenta (26.39) of contributing trajectories should coincide

$$p_i(q,q,E) - p'_i(q,q,E) = 0\,, \qquad q \in j\text{th periodic orbit}\,, \tag{27.1}$$

so the trace receives contributions only from those long classical trajectories which are *periodic* in the full phase space.

For a periodic orbit the natural coordinate system is the intrinsic one, with $q_\parallel$ axis pointing in the $\dot{q}$ direction along the orbit, and $q_\perp$, the rest of the coordinates transverse to $\dot{q}$. The jth periodic orbit contribution to the trace of the semiclassical Green's function in the intrinsic coordinates is

$$\mathrm{tr}\, G_j(E) = \frac{1}{i\hbar(2\pi\hbar)^{(d-1)/2}} \oint_j \frac{dq_\parallel}{\dot{q}} \int_j d^{d-1}q_\perp |\det D_\perp^j|^{1/2} e^{\frac{i}{\hbar}S_j - \frac{i\pi}{2}m_j}\,,$$

where the integration in $q_\parallel$ goes from 0 to L_j, the geometric length of small tube around the orbit in the configuration space. As always, in the stationary phase approximation we worry only about the fast variations in

the phase $S_j(q_\parallel, q_\perp, E)$, and assume that the density varies smoothly and is well approximated by its value $D^j_\perp(q_\parallel, 0, E)$ on the classical trajectory, $q_\perp = 0$. The topological index $m_j(q_\parallel, q_\perp, E)$ is an integer which does not depend on the initial point $q_\parallel$ and not change in the infinitesimal neighborhood of an isolated periodic orbit, so we set $m_j(E) = m_j(q_\parallel, q_\perp, E)$.

The transverse integration is again carried out by the stationary phase method, with the phase stationary on the periodic orbit, $q_\perp = 0$. The result of the transverse integration can depend only on the parallel coordinate

$$\mathrm{tr}\, G_j(E) = \frac{1}{i\hbar} \oint \frac{dq_\parallel}{\dot{q}} \left| \frac{\det D_{\perp j}(q_\parallel, 0, E)}{\det D'_{\perp j}(q_\parallel, 0, E)} \right|^{1/2} e^{\frac{i}{\hbar} S_j - \frac{i\pi}{2} m_j},$$

where the new determinant in the denominator, $\det D'_{\perp j} =$

$$\det \left(\frac{\partial^2 S(q, q', E)}{\partial q_{\perp i} \partial q_{\perp j}} + \frac{\partial^2 S(q, q', E)}{\partial q'_{\perp i} \partial q_{\perp j}} + \frac{\partial^2 S(q, q', E)}{\partial q_{\perp i} \partial q'_{\perp j}} + \frac{\partial^2 S(q, q', E)}{\partial q'_{\perp i} \partial q'_{\perp j}} \right),$$

is the determinant of the second derivative matrix coming from the stationary phase integral in transverse directions. Mercifully, this integral also removes most of the $2\pi\hbar$ prefactors in (??).

The ratio $\det D_{\perp j} / \det D'_{\perp j}$ is here to enforce the periodic boundary condition for the semiclassical Green's function evaluated on a periodic orbit. It can be given a meaning in terms of the monodromy matrix of the periodic orbit by following observations

$$\begin{aligned} \det D_\perp &= \left\| \frac{\partial p'_\perp}{\partial q_\perp} \right\| = \left\| \frac{\partial (q'_\perp, p'_\perp)}{\partial (q_\perp, q'_\perp)} \right\| \\ \det D'_\perp &= \left\| \frac{\partial p_\perp}{\partial q_\perp} - \frac{\partial p'_\perp}{\partial q_\perp} + \frac{\partial p_\perp}{\partial q'_\perp} - \frac{\partial p'_\perp}{\partial q'_\perp} \right\| = \left\| \frac{\partial (p_\perp - p'_\perp, q_\perp - q'_\perp),}{\partial (q_\perp, q'_\perp)} \right\| . \end{aligned}$$

Defining the $2(d-1)$-dimensional transverse vector $x_\perp = (q_\perp, p_\perp)$ in the full phase space we can express the ratio

$$\begin{aligned} \frac{\det D'_\perp}{\det D_\perp} &= \left\| \frac{\partial (p_\perp - p'_\perp, q_\perp - q'_\perp)}{\partial (q'_\perp, p'_\perp)} \right\| = \left\| \frac{\partial (x_\perp - x'_\perp)}{\partial x'_\perp} \right\| \\ &= \det \left(\mathbf{J} - \mathbf{1} \right) , \end{aligned} \tag{27.2}$$

in terms of the monodromy matrix $\mathbf{J}$ for a surface of section transverse to the orbit within the constant energy $E = H(q, p)$ shell.

The classical periodic orbit action $S_j(E) = \oint p(q_{||}, E)dq_{||}$ is an integral around a loop defined by the periodic orbit, and does not depend on the starting point $q_{||}$ along the orbit, see fig. 27.2. The eigenvalues of the monodromy matrix are also independent of where $\mathbf{J}_j$ is evaluated along the orbit, so $\det(1 - \mathbf{J}_j)$ can also be taken out of the the $q_{||}$ integral

$$\mathrm{tr}\, G_j(E) = \frac{1}{i\hbar} \sum_j \frac{1}{|\det(1 - \mathbf{J}_j)|^{1/2}} e^{r(\frac{i}{\hbar}S_j - \frac{i\pi}{2}m_j)} \oint \frac{dq_{||}}{\dot{q}_{||}} .$$

Here we have assumed that $\mathbf{J}_j$ has no marginal eigenvalues. The determinant of the monodromy matrix, the action $S_p(E) = \oint p(q_{||}, E)dq_{||}$ and the topological index are all classical invariants of the periodic orbit. The integral in the parallel direction we now do exactly.

First we take into account the fact that any repeat of a periodic orbit is also a periodic orbit. The action and the topological index are additive along the trajectory, so for rth repeat they simply get multiplied by r. The monodromy matrix of the rth repeat of a prime cycle p is (by the chain rule for derivatives) $\mathbf{J}_p^r$, where $\mathbf{J}_p$ is the prime cycle monodromy matrix. Let us denote the time period of the prime cycle p, the single, shortest traversal of a periodic orbit by T_p. The remaining integral can be carried out by change of variables $dt = dq_{||}/\dot{q}(t)$

$$\int_0^{L_p} \frac{dq_{||}}{\dot{q}(t)} = \int_0^{T_p} dt = T_p .$$

Note that the spatial integral corresponds to a *single* traversal. If you do not see why this is so, rethink the derivation of the classical trace formula (11.19) - that derivation takes only three pages of text. Regrettably, in the quantum case we do not know of an honest derivation that takes less than 30 pages. The final result, the *Gutzwiller trace formula*

$$\mathrm{tr}\, G_{sc}(E) = \mathrm{tr}\, G_0(E) + \frac{1}{i\hbar} \sum_p T_p \sum_{r=1}^{\infty} \frac{1}{|\det(1 - \mathbf{J}_p^r)|^{1/2}} e^{r(\frac{i}{\hbar}S_p - \frac{i\pi}{2}m_p)} , \quad (27.3)$$

an expression for the trace of the semiclassical Green's function in terms of periodic orbits, is beautiful in its simplicity and elegance.

The topological index $m_p(E)$ counts the number of changes of sign of the matrix of second derivatives evaluated along the prime periodic orbit p. By now we have gone through so many stationary phase approximations that you have surely lost track of what the total $m_p(E)$ actually is. The

rule is this: The topological index of a closed curve in a 2-d phase space is the sum of the number of times the partial derivatives $\frac{\partial p_i}{\partial q_i}$ for each dual pair (q_i, p_i), $i = 1, 2, \ldots, d$ (no sum on i) change their signs as one goes once around the curve.

27.1.1 Average density of states

We still have to evaluate $\mathrm{tr}\, G_0(E)$, the contribution coming from the infinitesimal trajectories. The real part of $\mathrm{tr}\, G_0(E)$ is infinite in the $q' \to q$ limit, so it makes no sense to write it down explicitly here. However, the imaginary part is finite, and plays an important role in the density of states formula, which we derive next.

The semiclassical contribution to the density of states (23.16) is given by the imaginary part of the Gutzwiller trace formula (27.3) multiplied with $-1/\pi$. The contribution coming from the zero length trajectories is the imaginary part of (26.47) for $q' \to q$ integrated over the configuration space

$$d_0(E) = -\frac{1}{\pi} \int d^d q \, \mathrm{Im}\, G_0(q, q, E),$$

The resulting formula has a pretty interpretation; it estimates the number of quantum states that can be accomodated up to the energy E by counting the available quantum cells in the phase space. This number is given by the *Weyl rule* , as the ratio of the phase space volume bounded by energy E divided by h^d, the volume of a quantum cell,

$$N_{sc}(E) = \frac{1}{h^d} \int d^d p d^d q \, \Theta(E - H(q,p)) \,. \tag{27.4}$$

where $\Theta(x)$ is the Heaviside function (23.21). $N_{sc}(E)$ is an estimate of the spectral staircase (23.20), so its derivative yields the average density of states

$$d_0(E) = \frac{d}{dE} N_{sc}(E) = \frac{1}{h^d} \int d^d p d^d q \, \delta(E - H(q,p)) \,, \tag{27.5}$$

precisely the semiclassical result (27.6). For Hamiltonians of type $p^2/2m + V(q)$, the energy shell volume in (27.5) is a sphere of radius $\sqrt{2m(E - V(q))}$. The surface of a d-dimensional sphere of radius r is $\pi^{d/2} r^{d-1}/\Gamma(d/2)$, so the

27.3
page 522

average density of states is given by

$$d_0(E) = \frac{2m}{\hbar^d 2^d \pi^{d/2} \Gamma(d/2)} \int_{V(q)<E} d^d q \, [2m(E - V(q))]^{d/2-1} \,, \qquad (27.6)$$

and

$$N_{sc}(E) = \frac{1}{h^d} \frac{\pi^{d/2}}{\Gamma(1 + d/2)} \int_{V(q)<E} d^d q \, [2m(E - V(q))]^{d/2} \,. \qquad (27.7)$$

Physically this means that at a fixed energy the phase space can support $N_{sc}(E)$ distinct eigenfunctions; anything finer than the quantum cell h^d cannot be resolved, so the quantum phase space is effectively finite dimensional. The average density of states is of a particularly simple form in one spatial dimension

27.4
page 522

$$d_0(E) = \frac{T(E)}{2\pi\hbar} \,, \qquad (27.8)$$

where $T(E)$ is the period of the periodic orbit of fixed energy E. In two spatial dimensions the average density of states is

$$d_0(E) = \frac{m\mathcal{A}(E)}{2\pi\hbar^2} \,, \qquad (27.9)$$

where $\mathcal{A}(E)$ is the classically allowed area of configuration space for which $V(q) < E$.

27.5
page 522

The semiclassical density of states is a sum of the average density of states and the oscillation of the density of states around the average, $d_{sc}(E) = d_0(E) + d_{osc}(E)$, where

$$d_{osc}(E) = \frac{1}{\pi\hbar} \sum_p T_p \sum_{r=1}^{\infty} \frac{\cos(rS_p(E)/\hbar - rm_p\pi/2)}{|\det(1 - \mathbf{J}_p^r)|^{1/2}} \qquad (27.10)$$

follows from the trace formula (27.3).

27.1.2 Regularization of the trace

The real part of the $q' \to q$ zero length Green's function (26.47) is ultraviolet divergent in dimensions $d > 1$, and so is its formal trace (23.16). The short

distance behavior of the real part of the Green's function can be extracted from the real part of (26.47) by using the Bessel function expansion for small z

$$Y_\nu(z) \approx \begin{cases} -\frac{1}{\pi}\Gamma(\nu)\left(\frac{z}{2}\right)^{-\nu} & \text{for } \nu \neq 0 \\ \frac{2}{\pi}(\ln(z/2)+\gamma) & \text{for } \nu = 0 \end{cases} ,$$

where $\gamma = 0.577...$ is the Euler constant. The real part of the Green's function for short distance is dominated by the singular part

$$G_{sing}(|q-q'|,E) = \begin{cases} -\frac{m}{2\hbar^2\pi^{\frac{d}{2}}}\Gamma((d-2)/2)\frac{1}{|q-q'|^{d-2}} & \text{for } d \neq 2 \\ \frac{m}{2\pi\hbar^2}(\ln(2m(E-V)|q-q'|/2\hbar)+\gamma) & \text{for } d = 2 \end{cases} .$$

The *regularized* Green's function

$$G_{reg}(q,q',E) = G(q,q',E) - G_{sing}(|q-q'|,E)$$

is obtained by subtracting the $q' \to q$ ultraviolet divergence. For the regularized Green's function the Gutzwiller trace formula is

$$\mathrm{tr}\, G_{reg}(E) = -i\pi d_0(E) + \frac{1}{i\hbar}\sum_p T_p \sum_{r=1}^{\infty} \frac{e^{r(\frac{i}{\hbar}S_p(E) - \frac{i\pi}{2}m_p(E))}}{|\det(1-\mathbf{J}_p^r)|^{1/2}} . \qquad (27.11)$$

Now you stand where Gutzwiller stood in 1990. You hold the trace formula in your hands. You have no clue how good is the $\hbar \to 0$ approximation, how to take care of the sum over an infinity of periodic orbits, and whether the formula converges at all.

27.2 Semiclassical spectral determinant

The problem with trace formulas is that they diverge where we need them, at the individual energy eigenvalues. What to do? Much of the quantum chaology literature responds to the challenge of wrestling the trace formulas by replacing the delta functions in the density of states (23.17) by gaussians. But there is no need to do this - we can compute the eigenenergies without any further ado by remembering that the smart way to determine the eigenvalues of linear operators is by determining zeros of their spectral determinants.

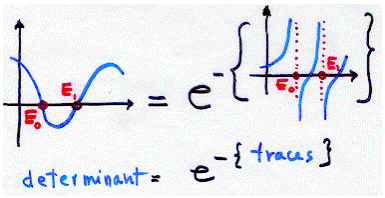

Figure 27.3: A sketch of how spectral determinants convert poles into zeros: The trace shows $1/(E-E_n)$ type singularities at the eigenenergies while the spectral determinant goes smoothly through zeroes.

A sensible way to compute energy levels is to construct the spectral determinant whose zeroes yield the eigenenergies, $\det(\hat{H}-E)_{sc}=0$. A first guess might be that the spectral determinant is the Hadamard product of form

$$\det(\hat{H}-E)=\prod_n (E-E_n),$$

but this product is not well defined, since for fixed E we multiply larger and larger numbers $(E-E_n)$. This problem is dealt with by *regularization*, discussed below in appendix 27.1.2. Here we offer an impressionistic sketch of regularization.

The logarithmic derivative of $\det(\hat{H}-E)$ is the (formal) trace of the Green's function

$$-\frac{d}{dE}\ln\det(\hat{H}-E)=\sum_n \frac{1}{E-E_n}=\mathrm{tr}\, G(E).$$

This quantity, not surprisingly, is divergent again. The relation, however, opens a way to derive a convergent version of $\det(\hat{H}-E)_{sc}$, by replacing the trace with the regularized trace

$$-\frac{d}{dE}\ln\det(\hat{H}-E)_{sc}=\mathrm{tr}\, G_{reg}(E).$$

The regularized trace still has $1/(E-E_n)$ poles at the semiclassical eigenenergies, poles which can be generated only if $\det(\hat{H}-E)_{sc}$ has a zero at $E=E_n$, see fig. 27.3. By integrating and exponentiating we obtain

$$\det(\hat{H}-E)_{sc}=\exp\left(-\int^E dE'\,\mathrm{tr}\, G_{reg}(E')\right)$$

Now we can use (27.11) and integrate the terms coming from periodic orbits, using the relation (26.16) between the action and the period of a periodic orbit, $dS_p(E)=T_p(E)dE$, and the relation (23.20) between the density

of states and the spectral staircase, $dN_{sc}(E) = d_0(E)dE$. We obtain the *semiclassical zeta function*

$$\det\left(\hat{H}-E\right)_{sc} = e^{i\pi N_{sc}(E)} \exp\left(-\sum_p \sum_{r=1}^{\infty} \frac{1}{r} \frac{e^{ir(S_p/\hbar - m_p\pi/2)}}{|\det\left(1-\mathbf{J}_p^r\right)|^{1/2}}\right) . \quad (27.12)$$

☞ chapter 15

We already know from the study of classical evolution operator spectra of chapter 12 that this can be evaluated by means of cycle expansions. The beauty of this formula is that everything on the right side – the cycle action S_p, the topological index m_p and monodromy matrix $\mathbf{J}_p$ determinant – is intrinsic, coordinate-choice independent property of the cycle p.

27.3 One-dimensional systems

It has been a long trek, a stationary phase upon stationary phase. Let us check whether the result makes sense even in the simplest case, for quantum mechanics in one spatial dimension.

In one dimension the average density of states follows from the one-dimensional form of the oscillating density (27.10) and of the average density (27.8)

$$d(E) = \frac{T_p(E)}{2\pi\hbar} + \sum_r \frac{T_p(E)}{\pi\hbar} \cos(rS_p(E)/\hbar - rm_p(E)\pi/2). \quad (27.13)$$

The classical particle oscillates in a single potential well with period $T_p(E)$. There is no monodromy matrix to evaluate, as in one dimension there is only the parallel coordinate, and no transverse directions. The r repetition sum in (27.13) can be rewritten by using the Fourier series expansion of a delta spike train

$$\sum_{n=-\infty}^{\infty} \delta(x-n) = \sum_{k=-\infty}^{\infty} e^{i2\pi kx} = 1 + \sum_{k=1}^{\infty} 2\cos(2\pi kx).$$

We obtain

$$d(E) = \frac{T_p(E)}{2\pi\hbar} \sum_n \delta(S_p(E)/2\pi\hbar - m_p(E)/4 - n). \quad (27.14)$$

This expression can be simplified by using the relation (26.16) between T_p and S_p, and the identity (7.7) $\delta(x-x^*) = |f'(x)|\delta(f(x))$, where x^* is the

only zero of the function $f(x^*) = 0$ in the interval under consideration. We obtain

$$d(E) = \sum_n \delta(E - E_n),$$

where the energies E_n are the zeroes of the arguments of delta functions in (27.14)

$$S_p(E_n)/2\pi\hbar = n - m_p(E)/4\,,$$

where $m_p(E) = m_p = 2$ for smoth potential at both turning points, and $m_p(E) = m_p = 4$ for two billiard (infinite potential) walls. These are precisely the *Bohr-Sommerfeld quantized energies* E_n, defined by the condition

$$\oint p(q, E_n)dq = h\left(n - \frac{m_p}{4}\right). \tag{27.15}$$

In this way the trace formula recovers the well known 1-dimensional quantization rule. In one dimension, the average of states can be expressed from the quantization condition. At $E = E_n$ the exact number of states is n, while the average number of states is $n - 1/2$ since the staircase function $N(E)$ has a unit jump in this point

$$N_{sc}(E) = n - 1/2 = S_p(E)/2\pi\hbar - m_p(E)/4 - 1/2. \tag{27.16}$$

The 1-dimensional spectral determinant follows from (27.12) by dropping the monodromy matrix part and using (27.16)

$$\det\left(\hat{H} - E\right)_{sc} = e^{-\frac{i}{2\hbar}S_p + \frac{i\pi}{2}m_p} e^{-\sum_r \frac{1}{r} e^{\frac{i}{\hbar}rS_p - \frac{i\pi}{2}rm_p}}\,. \tag{27.17}$$

Summation yields a logarithm by $\sum_r t^r/r = -\ln(1-t)$ and we get

$$\begin{aligned}\det\left(\hat{H} - E\right)_{sc} &= e^{-\frac{i}{2\hbar}S_p + \frac{im_p}{4} + \frac{i\pi}{2}}\left(1 - e^{\frac{i}{\hbar}S_p - i\frac{m_p}{2}}\right) \\ &= 2\sin\left(S_p(E)/\hbar - m_p(E)/4\right)\,.\end{aligned}$$

So in one dimension, where there is only one periodic orbit for a given energy E, nothing is gained by going from the trace formula to the spectral determinant. The spectral determinant is a real function for real energies, and its zeros are again the Bohr-Sommerfeld quantized eigenenergies (27.15).

27.4 Two-dimensional systems

For flows in two configuration dimensions the monodromy matrix $\mathbf{J}_p$ has two eigenvalues Λ_p and $1/\Lambda_p$, as explained in sect. 5.1.1. Isolated periodic orbits can be elliptic or hyperbolic. Here we discuss only the hyperbolic case, when the eigenvalues are real and their absolute value is not equal to one. The determinant appearing in the trace formulas can be written in terms of the expanding eigenvalue as

$$|\det\left(1-\mathbf{J}_p^r\right)|^{1/2} = |\Lambda_p^r|^{1/2}\left(1-1/\Lambda_p^r\right)\ ,$$

and its inverse can be expanded as a geometric series

$$\frac{1}{|\det\left(1-\mathbf{J}_p^r\right)|^{1/2}} = \sum_{k=0}^{\infty}\frac{1}{|\Lambda_p^r|^{1/2}\Lambda_p^{kr}}.$$

With the 2-dimensional expression for the average density of states (27.9) the spectral determinant becomes

$$\begin{aligned}\det\left(\hat{H}-E\right)_{sc} &= e^{i\frac{m\mathcal{A}E}{2\hbar^2}}\exp\left(-\sum_p\sum_{r=1}^{\infty}\sum_{k=0}^{\infty}\frac{e^{ir(S_p/\hbar-m_p\pi/2)}}{r|\Lambda_p^r|^{1/2}\Lambda_p^{kr}}\right)\\ &= e^{i\frac{m\mathcal{A}E}{2\hbar^2}}\prod_p\prod_{k=0}^{\infty}\left(1-\frac{e^{\frac{i}{\hbar}S_p-\frac{i\pi}{2}m_p}}{|\Lambda_p|^{1/2}\Lambda_p^k}\right)\ . \qquad (27.18)\end{aligned}$$

Commentary

Remark 27.1 Zeta functions. For "zeta function" nomenclature, see remark 12.4 on page 229.

Résumé

Spectral determinants and dynamical zeta functions arise both in classical and quantum mechanics because in both the dynamical evolution can be described by the action of linear evolution operators on infinite-dimensional vector spaces. In quantum mechanics the periodic orbit theory arose from studies of semi-conductors, and the unstable periodic orbits have been measured in experiments on the very paradigm of Bohr's atom, the hydrogen atom, this time in strong external fields.

In practice, most "quantum chaos" calculations take the stationary phase approximation to quantum mechanics (the Gutzwiller trace formula, possibly improved by including tunneling periodic trajectories, diffraction corrections, *etc.*) as the point of departure. Once the stationary phase approximation is made, what follows is *classical* in the sense that all quantities used in periodic orbit calculations - actions, stabilities, geometrical phases - are classical quantities. The problem is then to understand and control the convergence of classical periodic orbit formulas.

While various periodic orbit formulas are formally equivalent, practice shows that some are preferable to others. Three classes of periodic orbit formulas are frequently used:

Trace formulas. The trace of the semiclassical Green's function

$$\mathrm{tr}\, G_{sc}(E) = \int d^d q\, G_{sc}(q,q,E)$$

is given by a sum over the periodic orbits (27.11). While easiest to derive, in calculations the trace formulas are inconvenient for anything other than the leading eigenvalue estimates, as they tend to be divergent in the region of physical interest. In classical dynamics trace formulas hide under a variety of appelations such as the $f-\alpha$ or multifractal formalism; in quantum mechanics they are known as the Gutzwiller trace formulas.

Zeros of *Ruelle or dynamical zeta functions*

$$1/\zeta(s) = \prod_p (1-t_p), \quad t_p = \frac{1}{\sqrt{\Lambda_p}} e^{\frac{i}{\hbar}S_p - i\pi m_p/2}$$

yield, in combination with cycle expansions, the semiclassical estimates of *quantum* resonances. For hyperbolic systems the dynamical zeta functions have good convergence and are a useful tool for determination of classical and quantum mechanical averages.

Spectral determinants, Selberg-type zeta functions, Fredholm determinants, functional determinants are the natural objects for spectral calculations, with convergence better than for dynamical zeta functions, but with less transparent cycle expansions. The 2-dimensional semiclassical spectral determinant (27.18)

$$\det\left(\hat{H}-E\right)_{sc} = \prod_p e^{i\pi N_{sc}(E)} \prod_{k=0}^{\infty} \left(1 - \frac{e^{iS_p/\hbar - i\pi m_p/2}}{|\Lambda_p|^{1/2}\Lambda_p^k}\right)$$

is a typical example. Most periodic orbit calculations are based on cycle expansions of such determinants.

As we have assumed repeatedly during the derivation of the trace formula that the periodic orbits are isolated, and do not form families (as is the case for integrable systems or in KAM tori of systems with mixed phase space), the formulas discussed so far are valid only for hyperbolic and elliptic periodic orbits.

For deterministic dynamical flows and number theory, spectral determinants and zeta functions are exact. The quantum-mechanical ones, derived by the Gutzwiller approach, are at best only the stationary phase approximations to the exact quantum spectral determinants, and for quantum mechanics an important conceptual problem arises already at the level of derivation of the semiclassical formulas; how accurate are they, and can the periodic orbit theory be systematically improved?

References

[27.1] M. Jammer, *The Conceptual Development of Quantum mechanics* (McGraw-Hill, New York 1966).

[27.2] J. Mehra and H. Rechtenberg, *The Historical Development of the Quantum Theory* (Springer, New York 1982).

[27.3] J.W.S. Rayleigh, *The Theory of Sound* (Macmillan, London 1896; reprinted by Dover, New York 1945).

[27.4] J.B. Keller, *Ann. Phys. (N.Y.)* **4**, 180 (1958).

[27.5] J.B. Keller and S.I. Rubinow, *Ann. Phys. (N.Y.)* **9**, 24 (1960).

[27.6] J.B. Keller, "A geometrical theory of diffraction", in *Calculus of variations and its applications*, *Proc. of Symposia in appl. math.* **8**, (McGraw-Hill, New York, 1958).

[27.7] J.B. Keller, *Calculus of Variations* **27**, (1958).

[27.8] V.P. Maslov, *Théorie des Perturbations et Métodes Asymptotiques* (Dunod, Paris, 1972).

[27.9] V.P. Maslov and M.V. Fedoriuk, *Semi-Classical Approximation in Quantum Mechanics* (Reidel, Boston 1981).

[27.10] V.I. Arnold, *Functional Anal. Appl.* **1**, 1 (1967).

[27.11] J.E. Marsden and T.S. Ratiu, *Introduction to Mechanics and Symmetry* (Springer, New York, 1994).

[27.12] N. Bleistein and R.A. Handelsman, *Asymptotic Expansions of Integrals* (Dover, New York 1986).

[27.13] R.G. Littlejohn, J. Stat. Phys. **68**, 7 (1992).

[27.14] L.D. Landau and E.M. Lifshitz, *Mechanics* (Pergamon, London, 1959).

[27.15] R.G. Littlejohn, *"Semiclassical structure of trace formulas"*, in G. Casati and B. Chirikov, eds., *Quantum Chaos*, (Cambridge University Press, Cambridge 1994).

[27.16] M.C. Gutzwiller, *J. Math. Phys.* **8**, 1979 (1967); **10**, 1004 (1969); **11**, 1791 (1970); **12**, 343 (1971).

[27.17] M.C. Gutzwiller, *J. Math. Phys.* **12**, 343 (1971)

[27.18] M.C. Gutzwiller, *Physica* **D5**, 183 (1982)

[27.19] M.C. Gutzwiller, *J. Phys. Chem.* **92**, 3154 (1984).

[27.20] A. Voros, *J. Phys.* **A 21**, 685 (1988).

[27.21] A. Voros, *Aspects of semiclassical theory in the presence of classical chaos*, *Prog. Theor. Phys. Suppl.* **116**, 17 (1994).

[27.22] P. Cvitanović and P.E. Rosenqvist, in G.F. Dell'Antonio, S. Fantoni and V.R. Manfredi, eds., *From Classical to Quantum Chaos, Soc. Italiana di Fisica Conf. Proceed.* **41**, pp. 57-64 (Ed. Compositori, Bologna 1993).

[27.23] A. Wirzba, *CHAOS* **2**, 77 (1992).

[27.24] P. Cvitanović, G. Vattay and A. Wirzba, *"Quantum fluids and classical determinants"*, in H. Friedrich and B. Eckhardt., eds., *Classical, Semiclassical and Quantum Dynamics in Atoms – in Memory of Dieter Wintgen*, *Lecture Notes in Physics* **485** (Springer, New York 1997), `chao-dyn/9608012`.

[27.25] E.B. Bogomolny, CHAOS **2**, 5 (1992).

[27.26] E.B. Bogomolny, *Nonlinearity* **5**, 805 (1992).

[27.27] E.A. Spiegel

[27.28] M. Kline, *Mathematical Thought from Ancient to Modern Times* (Oxford Univ. Press, Oxford 1972); on Monge and theory of characteristics - chapter 22.7.

[27.29] E.T. Bell, *Men of Mathematics* (Penguin, London 1937).

[27.30] R.P. Feynman, *Statistical Physics* (Addison Wesley, New York 1990).

[27.31] Goldstein, *Mechanics*, chapter 9.

[27.32] G. Tanner and D. Wintgen, *CHAOS* **2**, 53 (1992).

[27.33] P. Cvitanović and F. Christiansen, *CHAOS* **2**, 61 (1992).

[27.34] M.V. Berry and J.P. Keating, *J. Phys.* **A 23**, 4839 (1990).

[27.35] H.H. Rugh, *"Generalized Fredholm determinants and Selberg zeta functions for Axiom A dynamical systems"*, *Ergodic Theory Dynamical Systems* **16**, 805 (1996).

[27.36] B. Eckhard and G. Russberg, Phys. Rev. **E 47**, 1578 (1993).

[27.37] D. Ruelle, *Statistical Mechanics, Thermodynamical Formalism* (Addison-Wesley, Reading MA, 1987).

[27.38] P. Szépfalusy, T. Tél, A. Csordás and Z. Kovács, Phys. Rev. **A 36**, 3525 (1987).

[27.39] H.H. Rugh, Nonlinearity **5**, 1237 (1992) and H.H. Rugh, *Ph.D. Thesis* (Niels Bohr Institute, 1993).

[27.40] P. Cvitanović, P.E. Rosenqvist, H.H. Rugh and G. Vattay, *Scattering Theory - special issue*, CHAOS (1993).

[27.41] E.J. Heller, S. Tomsovic and A. Sepúlveda CHAOS **2**, *Periodic Orbit Theory - special issue*, 105, (1992).

[27.42] V.I. Arnold, *Geometrical Methods in the Theory of Ordinary Differential Equations*, (Springer, New York 1983).

[27.43] R. Dashen, B. Hasslacher and A. Neveu , "Nonperturbative methods and extended hadron models in field theory. 1. Semiclassical functional methods.", *Phys. Rev.* **D10**, 4114 (1974).

[27.44] V.I. Arnold, *Geometrical Methods in the Theory of Ordinary Differential Equations* (Springer, New York 1983).

Exercises

Exercise 27.1 **Monodromy matrix from second variations of the action.** *Show that*

$$D_{\perp j}/D'_{\perp j} = (\mathbf{1} - \mathbf{J}) \tag{27.19}$$

Exercise 27.2 **Jacobi gymnastics.** *Prove that the ratio of determinants in (O.27) can be expressed as*

$$\frac{\det D'_{\perp j}(q_\parallel, 0, E)}{\det D_{\perp j}(q_\parallel, 0, E)} = \det \begin{pmatrix} I - \mathbf{J}_{qq} & -\mathbf{J}_{qp} \\ -\mathbf{J}_{pq} & I - \mathbf{J}_{pp} \end{pmatrix} = \det (1 - \mathbf{J}_j) \,, \tag{27.20}$$

where $\mathbf{J}_j$ is the monodromy matrix of the periodic orbit.

Exercise 27.3 **Volume of d-dimensional sphere.** *Show that the volume of a d-dimensional sphere of radius r equals $\pi^{d/2} r^d / \Gamma(1 + d/2)$. Show that $\Gamma(1 + d/2) = \Gamma(d/2) d/2$.*

Exercise 27.4 **Average density of states in 1 dimension.** *Show that in one dimension the average density of states is given by (27.8)*

$$\bar{d}(E) = \frac{T(E)}{2\pi\hbar},$$

where $T(E)$ is the time period of the 1-dimensional motion and show that

$$\bar{N}(E) = \frac{S(E)}{2\pi\hbar} \,, \tag{27.21}$$

where $S(E) = \oint p(q, E)\, dq$ is the action of the orbit.

Exercise 27.5 **Average density of states in 2 dimensions.** *Show that in 2 dimensions the average density of states is given by (27.9)*

$$\bar{d}(E) = \frac{m\mathcal{A}(E)}{2\pi\hbar^2} \,,$$

where $\mathcal{A}(E)$ is the classically allowed area of configuration space for which $U(q) < E$.

Chapter 28

Quantum scattering

(A. Wirzba, P. Cvitanović and N. Whelan)

So far the trace formulas have been derived assuming that the system under consideration is bound. As we shall now see, we are in luck - the semiclassics of bound systems is all we need to understand the semiclassics for open, scattering systems as well. We start by a brief review of the quantum theory of elastic scattering of a point particle from a (repulsive) potential, and then develop the connection to the standard Gutzwiller theory for bound systems. We do this in two steps - first, a heuristic derivation which helps us understand in what sense density of states is "density", and then we sketch a general derivation of the central result of the spectral theory of quantum scattering, the Krein-Friedel-Lloyd formula. The end result is that we establish a connection between the scattering resonances (both positions and widths) of an open quantum system and the poles of the trace of the Green function, which we learned to analyze in earlier chapters.

28.1 Density of states

For a scattering problem the density of states (23.17) appear ill defined since formulas such as (27.6) involve integration over infinite spatial extent. What we will now show is that a quantity that makes sense physically is the difference of two densities - the first with the scatterer present and the second with the scatterer absent.

In nonrelativistic dynamics the relative motion can be separated from the center-of-mass motion. Therefore the elastic scattering of two particles can be treated as the scattering of one particle from a static potential $V(q)$. We will study the scattering of a point-particle of (reduced) mass m by

a short-range potential $V(q)$, excluding *inter alia* the Coulomb potential. (The Coulomb potential decays slowly as a function of q so that various asymptotic approximations which apply to general potentials fail for it.) Although we can choose the spatial coordinate frame freely, it is advisable to place its origin somewhere near the geometrical center of the potential. The scattering problem is solved, if a scattering solution to the time-independent Schrödinger equation (23.5)

$$\left(-\frac{\hbar^2}{2m}\frac{\partial^2}{\partial q^2} + V(q)\right)\phi_{\vec{k}}(q) = E\phi_{\vec{k}}(q) \tag{28.1}$$

can be constructed. Here E is the energy, $\vec{p} = \hbar\vec{k}$ the initial momentum of the particle, and $\vec{k}$ the corresponding wave vector.

When the argument $r = |q|$ of the wave function is large compared to the typical size a of the scattering region, the Schrödinger equation effectively becomes a free particle equation because of the short-range nature of the potential. In the asymptotic domain $r \gg a$, the solution $\phi_{\vec{k}}(q)$ of (28.1) can be written as superposition of ingoing and outgoing solutions of the free particle Schrödinger equation for fixed angular momentum:

$$\phi(q) = A\phi^{(-)}(q) + B\phi^{(+)}(q)\,, \qquad (+ \text{ boundary conditions})\,,$$

where in 1-dimensional problems $\phi^{(-)}(q)$, $\phi^{(+)}(q)$ are the "left", "right" moving plane waves, and in higher-dimensional scattering problems the "incoming", "outgoing" radial waves, with the constant matrices A, B fixed by the boundary conditions. What are the boundary conditions? The scatterer can modify only the outgoing waves (see fig. 28.1), since the incoming ones, by definition, have yet to encounter the scattering region. This defines the quantum mechanical scattering matrix, or the S *matrix*

$$\phi_m(r) = \phi^{(-)}_m(r) + S_{mm'}\phi^{(+)}_{m'}(r)\,. \tag{28.2}$$

For concreteness, we have specialized to two dimensions, although the final formula is true for arbitrary dimensions. The indices m and m' are the angular momenta quantum numbers for the incoming and outgoing state of the scattering wave function, labeling the S-matrix elements $S_{mm'}$. More generally, given a set of quantum numbers β, γ, the S matrix is a collection $S_{\beta\gamma}$ of transition amplitudes $\beta \to \gamma$ normalized such that $|S_{\beta\gamma}|^2$ is the probability of the $\beta \to \gamma$ transition. The total probability that the ingoing state β ends up in some outgoing state must add up to unity

$$\sum_\gamma |S_{\beta\gamma}|^2 = 1\,, \tag{28.3}$$

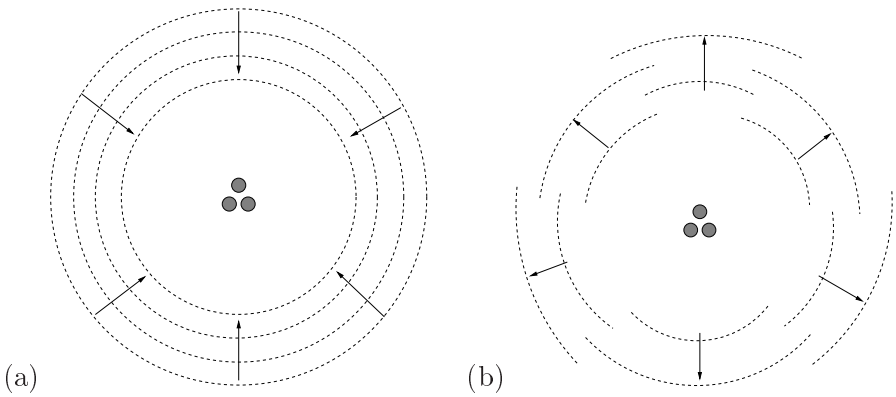

Figure 28.1: (a) *Incoming* spherical waves running into an obstacle. (b) Superposition of *outgoing* spherical waves scattered from an obstacle.

so the S matrix is unitary: $\mathbf{S}^\dagger\mathbf{S} = \mathbf{S}\mathbf{S}^\dagger = \mathbf{1}$.

We have already encountered a solution to the 2-dimensional problem; free particle propagation Green's function (26.47) is a radial solution, given in terms of the Hankel function

$$G_0(r,0,E) = -\frac{im}{2\hbar^2} H_0^{(+)}(kr)\,,$$

where we have used $S_0(r,0,E)/\hbar = kr$ for the action. The mth angular momentum eigenfunction is proportional to $\phi_m^{(\pm)}(q) \propto H_m^{(\pm)}(kr)$, and given a potential $V(q)$ we can in principle compute the infinity of matrix elements $S_{mm'}$. We will not need much information about $H_m^{(t)}(kr)$, other than that for large r its asymptotic form is

$$H^\pm \propto e^{\pm ikr}$$

In general, the potential $V(q)$ is not radially symmetric and (28.1) has to be solved numerically, by explicit integration, or by diagonalizing a large matrix in a specific basis. To simplify things a bit, we assume for the time being that a radially symmetric scatterer is centered at the origin; the final formula will be true for arbitrary asymmetric potentials. Then the solutions of the Schrödinger equation (23.5) are separable, $\phi_m(q) = \phi(r)e^{im\theta}$, $r = |q|$, the scattering matrix cannot mix different angular momentum eigenstates, and S is diagonal in the radial basis (28.2) with matrix elements given by

$$S_m(k) = e^{2i\delta_m(k)}. \tag{28.4}$$

The matrix is unitary so in a diagonal basis all entries are pure phases. This means that an incoming state of the form $H_m^{(-)}(kr)e^{im\theta}$ gets scattered

into an outgoing state of the form $S_m(k)H_m^{(+)}(kr)e^{im\theta}$, where $H_m^{(\mp)}(z)$ are incoming and outgoing Hankel functions respectively. We now embed the scatterer in a infinite cylindrical well of radius R, and will later take $R \to \infty$. Angular momentum is still conserved so that each eigenstate of this (now bound) problem corresponds to some value of m. For large $r \gg a$ each eigenstate is of the asymptotically free form

$$\begin{aligned} \phi_m(r) &\approx e^{im\theta}\left(S_m(k)H_m^{(+)}(kr) + H_m^{(-)}(kr)\right) \\ &\approx \cdots \cos(kr + \delta_m(k) - \chi_m)\,, \end{aligned} \tag{28.5}$$

where $\cdots$ is a common prefactor, and $\chi_m = m\pi/2 + \pi/4$ is an annoying phase factor from the asymptotic expansion of the Hankel functions that will play no role in what follows.

The state (28.5) must satisfy the external boundary condition that it vanish at $r = R$. This implies the quantization condition

$$k_n R + \delta_m(k_n) - \chi_m = \pi\,(n + 12)\ .$$

We now ask for the difference in the eigenvalues of two consecutive states of fixed m. Since R is large, the density of states is high, and the phase $\delta_m(k)$ does not change much over such a small interval. Therefore, to leading order we can include the effect of the change of the phase on state $n+1$ by Taylor expanding. is

$$k_{n+1}R + \delta_m(k_n) + (k_{n+1} - k_n)\delta'_m(k_n) - \chi_m \approx \pi + \pi(n + 12)\,.$$

Taking the difference of the two equations we obtain $\Delta k \approx \pi(R+\delta'_m(k))^{-1}$. This is the eigenvalue spacing which we now interpret as the inverse of the density of states within m angular momentum sbuspace

$$d_m(k) \approx \frac{1}{\pi}\left(R + \delta'_m(k)\right).$$

The R term is essentially the $1-d$ Weyl term (27.8), appropriate to $1-d$ radial quantization. For large R, the dominant behavior is given by the size of the circular enclosure with a correction in terms of the derivative of the scattering phase shift, approximation accurate to order $1/R$. However, not all is well: the area under consideration tends to infinity. We regularize this by subtracting from the result from the free particle density of states $d_0(k)$, for the same size container, but this time without any scatterer, fig. 28.2. We also sum over all m values so that

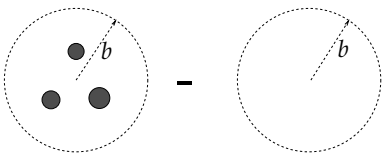

Figure 28.2: The "difference" of two bounded reference systems, one with and one without the scattering system.

$$d(k) - d_0(k) = \frac{1}{\pi}\sum_m \delta'_m(k) = \frac{1}{2\pi i}\sum_m \frac{d}{dk}\log S_m$$
$$= \frac{1}{2\pi i}\mathrm{Tr}\left(S^\dagger \frac{dS}{dk}\right). \qquad (28.6)$$

The first line follows from the definition of the phase shifts (28.4) while the second line follows from the unitarity of S so that $S^{-1} = S^\dagger$. We can now take the limit $R \to \infty$ since the R dependence has been cancelled away.

This is essentially what we want to prove since for the left hand side we already have the semiclassical theory for the trace of the difference of Green's functions,

$$d(k) - d_0(k) = -\frac{1}{2\pi k}\mathrm{Im}\left(\mathrm{tr}\left(G(k) - G_0(k)\right)\right). \qquad (28.7)$$

There are a number of generalizations. This can be done in any number of dimensions. It is also more common to do this as a function of energy and not wave number k. However, as the asymptotic dynamics is free wave dynamics labeled by the wave number k, we have adapted k as the natural variable in the above discussion.

Finally, we state without proof that the relation (28.6) applies even when there is no circular symmetry. The proof is more difficult since one cannot appeal to the phase shifts δ_m but must work directly with a non-diagonal S matrix.

28.2 Quantum mechanical scattering matrix

The results of the previous section indicate that there is a connection between the scattering matrix and the trace of the quantum Green's function (more formally between the difference of the Green's function with and without the scattering center.) We now show how this connection can be derived in a more rigorous manner. We will also work in terms of the energy E rather than the wavenumber k, since this is the more usual exposition. Suppose particles interact via forces of sufficiently short range, so that in the remote past they were in a free particle state labelled β, and

in the distant future they will likewise be free, in a state labelled γ. In the Heisenberg picture the S-matrix is defined as $\mathbf{S} = \Omega_- \Omega_+^\dagger$ in terms of the Møller operators

$$\Omega_\pm = \lim_{t\to\pm\infty} e^{iHt/\hbar} e^{-iH_0 t/\hbar} \ , \tag{28.8}$$

where H is the full Hamiltonian, whereas H_0 is the free Hamiltonian. In the interaction picture the S-matrix is given by

$$\begin{aligned} \mathbf{S} &= \Omega_+^\dagger \Omega_- = \lim_{t\to\infty} e^{iH_0 t/\hbar} e^{-2iHt/\hbar} e^{iH_0 t/\hbar} \\ &= T \exp\left(-i \int_{-\infty}^{+\infty} dt H'(t) \right) \ , \end{aligned} \tag{28.9}$$

where $H' = V = H - H_0$ is the interaction Hamiltonian and T is the time-ordering operator. In stationary scattering theory the S matrix has the following spectral representation

$$\begin{aligned} S &= \int_0^\infty dE\, S(E) \delta(H_0 - E) \\ S(E) &= Q_+(E) Q_-^{-1}(E), \qquad Q_\pm(E) = \mathbf{1} + (H_0 - E \pm i\epsilon)^{-1} V \end{aligned} \tag{28.10}$$

such that

$$\mathrm{Tr}\left[S^\dagger(E) \frac{d}{dE} S(E) \right] = \mathrm{Tr}\left[\frac{1}{H_0 - E - i\epsilon} - \frac{1}{H - E - i\epsilon} - (\epsilon \leftrightarrow -\epsilon) \right] \ . \tag{28.11}$$

☞ appendix K

The manipulations leading to (28.11) are justified if the operators $Q_\pm(E)$ can be linked to trace-class operators.

We can now use this result to derive the Krein-Lloyd formula which is the central result of this chapter. The Krein-Lloyd formula provides the connection between the trace of the Green's function and the poles of the scattering matrix, implicit in all of the trace formulas for open quantum systems which will be presented in the subsequent chapters.

28.3 Krein-Friedel-Lloyd formula

The link between quantum mechanics and semiclassics for scattering problems is provided by the semiclassical limit of the Krein-Friedel-Lloyd sum

for the spectral density which we now derive. This derivation builds on the results of the last section and extends the discussion of the opening section.

In chapter 26 we linked the spectral density (see (23.17)) of a bounded system

$$d(E) \equiv \sum_n \delta(E_n - E) \tag{28.12}$$

via the identity

$$\begin{aligned} \delta(E_n - E) &= -\lim_{\epsilon\to 0} \frac{1}{\pi} \mathrm{Im} \frac{1}{E - E_n + i\epsilon} \\ &= -\lim_{\epsilon\to 0} \frac{1}{\pi} \mathrm{Im} \langle E_n | \frac{1}{E - H + i\epsilon} | E_n \rangle \\ &= \frac{1}{2\pi\, i} \lim_{\epsilon\to 0} \left\langle E_n \left| \frac{1}{E - H - i\epsilon} - \frac{1}{E - H + i\epsilon} \right| E_n \right\rangle \end{aligned} \tag{28.13}$$

to the trace of the Green's function (27.1.1). Furthermore, in the semiclassical approximation, the trace of the Green's function is given by the Gutzwiller trace formula (27.11) in terms of a smooth Weyl term and an oscillating contribution of periodic orbits.

Therefore, the task of constructing the semiclassics of a scattering system is completed, if we can find a connection between the spectral density $d(E)$ and the scattering matrix S. We will see that (28.11) provides the clue. Note that the right hand side of (28.11) has nearly the structure of (28.13) when the latter is inserted into (28.12). The principal difference between these two types of equations is that the S matrix refers to *outgoing* scattering wave functions which are not normalizable and which have a *continuous* spectrum, whereas the spectral density $d(E)$ refers to a bound system with normalizable wave functions with a discrete spectrum. Furthermore, the bound system is characterized by a *hermitian* operator, the Hamiltonian H, whereas the scattering system is characterized by a *unitary* operator, the S-matrix. How can we reconcile these completely different classes of wave functions, operators and spectra? The trick is to put our scattering system into a finite box as in the opening section. We choose a spherical conatiner with radius R and with its center at the center of our finite scattering system. Our scattering potential $V(\vec{r})$ will be unaltered within the box, whereas at the box walls we will choose an infinitely high potential, with the Dirichlet boundary conditions at the outside of the box:

$$\phi(\vec{r})|_{r=R} = 0\,. \tag{28.14}$$

In this way, for any finite value of the radius R of the box, we have mapped our scattering system into a bound system with a spectral density $d(E;R)$ over discrete eigenenergies $E_n(R)$. It is therefore important that our scattering potential was chosen to be short-ranged to start with. (Which explains why the Coulomb potential requires special care.) The hope is that in the limit $R \to \infty$ we will recover the scattering system. But some care is required in implementing this. The smooth Weyl term $\bar{d}(E;R)$ belonging to our box with the enclosed potential V diverges for a spherical two-dimensional box of radius R quadratically, as $\pi R^2/(4\pi)$ or as R^3 in the three-dimensional case. This problem can easily be cured if the spectral density of an empty reference box of the *same* size (radius R) is subtracted (see fig. 28.2). Then all the divergences linked to the increasing radius R in the limit $R \to \infty$ drop out of the difference. Furthermore, in the limit $R \to \infty$ the energy-eigenfunctions of the box are only normalizable as a delta distribution, similarly to a plane wave. So we seem to recover a continous spectrum. Still the problem remains that the wave functions do not discriminate between incoming and outgoing waves, whereas this symmetry, namely the hermiticity, is broken in the scattering problem. The last problem can be tackled if we replace the spectral density over discrete delta distributions by a smoothed spectral density with a small finite imaginary part η in the energy E:

$$d(E+i\eta;R) \equiv \frac{1}{i\,2\pi} \sum_n \left\{ \frac{1}{E-E_n(R)-i\eta} - \frac{1}{E-E_n(R)+i\eta} \right\} . \quad (28.15)$$

Note that $d(E+i\eta;R) \neq d(E-i\eta;R) = -d(E+i\eta;R)$. By the introduction of the positive *finite* imaginary part η the time-dependent behavior of the wave function has effectively been altered from an oscillating one to a decaying one and the hermiticity of the Hamiltonian is removed. Finally the limit $\eta \to 0$ can be carried out, respecting the order of the limiting procedures. First the limit $R \to \infty$ has to be performed for a *finite* value of η, only then the limit $\eta \to 0$ is allowed. In practice, one can try to work with a finite value of R, but then it will turn out (see below) that the scattering system is only recovered if $R\sqrt{\eta} \gg 1$.

Let us summarize the relation between the smoothed spectral densities $d(E+i\eta;R)$ of the boxed potential and $d^{(0)}(E+i\eta;R)$ of the empty reference system and the S matrix of the corresponding scattering system:

$$\begin{aligned} \lim_{\eta\to+0} \lim_{R\to\infty} \Big(d(E+i\eta;R) - d^{(0)}(E+i\eta;R) \Big) &= \frac{1}{2\pi i} \mathrm{Tr} \left[S^\dagger(E) \frac{d}{dE} S(E) \right] \\ = \frac{1}{2\pi i} \mathrm{Tr} \frac{d}{dE} \ln S(E) &= \frac{1}{2\pi i} \frac{d}{dE} \ln \det S(E) \end{aligned} \quad (28.16)$$

This is the *Krein-Friedel-Lloyd formula*. It replaces the scattering problem by the difference of two bounded reference billiards of the same radius

R which finally will be taken to infinity. The first billiard contains the scattering region or potentials, whereas the other does not (see fig. 28.2). Here $d(E+i\eta;R)$ and $d^{(0)}(E+i\eta;R)$ are the *smoothed* spectral densities in the presence or in the absence of the scatterers, respectively. In the semiclassical approximation, they are replaced by a Weyl term (27.10) and an oscillating sum over periodic orbits. As in (27.2), the trace formula (28.16) can be integrated to give a relation between the smoothed staircase functions and the determinant of the S-matrix:

$$\lim_{\eta\to+0}\lim_{R\to\infty}\Big(N(E+i\eta;R)-N^{(0)}(E+i\eta;R)\Big) \;=\; \frac{1}{2\pi i}\ln\det S(E) \qquad (28.17)$$

Furthermore, in both versions of the Krein-Friedel-Lloyd formulas the energy argument $E+i\eta$ can be replaced by the wavenumber argument $k+i\eta'$. These expressions only make sense for wave numbers on or above the real k-axis. In particular, if k is chosen to be real, η' must be greater than zero. Otherwise, the exact left hand sides (28.17) and (28.16) would give discontinuous staircase or even delta function sums, respectively, whereas the right hand sides are continuous to start with, since they can be expressed by continuous phase shifts. Thus the order of the two limits in (28.17) and (28.16) is essential.

The necessity of the $+i\eta$ prescription can also be understood by purely phenomenological considerations in the semiclassical approximation: Without the $i\eta$ term there is no reason why one should be able to neglect spurious periodic orbits which are there solely because of the introduction of the confining boundary. The subtraction of the second (empty) reference system removes those spurious periodic orbits which never encounter the scattering region – in addition to the removal of the divergent Weyl term contributions in the limit $R\to\infty$. The periodic orbits that encounter both the scattering region and the external wall would still survive the first limit $R\to\infty$, if they were not exponentially suppressed by the $+i\eta$ term because of their

$$e^{iL(R)\sqrt{2m(E+i\eta)}} = e^{iL(R)k}\, e^{-L(R)\eta'}$$

behavior. As the length $L(R)$ of a spurious periodic orbit grows linearly with the radius R. The bound $R\eta'\gg 1$ is an essential precondition on the suppression of the unwanted spurious contributions of the container if the Krein-Friedel-Lloyd formulas (28.16) and (28.17) are evaluated at a finite value of R.

28.1
page 536

Finally, the semiclassical approximation can also help us in the interpretation of the Weyl term contributions for scattering problems. In scattering problems the Weyl term appears with a negative sign. The reason is the

subtraction of the empty container from the container with the potential. If the potential is a dispersing billiard system (or a finite collection of dispersing billiards), we expect an excluded volume (or the sum of excluded volumes) relative to the empty container. In other words, the Weyl term contribution of the empty container is larger than of the filled one and therefore a negative net contribution is left over. Secondly, if the scattering potential is a collection of a finite number of non-overlapping scattering regions, the Krein-Friedel-Lloyd formulas show that the corresponding Weyl contributions are completely independent of the position of the single scatterers, as long as these do not overlap.

28.4 Wigner time delay

The term $\frac{d}{dE}\ln\det S$ in the density formula (28.16) is dimensionally time. This suggests another, physically important interpretation of such formulas for scattering systems, the Wigner delay, defined as

$$\begin{aligned} d(k) &= \frac{d}{dk}\mathrm{Argdet}\left(\mathbf{S}(k)\right) \\ &= -i\frac{d}{dk}\log\det\left(\mathbf{S}(k)\right) \\ &= -i\,\mathrm{tr}\left(\mathbf{S}^\dagger(k)\frac{d\mathbf{S}}{dk}(k)\right) \end{aligned} \tag{28.18}$$

and can be shown to equal the total delay of a wave packet in a scattering system. We now review this fact.

A related quantity is the total scattering *phase shift* $\Theta(k)$ defined as

$$\det\mathbf{S}(k) = e^{+i\,\Theta(k)}\,,$$

so that $d(k) = \frac{d}{dk}\Theta(k)$.

The time delay may be both positive and negative, reflecting attractive respectively repulsive features of the scattering system. To elucidate the connection between the scattering determinant and the time delay we study a plane wave:

The phase of a wave packet will have the form:

$$\phi = \vec{k}\cdot\vec{x} - \omega\,t \;+\; \Theta\,.$$

Here the term in the parenthesis refers to the phase shift that will occur if scattering is present. The center of the wave packet will be determined by the principle of stationary phase:

$$0 = d\phi = d\vec{k} \cdot \vec{x} - d\omega\, t \; + \; d\Theta\,.$$

Hence the packet is located at

$$\vec{x} = \frac{\partial \omega}{\partial \vec{k}}\, t \; - \frac{\partial \Theta}{\partial \vec{k}}\,.$$

The first term is just the group velocity times the given time t. Thus the the packet is retarded by a length given by the derivative of the phase shift with respect to the wave vector $\vec{k}$. The arrival of the wave packet at the position $\vec{x}$ will therefore be delayed. This *time delay* can similarly be found as

$$\tau(\omega) = \frac{\partial \Theta(\omega)}{\partial \omega}.$$

To show this we introduce the *slowness* of the phase $\vec{s} = \vec{k}/\omega$ for which $\vec{s} \cdot \vec{v}_g = 1$, where $\vec{v}_g$ is the group velocity to get

$$d\vec{k} \cdot \vec{x} = \vec{s} \cdot \vec{x}\, d\omega = \frac{x}{v_g}\, d\omega\,,$$

since we may assume $\vec{x}$ is parallel to the group velocity (consistent with the above). Hence the arrival time becomes

$$t = \frac{x}{v_g} \; + \frac{\partial \Theta(\omega)}{\partial \omega}\,.$$

If the scattering matrix is not diagonal, one interprets

$$\Delta t_{ij} = \mathrm{Re}\left(-i\, S_{ij}^{-1} \frac{\partial S_{ij}}{\partial \omega}\right) = \mathrm{Re}\left(\frac{\partial \Theta_{ij}}{\partial \omega}\right)$$

as the delay in the jth scattering channel after an injection in the ith. The probability for appearing in channel j goes as $|S_{ij}|^2$ and therefore the average delay for the incoming states in channel i is

$$\begin{aligned} \langle \Delta t_i \rangle &= \sum_j |S_{ij}|^2 \Delta t_{ij} = \mathrm{Re}\,(-i \sum_j S_{ij}^* \frac{\partial S_{ij}}{\partial \omega}) = \mathrm{Re}\,(-i\, \mathbf{S}^\dagger \cdot \frac{\partial \mathbf{S}}{\partial \omega})_{ii} \\ &= -i \left(\mathbf{S}^\dagger \cdot \frac{\partial \mathbf{S}}{\partial \omega}\right)_{ii}\,, \end{aligned}$$

where we have used the derivative, $\partial/\partial\omega$, of the unitarity relation $\mathbf{S}\cdot\mathbf{S}^\dagger = \mathbf{1}$ valid for real frequencies. This discussion can in particular be made for wave packets related to partial waves and superpositions of these like an incoming plane wave corresponding to free motion. The total Wigner delay therefore corresponds to the sum over all channel delays (28.18).

Commentary

Remark 28.1 Krein-Friedel-Lloyd formula. The Krein-Friedel-Lloyd formula (28.16) was derived in refs. [28.3, 28.4, 28.5, 28.6], see also refs. [28.7, 28.8, 28.9, 28.10, 28.11].

Remark 28.2 Weyl term for empty container. For a discussion of why the Weyl term contribution of the empty container is larger than of the filled one and therefore a negative net contribution is left over, see ref. [28.9].

References

[28.1] W. Thirring, *Quantum mechanics of atoms and molecules*, *A course in mathematical physics* Vol. **3** (Springer, New York, 1979). (Springer, Wien 1979).

[28.2] A. Messiah, *Quantum Mechanics, Vol.* **I** (North-Holland, Amsterdam, 1961).

[28.3] M.G. Krein, *On the Trace Formula in Perturbation Theory*, Mat.. Sborn. (N.S.) **33** (1953) 597-626; *Perturbation Determinants and Formula for Traces of Unitary and Self-adjoint Operators*, Sov. Math.-Dokl. **3** (1962) 707-710. M.S. Birman and M.G. Krein, *On the Theory of Wave Operators and Scattering Operators*, Sov. Math.-Dokl. **3** (1962) 740-744.

[28.4] J. Friedel, Nuovo Cim. Suppl. **7** (1958) 287–301.

[28.5] P. Lloyd, Wave propagation through an assembly of spheres. II. The density of single-particle eigenstates, *Proc. Phys. Soc.* **90** (1967) 207–216.

[28.6] P. Lloyd and P.V. Smith, Multiple-scattering theory in condensed materials, *Adv. Phys.* **21** (1972) 69–142, and references therein.

[28.7] R. Balian and C. Bloch, Solution of the Schrödinger Equation in Terms of Classical Paths, *Ann. Phys. (N.Y.)* **85** (1974) 514–545.

[28.8] P. Gaspard and S.A. Rice, Semiclassical quantization of the scattering from a classically chaotic repellor, *J. Chem. Phys.* **90** (1989) 2242–2254.

[28.9] P. Scherer, *Quantenzustände eines klassisch chaotischen Billards*, Ph.D. thesis, Univ. Köln (Berichte des Forschungszentrums Jülich 2554, ISSN 0366-0885, Jülich, Nov. 1991).

[28.10] P. Gaspard, Scattering Resonances: Classical and Quantum Dynamics, in: *Proceedings of the Int. School of Physics "Enrico Fermi"*, Course CXIX, Varena, 23 July - 2 August 1991, eds G. Casati, I. Guarneri and U. Smilansky (North-Holland, Amsterdam, 1993).

[28.11] A. Norcliffe and I. C. Percival, J. Phys. B **1**, 774 (1968); L. Schulman, Phys. Rev. **176**, 1558 (1968).

[28.12] E.P. Wigner, *Phys. Rev.* **98**, 145 (1955).

[28.13] F.T. Smith, *Phys. Rev.* **118**, 349 (1960).

[28.14] A. Wirzba, *Quantum Mechanics and Semiclassics of Hyperbolic n-Disk Scattering*, *Physics Reports* **309**, 1-116 (1999); `chao-dyn/9712015`.

[28.15] V. A. Gopar, P. A. Mello, and M. Buttiker, Phys. Rev. Lett. 77, 3005 (1996).

[28.16] P. W. Brouwer, K. M. Frahm, and C. W. J. Beenakker, Phys. Rev. Lett. 78, 4737 (1997).

[28.17] Following the thesis of Eisenbud, the local delay time Dtab is defined in ref. [28.13] as the appearance of the peak in the outgoing signal in channel b after the injection of a wave packet in channel a. Our definition of the local delay time tab in Eq. (1) coincides with the definition of Dtab in the limit of narrow bandwidth pulses, as shown in Eq. (3).

[28.18] E. Doron and U. Smilansky, Phys. Rev. Lett. 68, 1255 (1992).

[28.19] G. Iannaccone, Phys. Rev. B 51, 4727 (1995).

[28.20] V. Gasparian, T. Christen, and M. Büttiker, Phys. Rev. A 54, 4022 (1996).

[28.21] For a complete and insightful review see Y. V. Fyodorv and H.-J. Sommers, J. Math. Phys. 38, 1918 (1997).

[28.22] R. Landauer and Th. Martin, Rev. Mod. Phys. 66, 217 (1994). j

[28.23] E. H. Hauge and J. A. Støveng, Rev. Mod. Phys. 61, 917 (1989).

Exercises

Exercise 28.1 Spurious orbits under the Krein-Friedel-Lloyd contruction. *Draw examples for the three types of period orbits under the Krein-Friedel-Lloyd construction: (a) the genuine periodic orbits of the scattering region, (b) spurious periodic orbits which can be removed by the subtraction of the reference system, (c) spurious periodic orbits which cannot be removed by this subtraction. What is the role of the double limit $\eta \to 0$, container size $b \to \infty$?*

Exercise 28.2 The one-disk scattering wave function. *Derive the one-disk scattering wave function.*

(Andreas Wirzba)

Exercise 28.3 Quantum two-disk scattering. *Compute the quasiclassical spectral determinant*

$$Z(\varepsilon) = \prod_{p,j,l} \left(1 - \frac{t_p}{\Lambda_p^{j+2l}}\right)^{j+1}$$

for the two disk problem. Use the geometry

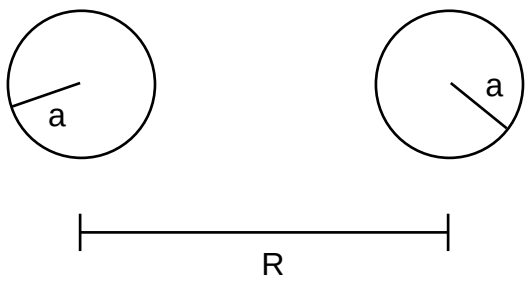

The full quantum mechanical version of this problem can be solved by finding the zeros in k for the determinant of the matrix

$$M_{m,n} = \delta_{m,n} + \frac{(-1)^n}{2} \frac{J_m(ka)}{H_n^{(1)}(ka)} \left(H_{m-n}^{(1)}(kR) + (-1)^n H_{m+n}^{(1)}(kR) \right) ,$$

where J_n is the nth Bessel function and $H_n^{(1)}$ is the Hankel function of the first kind. Find the zeros of the determinant closest to the origin by solving $\det M(k) = 0$. (Hints: notice the structure $M = I + A$ to approximate the determinant; or read Chaos **2**, *79 (1992))*

Exercise 28.4 Pinball topological index. *Upgrade your pinball simulator so that it computes the topological index for each orbit it finds.*

Chapter 29

Helium atom

> "But," Bohr protested, "nobody will believe me unless I can explain every atom and every molecule." Rutherford was quick to reply, "Bohr, you explain hydrogen and you explain helium and everybody will believe the rest."
> John Archibald Wheeler (1986)

(G. Tanner)

So far much has been said about 1-dimensional maps, game of pinball and other curious but rather idealized dynamical systems. If you have became impatient and started wondering what good are the methods learned so far in solving real physical problems, we have good news for you. We will show in this chapter that the concepts of symbolic dynamics, unstable periodic orbits, and cycle expansions are essential tools to understand and calculate classical and quantum mechanical properties of nothing less than the helium, a dreaded three-body Coulomb problem.

This sounds almost like one step too much at a time; we all know how rich and complicated the dynamics of the three-body problem is – can we really jump from three static disks directly to three charged particles moving under the influence of their mutually attracting or repelling forces? It turns out, we can, but we have to do it with care. The full problem is indeed not accessible in all its detail, but we are able to analyze a somewhat simpler subsystem – collinear helium. This system plays an important role in the classical dynamics of the full three-body problem and its quantum spectrum.

The main work in reducing the quantum mechanics of helium to a semiclassical treatment of collinear helium lies in understanding why we are allowed to do so. We will not worry about this too much in the beginning;

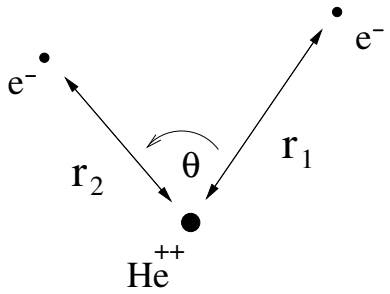

Figure 29.1: Coordinates for the helium three body problem in the plane.

after all, 80 years and many failed attempts separate Heisenberg, Bohr and others in the 1920ties from the insights we have today on the role chaos plays for helium and its quantum spectrum. We will introduce collinear helium in sect. 29.1 and discuss its dynamics in some detail. We will learn how to integrate and find periodic orbits and how to determine the relevant eigenvalues of the Jacobian matrix. We will explain in sect. 29.2 why a quantization of the collinear dynamics in helium will enable us to find parts of the full helium spectrum; we then set up the semiclassical spectral determinant and evaluate its cycle expansion. A full quantum justification of this treatment of helium is briefly discussed in sect. 29.2.1.

29.1 Classical dynamics of collinear helium

The full classical helium system consists of two electrons of mass m_e and charge $-e$ moving about a positively charged nucleus of mass m_{he} and charge $+2e$.

The helium electron-nucleus mass ratio $m_{he}/m_e = 1836$ is so large that we may work in the infinite nucleus mass approximation $m_{he} = \infty$, fixing the nucleus at the origin. Finite nucleus mass effects can be taken into account without any substantial difficulty. We are now left with two electrons moving in three spatial dimensions around the origin. The total angular momentum of the combined electron system is still conserved. In the special case of angular momentum $L = 0$, the electrons move in a fixed plane containing the nucleus. The three body problem can then be written in terms of three independent coordinates only, the electron-nucleus distances r_1 and r_2 and the inter-electron angle Θ, see fig. 29.1.

29.2
page 563

This looks like something we can lay our hands on; the problem has been reduced to three degrees of freedom, six phase space coordinates in all, and the total energy is conserved. But let us go one step further; the electrons are attracted by the nucleus but repelled by each other. They will tend to stay as far away from each other as possible, preferably on opposite sides of the nucleus. It is thus worth having a closer look at the situation where the three particles are all on a line with the nucleus being

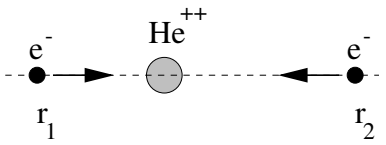

Figure 29.2: Collinear helium, with the two electrons on opposite sides of the nucleus.

somewhere between the two electrons. If we, in addition, let the electrons have momenta pointing towards the nucleus as in fig. 29.2, then there is no force acting on the electrons perpendicular to the common interparticle axis. That is, if we start the classical system on the dynamical subspace $\Theta = \pi$, $\frac{d}{dt}\Theta = 0$, the three particles will remain in this *collinear configuration* for all times.

29.1.1 Scaling

In what follows we will restrict the dynamics to this collinear subspace. It is a system of two degrees of freedom with the Hamiltonian

$$H = \frac{1}{2m_e}\left(p_1^2 + p_2^2\right) - \frac{2e}{r_1} - \frac{2e}{r_2} + \frac{e}{r_1 + r_2} = E\,, \tag{29.1}$$

where E is the total energy. We will first consider the dependence of the dynamics on the energy E. A simple analysis of potential versus kinetic energy tells us that if the energy is positive both electrons can escape to $r_i \to \infty$, $i = 1, 2$. More interestingly, a single electron can still escape even if E is negative, carrying away an unlimited amount of kinetic energy, as the total energy of the remaining inner electron has no lower bound. Not only that, but one electron *will* escape eventually for almost all starting conditions. The overall dynamics thus depends critically on whether $E > 0$ or $E < 0$. But how does the dynamics change otherwise with varying energy? Fortunately, not at all. Helium dynamics remains invariant under a change of energy up to a simple scaling transformation; a solution of the equations of motion at a fixed energy $E_0 = -1$ can be transformed into a solution at an arbitrary energy $E < 0$ by scaling the coordinates as

$$r_i(E) = \frac{e^2}{(-E)}\, r_i, \quad p_i(E) = \sqrt{-m_e E}\, p_i, \quad i = 1, 2\,,$$

together with a time transformation $t(E) = e^2 m_e^{1/2}(-E)^{-3/2}\, t$. We include the electron mass and charge in the scaling transformation in order to obtain a non–dimensionalized Hamiltonian of the form

$$H = \frac{p_1^2}{2} + \frac{p_2^2}{2} - \frac{2}{r_1} - \frac{2}{r_2} + \frac{1}{r_1 + r_2} = -1\,. \tag{29.2}$$

The case of negative energies chosen here is the most interesting one for us. It exhibits chaos, unstable periodic orbits and is responsible for the bound states and resonances of the quantum problem treated in sect. 29.2.

There is another classical quantity important for a semiclassical treatment of quantum mechanics, and which will also feature prominently in the discussion in the next section; this is the classical action (26.14) which scales with energy as

$$S(E) = \oint \mathrm{d}\mathbf{q}(E) \cdot \mathbf{p}(E) = \frac{e^2 m_e^{1/2}}{(-E)^{1/2}}\, S, \tag{29.3}$$

with S being the action obtained from (29.2) for $E = -1$, and coordinates $\mathbf{q} = (r_1, r_2)$, $\mathbf{p} = (p_1, p_2)$. For the Hamiltonian (29.2), the period of a cycle and its action are related by (26.16), $T_p = \frac{1}{2} S_p$.

29.1.2 Regularization of two–body collisions

Next, we have a closer look at the singularities in the Hamiltonian (29.2). Whenever two bodies come close to each other, accelerations become large, numerical routines require lots of small steps, and numerical precision suffers. No numerical routine will get us through the singularity itself, and in collinear helium electrons have no option but to collide with the nucleus. Hence a *regularization* of the differential equations of motions is a necessary prerequisite to any numerical work on such problems, both in celestial mechanics (where a spaceship executes close approaches both at the start and its destiantion) and in quantum mechanics (where much of semiclassical physics is dominated by returning classical orbits that probe the quantum wave function at the nucleus).

There is a fundamental difference between two–body collisions $r_1 = 0$ or $r_2 = 0$, and the triple collision $r_1 = r_2 = 0$. Two–body collisions can be regularized, with the singularities in equations of motion removed by a suitable coordinate transformation together with a time transformation preserving the Hamiltonian structure of the equations. Such regularization is not possible for the triple collision, and solutions of the differential equations can not be continued through the singularity at the origin. As we shall see, the chaos in collinear helium originates from this singularity of triple collisions.

A regularization of the two–body collisions is achieved by means of the Kustaanheimo–Stiefel (KS) transformation, which consists of a coordinate dependent time transformation which stretches the time scale near the origin, and a canonical transformation of the phase space coordinates. In

order to motivate the method, we apply it first to the 1-dimensional Kepler problem

$$H = \frac{1}{2}p^2 - \frac{2}{x} = E\,. \tag{29.4}$$

To warm up, consider the $E = 0$ case, starting at $x = 0$ at $t = 0$. Even though the equations of motion are singular at the intial point, we can immediately integrate

$$\frac{1}{2}\dot{x}^2 - \frac{2}{x} = 0$$

by means of separation of variables

$$\sqrt{x}dx = \sqrt{2}dt\,, \qquad x = (9/2)^{\frac{1}{3}}\, t^{\frac{2}{3}}\,, \tag{29.5}$$

and observe that the solution is not singular. The aim of regularization is to compensate for the infinite acceleration at the origin by introducing a fictitious time, in terms of which the passage through the origin is smooth.

A time transformation $dt = f(q,p)d\tau$ for a system described by a Hamiltonian $H(q,p) = E$ leaves the Hamiltonian structure of the equations of motion unaltered, if the Hamiltonian itself is transformed into $\mathcal{H}(q,p) = f(q,p)(H(q,p) - E)$. For the 1– dimensional Coulomb problem with (29.4) we choose the time transformation $dt = xd\tau$ which lifts the $|x| \to 0$ singularity in (29.4) and leads to a new Hamiltonian

$$\mathcal{H} = \frac{1}{2}xp^2 - 2 - Ex = 0. \tag{29.6}$$

The solution (29.5) is now parametrized by the fictitous time $d\tau$ through a pair of equations

$$x = \frac{1}{2}\tau^2\,, \qquad t = \frac{1}{6}\tau^3\,.$$

The equations of motion are, however, still singular as $x \to 0$:

$$\frac{d^2x}{d\tau^2} = -\frac{1}{2x}\frac{dx}{d\tau} + xE\,.$$

Appearance of the square root in (29.5) now suggests a canonical transformation of form

$$x = Q^2\,, \quad p = \frac{P}{2Q} \tag{29.7}$$

which maps the Kepler problem into that of a harmonic oscillator with Hamiltonian

$$H(Q,P) = \frac{1}{8}P^2 - EQ^2 = 2, \tag{29.8}$$

with all singularities completely removed.

We now apply this method to collinear helium. The basic idea is that one seeks a higher-dimensional generalization of the "square root removal" trick (29.7), by introducing a new vector Q with property $r = |Q|^2$. In this simple 1-dimensional example the KS transformation can be implemented by

$$r_1 = Q_1^2\,, \qquad r_2 = Q_2^2\,, \qquad p_1 = \frac{P_1}{2Q_1}\,, \qquad p_2 = \frac{P_2}{2Q_2} \tag{29.9}$$

29.1
page 563

and reparametrization of time by $d\tau = dt/r_1 r_2$. The singular behavior in the original momenta at r_1 or $r_2 = 0$ is again compensated by stretching the time scale at these points. The Hamiltonian structure of the equations of motions with respect to the new time τ is conserved, if we consider the Hamiltonian

$$H_{ko} = \frac{1}{8}(Q_2^2 P_1^2 + Q_1^2 P_2^2) - 2R_{12}^2 + Q_1^2 Q_2^2 \left(1 + \frac{1}{R_{12}^2}\right) = 0 \tag{29.10}$$

with $R_{12} = (Q_1^2 + Q_2^2)^{1/2}$. The equations of motion now have the form

$$\begin{aligned} \dot{P}_1 &= 2Q_1 \left[2 - \frac{P_2^2}{8} - Q_2^2\left(1 + \frac{Q_2^2}{R_{12}^4}\right)\right]; \qquad \dot{Q}_1 = \frac{1}{4}P_1 Q_2^2 \\ \dot{P}_2 &= 2Q_2 \left[2 - \frac{P_1^2}{8} - Q_1^2\left(1 + \frac{Q_1^2}{R_{12}^4}\right)\right]; \qquad \dot{Q}_2 = \frac{1}{4}P_2 Q_1^2. \end{aligned} \tag{29.11}$$

Individual electron–nucleus collisions at $r_1 = Q_1^2 = 0$ or $r_2 = Q_2^2 = 0$ no longer pose a problem to a numerical integration routine. The equations (29.11) are singular only at the triple collision $R_{12} = 0$, that is, when both electrons hit the nucleus at the same time.

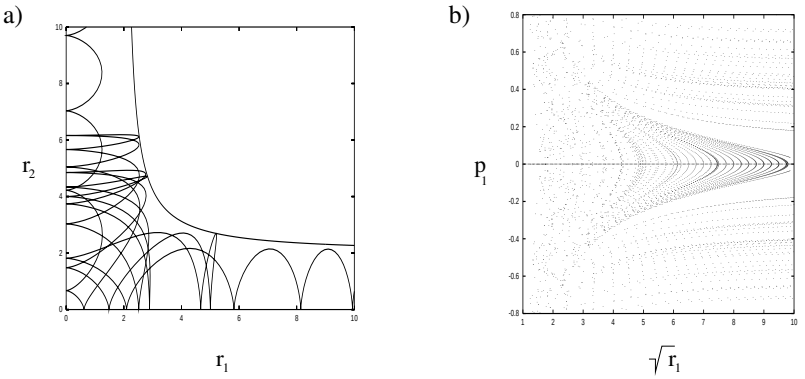

Figure 29.3: a) A typical trajectory in the $r_1 - r_2$ plane; the trajectory enters here along the r_1 axis and escapes to infinity along the r_2 axis; b) Poincaré map (r_2=0) for collinear helium. Strong chaos prevails for small r_1 near the nucleus.

The new coordinates and the Hamiltonian (29.10) are very useful when calculating trajectories for collinear helium; they are, however, less intuitive as a visualization of the three-body dynamics. We will therefore refer to the old coordinates r_1, r_2 when discussing the dynamics and the periodic orbits.

29.1.3 Chaos, symbolic dynamics and periodic orbits

Let us have a closer look at the dynamics in collinear helium. The electrons are attracted by the nucleus. During an electron–nucleus collision momentum is transferred between the inner and outer electron. The inner electron has a maximal screening effect on the charge of the nucleus, diminishing the attractive force on the outer electron. This electron – electron interaction is negligible if the outer electron is far from the nucleus at a collision and the overall dynamics is regular like in the 1-dimensional Kepler problem.

Things change drastically if both electrons approach the nucleus nearly simultaneously. The momentum transfer between the electrons depends now sensitively on how the particles approach the origin. Intuitively, these nearly missed triple collisions render the dynamics chaotic. A typical trajectory is plotted in fig. 29.3(a) where we used r_1 and r_2 as the relevant axis. The dynamics can also be visualized in a Poincaré surface of section, see fig. 29.3(b). We plot here the coordinate and momentum of the outer electron whenever the inner particle hits the nucleus, that is, r_1 or $r_2 = 0$. As the unstructured gray region of the Poincaré section for small r_1 illustrates, the dynamics is chaotic whenever the outer electron is close to the origin during a collision. Conversely, regular motions dominate whenever the outer electron is far from the nucleus. As one of the electrons escapes for almost any starting condition, the system is unbounded: one

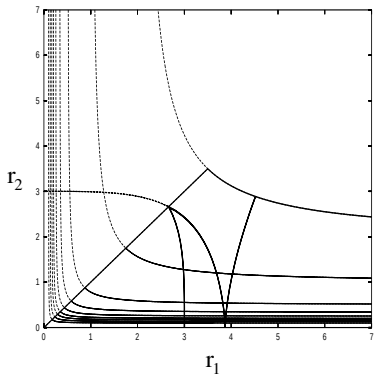

Figure 29.4: The cycle 011 in the fundamental domain $r_1 \geq r_2$ (full line) and in the full domain (dashed line).

electron (say electron 1) can escape, with an arbitrary amount of kinetic energy taken by the fugative. The remaining electron is trapped in a Kepler ellipse with total energy in the range $[-1, -\infty]$. There is no energy barrier which would separate the bound from the unbound regions of the phase space. From general kinematic arguments one deduces that the outer electron will not return when $p_1 > 0$, $r_2 \leq 2$ at $p_2 = 0$, the turning point of the inner electron. Only if the two electrons approach the nucleus almost symmetrically along the line $r_1 = r_2$, and pass close to the triple collision can the momentum transfer between the electrons be large enough to kick one of the particles out completely. In other words, the electron escape originates from the near triple collisions.

The collinear helium dynamics has some important properties which we now list.

Reflection symmetry

The Hamiltonian (29.1) is invariant with respect to electron–electron exchange; this symmetry corresponds to the mirror symmetry of the potential along the line $r_1 = r_2$, fig. 29.4. As a consequence, we can restrict ourselves to the dynamics in the *fundamental domain* $r_1 \geq r_2$ and treat a crossing of the diagonal $r_1 = r_2$ as a hard wall reflection. The dynamics in the full domain can then be reconstructed by unfolding the trajectory through back-reflections. As explained in chapter 19, the dynamics in the fundamental domain is the key to the factorization of spectral determinants, to be implemented here in (29.22). Note also the similarity between the fundamental domain of the collinear potential fig. 29.4, and the fundamental domain fig. 9.5(b) in the 3–disk system, a simpler problem with the same binary symbolic dynamics.

in depth:
sect. 19.6, p. 382

Symbolic dynamics

We have already made the claim that the triple collisions render the collinear helium fully chaotic. We have no proof of the assertion, but the analysis of the symbolic dynamics lends further credence to the claim.

The potential in (29.2) forms a ridge along the line $r_1 = r_2$. One can show that a trajectory passing the ridge must go through at least one two-body collision $r_1 = 0$ or $r_2 = 0$ before coming back to the diagonal $r_1 = r_2$. This suggests a *binary* symbolic dynamics corresponding to the dynamics in the fundamental domain $r_1 \geq r_2$; the symbolic dynamics is linked to the Poincaré map $r_2 = 0$ and the symbols 0 and 1 are defined as

0: if the trajectory is not reflected from the line $r_1 = r_2$ between two collisions with the nucleus $r_2 = 0$;

1: if a trajectory is reflected from the line $r_1 = r_2$ between two collisions with the nucleus $r_2 = 0$.

Empirically, the symbolic dynamics is complete for a Poincaré map in the fundamental domain, that is, there exists a one-to-one correspondence between binary symbol sequences and collinear trajectories in the fundamental domain, with exception of the $\overline{0}$ cycle.

Periodic orbits

The existence of a binary symbolic dynamics makes it easy to count the number of periodic orbits in the fundamental domain, as in sect. 10.5.2. However, mere existence of these cycles does not suffice to calculate semiclassical spectral determinants. We need to determine their phase space trajectories and calculate their periods, topological indices and stabilities. A restriction of the periodic orbit search to a suitable Poincaré surface of section, e.g. $r_2 = 0$ or $r_1 = r_2$, leaves us in general with a 2-dimensional search. Methods to find periodic orbits in multi-dimensional spaces have been described in chapter 14. They depend sensitively on good starting guesses. A systematic search for all orbits can be achieved only after combining multi-dimensional Newton methods with interpolation algorithms based on the binary symbolic dynamics phase space partitioning. All cycles up to symbol length 16 (some 8000 primitive cycles) have been computed by such methods, with some examples shown in fig. 29.5. All numerical evidence indicates that the dynamics of collinear helium is hyperbolic, and that all periodic orbits are unstable.

Note that the fixed point $\overline{0}$ cycle is not in this list. The $\overline{0}$ cycle would correspond to the situation where the outer electron sits at rest infinitely

far from the nucleus while the inner electron bounces back and forth into the nucleus. The orbit is the limiting case of an electron escaping to infinity with zero kinetic energy. The orbit is in the regular (that is separable) limit of the dynamics and is thus marginally stable. The existence of this orbit is also related to intermittent behavior generating the quasi–regular dynamics for large r_1 that we have already noted in fig. 29.3(b).

Search algorithm for an arbitrary periodic orbit is quite cumbersome to program. There is, however, a class of periodic orbits, orbits with symmetries, which can be easily found by a one-parameter search. The only symmetry left for the dynamics in the fundamental domain is time reversal symmetry; a time reversal symmetric periodic orbit is an orbit whose trajectory in phase space is mapped onto itself when changing $(p_1, p_2) \to (-p_1, -p_2)$, by reversing the direction of the momentum of the orbit. Such an orbit must be a "libration" or self-retracing cycle, an orbit that runs back and forth along the same path in the (r_1, r_2) plane. The cycles $\overline{1}$, $\overline{01}$ and $\overline{001}$ in fig. 29.5 are examples of self-retracing cycles. Luckily, the shortest cycles that we desire most ardently have this symmetry.

Why is this observation helpful? A self-retracing cycle must start perpendicular to the boundary of the fundamental domain, that is, on either of the axis $r_2 = 0$ or $r_1 = r_2$, or on the potential boundary $-\frac{2}{r_1} - \frac{2}{r_2} + \frac{1'}{r_1+r_2} = -1$. By shooting off trajectories perpendicular to the boundaries and monitoring the orbits returning to the boundary with the right symbol length we will find time reversal symmetric cycles by varying the starting point on the boundary as the only parameter. But how can we tell whether a given cycle is self-retracing or not? All the relevant information is contained in the itineraries; a cycle is self-retracing if its itinerary is invariant under time reversal symmetry (that is read backwards) and a suitable number of cyclic permutations. All binary strings up to length 5 fulfill this condition. The symbolic dynamics contains even more information; we can tell at which boundary the total reflection occurs. One finds that an orbit starts out perpendicular

- to the diagonal $r_1 = r_2$ if the itinerary is time reversal invariant and has an odd number of 1's; an example is the cycle $\overline{001}$ in fig. 29.5;
- to the axis $r_2 = 0$ if the itinerary is time reversal invariant and has an even number of symbols; an example is the cycle $\overline{0011}$ in fig. 29.5;
- to the potential boundary if the itinerary is time reversal invariant and has an odd number of symbols; an example is the cycle $\overline{011}$ in fig. 29.5.

All cycles up to symbol length 5 are time reversal invariant, the first two non-time reversal symmetric cycles are cycles $\overline{001011}$ and $\overline{001101}$ in fig. 29.5.

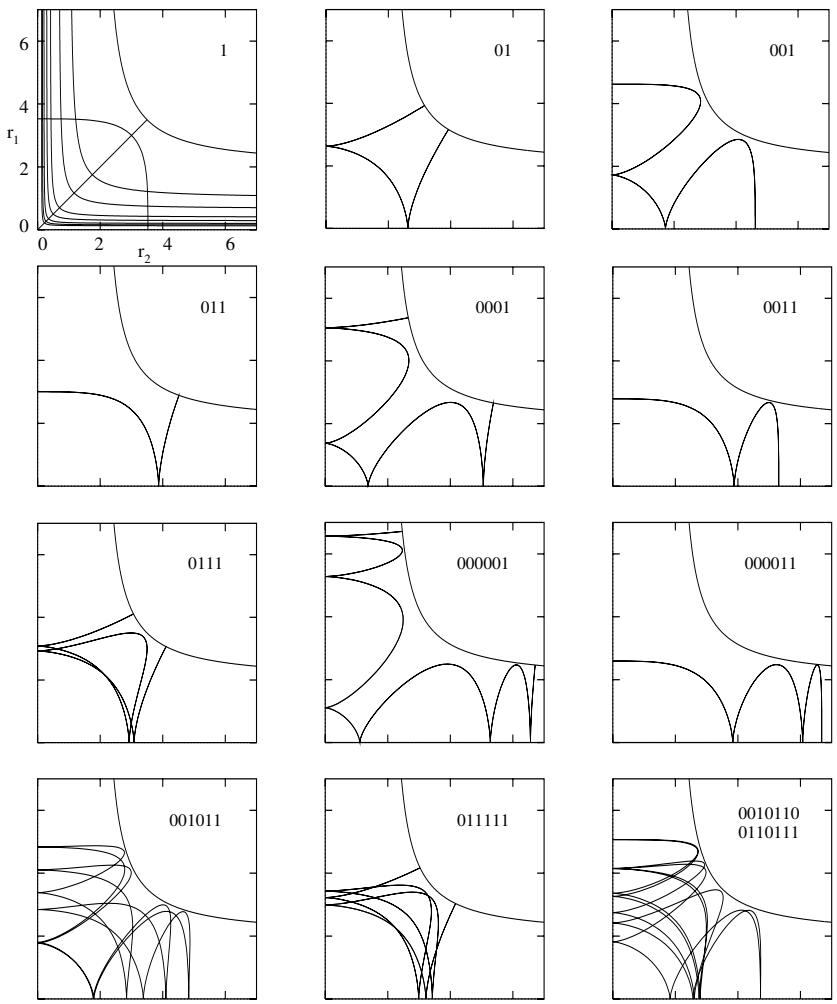

Figure 29.5: Some of the shortest cycles in collinear helium. The classical collinear electron motion is bounded by the potential barrier $-1 = -2/r_1 - 2/r_2 + 1/(r_1 + r_2)$ and the condition $r_i \geq 0$. The orbits are shown in the full r_1–r_2 domain, the itineraries refers to the dynamics in the $r_1 \geq r_2$ fundamental domain. The last figure, the 14-cycle 00101100110111, is an example of a typical cycle with no symmetry.

Their determination would require a two-parameter search. The two cycles are mapped onto each other by time reversal symmetry, that is, they have the same trace in the r_1–r_2 plane, but they trace out distinct cycles in the full phase space.

We are ready to integrate trajectories for classical collinear helium with the help of the equations of motions (29.11) and to find all cycles up to length 5. There is only one thing not yet in place; we need the governing equations for the matrix elements of the Jacobian matrix along a trajectory in order to calculate stability indices. We will provide the main equations in the next section, with the details of the derivation relegated to the appendix C.2.

29.5
page 563

29.1.4 Local coordinates, Jacobian matrix

In this section, we will derive the equations of motion for the Jacobian matrix along a collinear helium trajectory. The Jacobian matrix is 4-dimensional; the two trivial eigenvectors corresponding to the conservation of energy and displacements along a trajectory can, however, be projected out by suitable orthogonal coordinates transformations, see appendix C. We will give the transformation to local coordinates explicitly, here for the regularized coordinates (29.9), and state the resulting equations of motion for the reduced $[2 \times 2]$ Jacobian matrix.

The vector locally parallel to the trajectory is pointing in the direction of the phase space velocity (5.4)

$$v_m = \dot{x}_m(t) = \omega_{mn} \frac{\partial H}{\partial x_n} = (H_{P_1}, H_{P_2}, -H_{Q_1}, -H_{Q_2})^T,$$

with $H_{Q_i} = \frac{\partial H}{\partial Q_i}$, and $H_{P_i} = \frac{\partial H}{\partial P_i}$, $i = 1{,}2$. The vector perpendicular to a trajectory $x(t) = (Q_1(t), Q_2(t), P_1(t), P_2(t))$ and to the energy manifold is given by the gradient of the Hamiltonian (29.10)

$$\gamma = \nabla H = (H_{Q_1}, H_{Q_2}, H_{P_1}, H_{P_2})^T .$$

By symmetry $v_m \gamma_m = \omega_{mn} \frac{\partial H}{\partial x_n} \frac{\partial H}{\partial x_m}$, so the two vectors are orthogonal.

Next, we consider the orthogonal matrix

$$\begin{aligned} \mathbf{O}_{\gamma(t)} &= (\gamma_1, \gamma_2, \gamma/R, v) \qquad (29.12) \\ &= \begin{pmatrix} -H_{P_2}/R & H_{Q_2} & H_{Q_1}/R & H_{P_1} \\ H_{P_1}/R & -H_{Q_1} & H_{Q_2}/R & H_{P_2} \\ -H_{Q_2}/R & -H_{P_2} & H_{P_1}/R & -H_{Q_1} \\ H_{Q_1}/R & H_{P_1} & H_{P_2}/R & -H_{Q_2} \end{pmatrix} \end{aligned}$$

with $R = |\nabla H|^2 = (H_{Q_1}^2 + H_{Q_2}^2 + H_{P_1}^2 + H_{P_2}^2)$, which provides a transformation to local phase space coordinates centered on the trajectory $x(t)$ along the two vectors (γ, v). The vectors $\gamma_{1,2}$ are phase space vectors perpendicular to the trajectory and to the energy manifold in the 4-dimensional phase space of collinear helium. The Jacobian matrix (4.5) rotated to the local coordinate system by $\mathbf{O}$ then has the form

29.6
page 564

$$\mathbf{m} = \begin{pmatrix} m_{11} & m_{12} & * & 0 \\ m_{21} & m_{22} & * & 0 \\ 0 & 0 & 1 & 0 \\ * & * & * & 1 \end{pmatrix}, \quad \mathbf{J} = \mathbf{O}^{\mathbf{T}}\mathbf{m}\mathbf{O}\sigma$$

The linearized motion perpendicular to the trajectory on the energy manifold is described by the $[2 \times 2]$ matrix $\mathbf{m}$; the 'trivial' directions correspond to unit eigenvalues on the diagonal in the 3rd and 4th column and row.

The equations of motion for the reduced Jacobian matrix $\mathbf{m}$ are given by

$$\dot{\mathbf{m}} = \mathrm{l}(t)\mathbf{m}(t), \tag{29.13}$$

with $\mathbf{m}(0) = \mathbf{1}$. The matrix l depends on the trajectory in phase space and has the form

$$\mathrm{l} = \begin{pmatrix} l_{11} & l_{12} & * & 0 \\ l_{21} & l_{22} & * & 0 \\ 0 & 0 & 0 & 0 \\ * & * & * & 0 \end{pmatrix},$$

where the relevant matrix elements l_{ij} are given by

$$\begin{aligned} l_{11} &= \frac{1}{R}[2H_{Q_1Q_2}(H_{Q_2}H_{P_1} + H_{Q_1}H_{P_2}) \\ &\quad +(H_{Q_1}H_{P_1} - H_{Q_2}H_{P_2})(H_{Q_1Q_1} - H_{Q_2Q_2} - H_{P_1P_1} + H_{P_2P_2})] \\ l_{12} &= -2H_{Q_1Q_2}(H_{Q_1}H_{Q_2} - H_{P_1}H_{P_2}) \\ &\quad +(H_{Q_1}^2 + H_{P_2}^2)(H_{Q_2Q_2} + H_{P_1P_1}) + (H_{Q_2}^2 + H_{P_1}^2)(H_{Q_1Q_1} + H_{P_2P_2}) \\ l_{21} &= \frac{1}{R^2}[2(H_{Q_1P_2} + H_{Q_2P_1})(H_{Q_2}H_{P_1} + H_{Q_1}H_{P_8}) \\ &\quad -(H_{P_1}^2 + H_{P_2}^2)(H_{Q_1Q_1} + H_{Q_2Q_2}) - (H_{Q_1}^2 + H_{Q_2}^2)(H_{P_1P_1} + H_{P_2P_2})] \\ l_{22} &= -l_{11}\,. \end{aligned} \tag{29.14}$$

Here $H_{Q_iQ_j}$, $H_{P_iP_j}$, i, $j = 1, 2$ are the second partial derivatives of H with respect to the coordinates Q_i, P_i, evaluated at the phase space coordinate of the classical trajectory.

p	$S_p/2\pi$	$\ln \lvert\Lambda_p\rvert$	σ_p	m_p
1	1.82900	0.6012	0.5393	2
01	3.61825	1.8622	1.0918	4
001	5.32615	3.4287	1.6402	6
011	5.39451	1.8603	1.6117	6
0001	6.96677	4.4378	2.1710	8
0011	7.04134	2.3417	2.1327	8
0111	7.25849	3.1124	2.1705	8
00001	8.56618	5.1100	2.6919	10
00011	8.64306	2.7207	2.6478	10
00101	8.93700	5.1562	2.7291	10
00111	8.94619	4.5932	2.7173	10
01011	9.02689	4.1765	2.7140	10
01111	9.07179	3.3424	2.6989	10
000001	10.13872	5.6047	3.2073	12
000011	10.21673	3.0323	3.1594	12
000101	10.57067	6.1393	3.2591	12
000111	10.57628	5.6766	3.2495	12
001011	10.70698	5.3251	3.2519	12
001101	10.70698	5.3251	3.2519	12
001111	10.74303	4.3317	3.2332	12
010111	10.87855	5.0002	3.2626	12
011111	10.91015	4.2408	3.2467	12

Table 29.1: Action S_p (in units of 2π), Lyapunov exponent $|\Lambda_p|/T_p$ for the motion in the collinear plane, winding number σ_p for the motion perpendicular to the collinear plane, and the topological index m_p for all fundamental domain cycles up to topological length 6.

29.1.5 Getting ready

Now everything is in place: the regularized equations of motion can be implemented in a Runge–Kutta or any other integration scheme to calculate trajectories. We have a symbolic dynamics and know how many cycles there are and how to find them (at least up to symbol length 5). We know how to compute the Jacobian matrix whose eigenvalues enter the semiclassical spectral determinant (27.12). By (26.16) the action S_p is proportional to the period of the orbit, $S_p = 2T_p$.

There is, however, still a slight complication. Collinear helium is an invariant 4-dimensional subspace of the full helium phase space. If we restrict the dynamics to angular momentum equal zero, we are left with 6 phase space coordinates. That is not a problem when computing periodic orbits, they are oblivious to the other dimensions. However, the Jacobian matrix does pick up extra contributions. When we calculate the Jacobian matrix for the full problem, we must also allow for displacements out of the collinear plane, so the full Jacobian matrix for dynamics for $L = 0$ angular momentum is 6 dimensional. Fortunately, the linearized dynamics in and off the collinear helium subspace decouple, and the Jacobian matrix can be written in terms of two distinct $[2 \times 2]$ matrices, with trivial eigendirections providing the remaining two dimensions. The submatrix related to displacements off the linear configuration characterizes the linearized dynamics in the additional degree of freedom, the Θ-coordinate in fig. 29.1. It turns out that the linearized dynamics in the Θ coordinate is stable, corresponding to a bending type motion of the two electrons. We will need the stability exponents for all degrees of freedom in evaluating the semiclassical spectral determinant in sect. 29.2.

The numerical values of the actions, stability exponents, stability angles, and topological indices for the shortest cycles are listed in table 29.1.4. These numbers, needed for the semiclassical quantization implemented in the next section, an also be helpful in checking your own calculations.

29.2 Semiclassical quantization of collinear helium

Before we get down to a serious calculation of the helium quantum energy levels let us have a brief look at the overall structure of the spectrum. This will give us a preliminary feel for which parts of the helium spectrum are accessible with the help of our collinear model – and which are not. In order to keep the discussion as simple as possible and to concentrate on the semiclassical aspects of our calculations we offer here only a rough overview. For a guide to more detailed accounts see remark 29.4.

29.2.1 Structure of helium spectrum

We start by recalling Bohr's formula for the spectrum of hydrogen like one-electron atoms. The eigenenergies form a Rydberg series

$$E_N = -\frac{e^4 m_e}{\hbar^2}\frac{Z^2}{2N^2}\,, \tag{29.15}$$

where Ze is the charge of the nucleus and m_e is the mass of the electron. Through the rest of this chapter we adopt the atomic units $e = m_e = \hbar = 1$.

The simplest model for the helium spectrum is obtained by treating the two electrons as independent particles moving in the potential of the nucleus neglecting the electron–electron interaction. Both electrons are then bound in hydrogen like states; the inner electron will see a charge $Z = 2$, screening at the same time the nucleus, the outer electron will move in a Coulomb potential with effective charge $Z - 1 = 1$. In this way obtain a first estimate for the total energy

$$E_{N,n} = -\frac{2}{N^2} - \frac{1}{2n^2} \qquad \text{with} \quad n > N. \tag{29.16}$$

This double Rydberg formula contains already most of the information we need to understand the basic structure of the spectrum. The (correct) ionizations thresholds $E_N = -\frac{2}{N^2}$ are obtained in the limit $n \to \infty$, yielding the ground and excited states of the helium ion He^+. We will therefore refer to N as the principal quantum number. We also see that all states $E_{N,n}$ with $N \geq 2$ lie above the first ionization threshold for $N = 1$. As soon as we switch on electron-electron interaction these states are no longer bound states; they turn into resonant states which decay into a bound state of the helium ion and a free outer electron. This might not come as a big surprise if we have the classical analysis of the previous section in mind: we already found that one of the classical electrons will almost always escape after some finite time. More remarkable is the fact that the first, $N = 1$ series consists of true bound states for all n, an effect which can only be understood by quantum arguments.

The hydrogen-like quantum energies (29.15) are highly degenerate; states with different angular momentum but the same principal quantum number N share the same energy. We recall from basic quantum mechanics of hydrogen atom that the possible angular momenta for a given N span $l = 0, 1 \ldots N-1$. How does that affect the helium case? Total angular momentum L for the helium three-body problem is conserved. The collinear helium is a subspace of the classical phase space for $L = 0$; we thus expect that we can only quantize helium states corresponding to the total angular

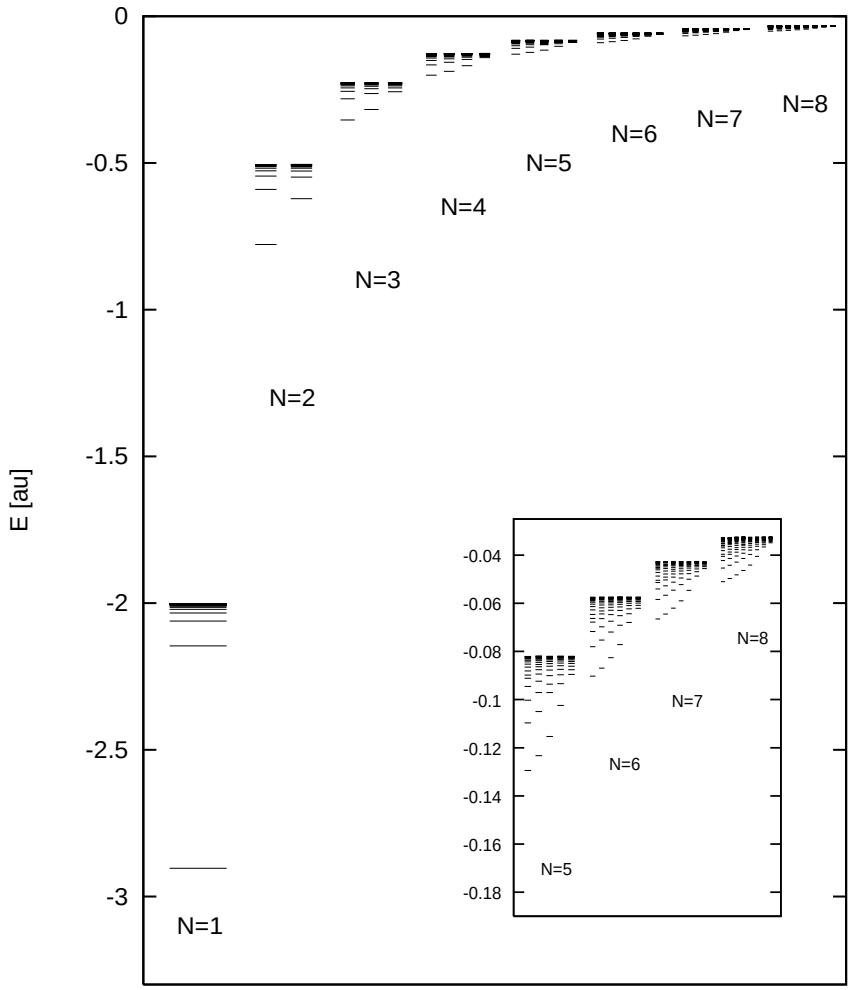

Figure 29.6: The exact quantum helium spectrum for $L = 0$. The energy levels denoted by bars have been obtained from full 3-dimensional quantum calculations [29.3].

momentum zero, a subspectrum of the full helium spectrum. Going back to our crude estimate (29.16) we may now attribute angular momenta to the two independent electrons, l_1 and l_2 say. In order to obtain total angular momentum $L = 0$ we need $l_1 = l_2 = l$ and $l_{z1} = -l_{z2}$, that is, there are N different states corresponding to $L = 0$ for fixed quantum numbers N, n. That means that we expect N different Rydberg series converging to each ionization threshold $E_N = -2/N^2$. This is indeed the case and the N different series can be identified also in the exact helium quantum spectrum, see fig. 29.6. The degeneracies between the different N Rydberg series corresponding to the same principal quantum number N, are removed by the electron-electron interaction. We thus already have a rather good idea of the coarse structure of the spectrum.

In the next step, we may even speculate which parts of the $L = 0$ spectrum can be reproduced by the semiclassical quantization of collinear helium. In the collinear helium, both classical electrons move back and forth along a common axis through the nucleus, so each has zero angular momentum. We therefore expect that collinear helium describes the Rydberg series with $l = l_1 = l_2 = 0$. These series are the energetically lowest states for fixed (N, n), corresponding to the Rydberg series on the outermost left side of the spectrum in fig. 29.6. We will see in the next section that this is indeed the case and that the collinear model holds down to the $N = 1$ bound state series, including even the ground state of helium! We will also find a semiclassical quantum number corresponding to the angular momentum l and show that the collinear model describes states for moderate angular momentum l as long as $l \ll N$. .

☞ remark 29.4

29.2.2 Semiclassical spectral determinant for collinear helium

Nothing but lassitude can stop us now from calculating our first semiclassical eigenvalues. The only thing left to do is to set up the spectral determinant in terms of the periodic orbits of collinear helium and to write out the first few terms of its cycle expansion with the help of the binary symbolic dynamics. The semiclassical spectral determinant (27.12) has been written as product over all cycles of the classical systems. The energy dependence in collinear helium enters the classical dynamics only through simple scaling transformations described in sect. 29.1.1 which makes it possible to write the semiclassical spectral determinant in the form

$$\det\left(\hat{H} - E\right)_{sc} = \exp\left(-\sum_p \sum_{r=1}^{\infty} \frac{1}{r} \frac{e^{ir(sS_p - m_p\frac{\pi}{2})}}{(-\det\left(1 - \mathbf{J}^r_{p\perp}\right))^{1/2} |\det\left(1 - \mathbf{J}^r_{p||}\right)|^{1/2}}\right), \quad (29.17)$$

with the energy dependence absorbed into the variable

$$s = \frac{e^2}{\hbar}\sqrt{\frac{m_e}{-E}},$$

obtained by using the scaling relation (29.3) for the action. As explained in sect. 29.1.4, the fact that the $[4 \times 4]$ Jacobian matrix decouples into two $[2 \times 2]$ submatrices corresponding to the dynamics *in* the collinear space and *perpendicular* to it makes it possible to write the denominator in terms of a product of two determinants. Stable and unstable degrees of freedom enter the trace formula in different ways, reflected by the absence of the modulus sign and the minus sign in front of $\det\left(1 - \mathbf{J}_\perp\right)$. The topological index m_p

corresponds to the unstable dynamics in the collinear plane. Note that the factor $e^{i\pi\bar{N}(E)}$ present in (27.12) is absent in (29.17). Collinear helium is an open system, that is the eigenenergies are resonances corresponding to the complex zeros of the semiclassical spectral determinant and the mean energy staircase $\bar{N}(E)$ not defined. In order to obtain a spectral determinant as an infinite product of the form (27.18) we may proceed as in (12.9) by expanding the determinants in (29.17) in terms of the eigenvalues of the corresponding Jacobian matrices. The matrix representing displacements perpendicular to the collinear space has eigenvalues of the form $\exp(\pm 2\pi i\sigma)$, reflecting stable linearized dynamics. σ is the full winding number along the orbit in the stable degree of freedom, multiplicative under multiple repetitions of this orbit .The eigenvalues corresponding to the unstable dynamics along the collinear axis are paired as $\{\Lambda, 1/\Lambda\}$ with $|\Lambda| > 1$ and real. As in (12.9) and (27.18) we may thus write

$$\begin{aligned}
&\left[-\det\left(1-\mathbf{J}_{\perp}^{r}\right)|\det\left(1-\mathbf{J}_{\parallel}^{r}\right)|\right]^{-1/2} \qquad (29.18)\\
&= \left[-(1-\Lambda^{r})(1-\Lambda^{-r})|(1-e^{2\pi i r\sigma})(1-e^{-2\pi i r\sigma})\right]^{-1/2}\\
&= \sum_{k,\ell=0}^{\infty}\frac{1}{|\Lambda^{r}|^{1/2}\Lambda^{rk}}e^{-ir(\ell+1/2)\sigma}\,.
\end{aligned}$$

The $\pm$ sign corresponds to the hyperbolic/inverse hyperbolic periodic orbits with positive/negative eigenvalues Λ. Using the relation (29.19) we see that the sum over r in (29.17) is the expansion of the logarithm, so the semiclassical spectral determinant can be rewritten as a product over dynamical zeta functions, as in (12.9):

$$\det\left(\hat{H}-E\right)_{sc} = \prod_{k=0}^{\infty}\prod_{m=0}^{\infty}\zeta_{k,m}^{-1} = \prod_{k=0}^{\infty}\prod_{m=0}^{\infty}\prod_{p}(1-t_{p}^{(k,m)})\,, \qquad (29.19)$$

where the cycle weights are given by

$$t_{p}^{(k,m)} = \frac{1}{|\Lambda|^{1/2}\Lambda^{k}}e^{i\left(sS_{p}-m_{p}\frac{\pi}{2}-4\pi(\ell+1/2)\sigma_{p}\right)}\,, \qquad (29.20)$$

and m_p is the topological index for the motion in the collinear plane which equals twice the topological length of the cycle. The two independent directions perpendicular to the collinear axis lead to a twofold degeneracy in this degree of freedom which accounts for an additional factor 2 in front of the winding number σ. The values for the actions, winding numbers and stability indices of the shortest cycles in collinear helium are listed in table 29.1.4.

The integer indices ℓ and k play very different roles in the semiclassical spectral determinant (29.19). A linearized approximation of the flow along a cycle corresponds to a harmonic approximation of the potential in the vicinity of the trajectory. Stable motion corresponds to a harmonic oscillator potential, unstable motion to an inverted harmonic oscillator. The index ℓ which contributes as a phase to the cycle weights in the dynamical zeta functions can therefore be interpreted as a harmonic oscillator quantum number; it corresponds to vibrational modes in the Θ coordinate and can in our simplified picture developed in sect. 29.2.1 be related to the quantum number $l = l_1 = l_2$ representing the single particle angular momenta. Every distinct ℓ value corresponds to a full spectrum which we obtain from the zeros of the semiclassical spectral determinant $1/\zeta_\ell$ keeping ℓ fixed. The harmonic oscillator approximation will eventually break down with increasing off-line excitations and thus increasing ℓ. The index k corresponds to 'excitations' along the unstable direction and can be identified with local resonances of the inverted harmonic oscillator centered on the given orbit. The cycle contributions $t_p^{(k,m)}$ decrease exponentially with increasing k. Higher k terms in an expansion of the determinant give corrections which become important only for large negative imaginary s values. As we are interested only in the leading zeros of (29.19), that is the zeros closest to the real energy axis, it is sufficient to take only the $k = 0$ terms into account.

Next, let us have a look at the discrete symmetries discussed in sect. 29.1.3. Collinear helium has a C_2 symmetry as it is invariant under reflection across the $r_1 = r_2$ line corresponding to the electron-electron exchange symmetry. As explained in sects. 19.1.2 and 19.5, we may use this symmetry to factorize the semiclassical spectral determinant. The spectrum corresponding to the states symmetric or antisymmetric with respect to reflection can be obtained by writing the dynamical zeta functions in the symmetry factorized form

$$1/\zeta^{(\ell)} = \prod_a (1 - t_a)^2 \prod_{\tilde{s}} (1 - t_{\tilde{s}}^2)\,. \tag{29.21}$$

Here, the first product is taken over all asymmetric prime cycles, that is cycles that are not self-dual under the C_2 symmetry. Such cycles come in pairs, as two equivalent orbits are mapped into each other by the symmetry transformation. The second product runs over all self-dual cycles; these orbits cross the axis $r_1 = r_2$ twice at a right angle. The self-dual cycles close in the fundamental domain $r_1 \leq r_2$ already at half the period compared to the orbit in the full domain, and the cycle weights $t_{\tilde{s}}$ in (29.21) are the weights of fundamental domain cycles. The C_2 symmetry now leads to the

factorization of (29.21) $1/\zeta = \zeta_+^{-1}\zeta_-^{-1}$, with

$$
\begin{aligned}
1/\zeta_+^{(\ell)} &= \prod_a (1-t_a) \prod_{\tilde{s}} (1-t_{\tilde{s}}) \,, \\
1/\zeta_-^{(\ell)} &= \prod_a (1-t_a) \prod_{\tilde{s}} (1+t_{\tilde{s}}) \,,
\end{aligned}
\tag{29.22}
$$

setting $k = 0$ in what follows. The symmetric subspace resonances are given by the zeros of $1/\zeta_+^{(\ell)}$, antisymmetric resonances by the zeros of $1/\zeta_-^{(\ell)}$, with the two dynamical zeta functions defined as products over orbits in the fundamental domain. The symmetry properties of an orbit can be read off directly from its symbol sequence, as explained in sect. 29.1.3. An orbit with an odd number of 1's in the itinerary is self-dual under the C_2 symmetry and enters the spectral determinant in (29.22) with a negative or a positive sign, depending on the symmetry subspace under consideration.

29.2.3 Cycle expansion results

So far we have established a factorized form of the semiclassical spectral determinant and have thereby picked up two *good quantum numbers*; the quantum number m has been identified with an excitation of the bending vibrations, the exchange symmetry quantum number ± 1 corresponds to states being symmetric or antisymmetric with respect to the electron-electron exchange. We may now start writing down the binary cycle expansion (15.5) and determine the zeros of spectral determinant. There is, however, still another problem: there is no cycle 0 in the collinear helium. The symbol sequence $\overline{0}$ corresponds to the limit of an outer electron fixed with zero kinetic energy at $r_1 = \infty$, the inner electron bouncing back and forth into the singularity at the origin. This introduces intermittency in our system, a problem discussed in chapter 18. We note that the behavior of cycles going far out in the channel r_1 or $r_2 \to \infty$ is very different from those staying in the near core region. A cycle expansion using the binary alphabet reproduces states where both electrons are localized in the near core regions: these are the lowest states in each Rydberg series. The states converging to the various ionization thresholds $E_N = -2/N^2$ correspond to eigenfunctions where the wave function of the outer electron is stretched far out into the ionization channel $r_1, r_2 \to \infty$. To include those states, we have to deal with the dynamics in the limit of large r_1, r_2. This turns out to be equivalent to switching to a symbolic dynamics with an infinite alphabet. With this observation in mind, we may write the cycle expansion (....) for a binary alphabet without the $\overline{0}$ cycle as

☞ remark 29.5

$$1/\zeta^{\ell}(s) = 1 - t_1^{(\ell)} - t_{01}^{(\ell)} - [t_{001}^{(\ell)} + t_{011}^{(\ell)} - t_{01}^{(\ell)} t_1^{(\ell)}] - [t_{0001}^{(\ell)} + t_{0011}^{(\ell)} - t_{001}^{(\ell)} t_1^{(\ell)} + t_{0111}^{(\ell)} - t_{011}^{(\ell)} t_1^{(\ell)}] - \ldots \quad (29.23)$$

The weights $t_p^{(\ell)}$ are given in (29.19), with contributions of orbits and composite orbits of the same total symbol length collected within square brackets. The cycle expansion depends only on the classical actions, stability indices and winding numbers, given for orbits up to length 6 in table 29.1.4. To get reacquainted with the cycle expansion formula (29.23), consider a truncation of the series after the first term

$$1/\zeta^{(\ell)}(s) \approx 1 - t_1 \,.$$

The quantization condition $1/\zeta^{(\ell)}(s) = 0$ leads to

$$E_{m,N} = -\frac{(S_1/2\pi)^2}{[m + \frac{1}{2} + 2(N + \frac{1}{2})\sigma_1]^2}, \qquad m, N = 0, 1, 2, \ldots \,, \quad (29.24)$$

with $S_1/2\pi = 1.8290$ for the action and $\sigma_1 = 0.5393$ for the winding number, see table 29.1.4, the 1 cycle in the fundamental domain. This cycle can be described as the *asymmetric stretch* orbit, see fig. 29.5. The additional quantum number N in (29.24) corresponds to the principal quantum number defined in sect. 29.2.1. The states described by the quantization condition (29.24) are those centered closest to the nucleus and correspond therefore to the lowest states in each Rydberg series (for a fixed m and N values), in fig. 29.6. The simple formula (29.24) gives already a rather good estimate for the ground state of helium! Results obtained from (29.24) are tabulated in table 29.2, see the 3rd column under $j = 1$ and the comparison with the full quantum calculations.

In order to obtain higher excited quantum states, we need to include more orbits in the cycle expansion (29.23), covering more of the phase space dynamics further away from the center. Taking longer and longer cycles into account, we indeed reveal more and more states in each N-series for fixed m. This is illustrated by the data listed in table 29.2 for symmetric states obtained from truncations of the cycle expansion of $1/\zeta_+$.

29.7
page 564

Results of the same quality are obtained for antisymmetric states by calculating the zeros of $1/\zeta_-^{(\ell)}$. Repeating the calculation with $\ell = 1$ or higher in (29.22) reveals states in the Rydberg series which are to the right of the energetically lowest series in fig. 29.6.

N	n	$j=1$	$j=4$	$j=8$	$j=12$	$j=16$	$-E_{\rm qm}$
1	1	3.0970	2.9692	2.9001	2.9390	2.9248	2.9037
2	2	0.8044	0.7714	0.7744	0.7730	0.7727	0.7779
2	3	—	0.5698	0.5906	0.5916	0.5902	0.5899
2	4	—	—	—	0.5383	0.5429	0.5449
3	3	0.3622	0.3472	0.3543	0.3535	0.3503	0.3535
3	4	—	—	0.2812	0.2808	0.2808	0.2811
3	5	—	—	0.2550	0.2561	0.2559	0.2560
3	6	—	—	—	0.2416	0.2433	0.2438
4	4	0.2050	0.1962	0.1980	0.2004	0.2012	0.2010
4	5	—	0.1655	0.1650	0.1654	0.1657	0.1657
4	6	—	—	0.1508	0.1505	0.1507	0.1508
4	7	—	—	0.1413	0.1426	0.1426	0.1426

Table 29.2: Collinear helium, real part of the symmetric subspace resonances obtained by a cycle expansion (29.23) up to cycle length j. The exact quantum energies [29.3] are in the last column. The states are labeled by their principal quantum numbers. A dash as an entry indicates a missing zero at that level of approximation.

Commentary

Remark 29.1 Sources. The full 3-dimensional Hamiltonian after elimination of the center of mass coordinates, and an account of the finite nucleus mass effects is given in ref. [29.2]. The general two–body collision regularizing Kustaanheimo–Stiefel transformation [29.5], a generalization of Levi-Civita's [29.13] Pauli matrix two–body collision regularization for motion in a plane, is due to Kustaanheimo [29.12] who realized that the correct higher-dimensional generalization of the "square root removal" trick (29.7), by introducing a vector Q with property $r = |Q|^2$, is the same as Dirac's trick of getting linear equation for spin $1/2$ fermions by means of spinors. Vector spaces equipped with a product and a known satisfy $|Q \cdot Q| = |Q|^2$ define *normed algebras*. They appear in various physical applications - as quaternions, octonions, spinors. The technique was originally developed in celestial mechanics [29.6] to obtain numerically stable solutions for planetary motions. The basic idea was in place as early as 1931, when H. Hopf [29.14] used a KS transformation in order to illustrate a Hopf's invariant. The KS transformation for the collinear helium was introduced in ref. [29.2].

Remark 29.2 Complete binary symbolic dynamics. No stable periodic orbit and no exception to the binary symbolic dynamics of the collinear helium cycles have been found in numerical investigations. A proof that all cycles are unstable, that they are uniquely labelled by the binary symbolic dynamcis, and that this dynamics is complete

is, however, still missing. The conjectured Markov partition of the phase space is given by the triple collision manifold, that is by those trajectories which start in or end at the singular point $r_1 = r_2 = 0$. See also ref. [29.2].

Remark 29.3 Spin and particle exchange symmetry. In our presentation of collinear helium we have completely ignored all dynamical effects due to the spin of the particles involved, such as the electronic spin-orbit coupling. Electrons are fermions and that determines the symmetry properties of the quantum states. The total wave function, including the spin degrees of freedom, must be antisymmetric under the electron-electron exchange transformation. That means that a quantum state symmetric in the position variables must have an antisymmetric spin wave function, i.e. the spins are antiparallel and the total spin is zero (singletstate). Antisymmetric states have symmetric spin wave function with total spin 1 (tripletstates). The threefold degeneracy of spin 1 states is lifted by the spin-orbit coupling.

Remark 29.4 Helium quantum numbers. The classification of the helium states in terms of single electron quantum numbers, sketched in sect. 29.2.1, prevailed until the 1960's; a growing discrepancy between experimental results and theoretical predictions made it necessary to refine this picture. In particular, the different Rydberg series sharing a given N-quantum number correspond, roughly speaking, to a quantization of the inter electronic angle Θ, see fig. 29.1, and can not be described in terms of single electron quantum numbers l_1, l_2. The fact that something is slightly wrong with the single electron picture laid out in sect. 29.2.1 is highlighted when considering the collinear configuration where both electrons are on the *same* side of the nucleus. As both electrons again have angular momentum equal to zero, the corresponding quantum states should also belong to single electron quantum numbers $(l_1, l_2) = (0, 0)$. However, the single electron picture breaks down completely in the limit $\Theta = 0$ where electron-electron interaction becomes the dominant effect. The quantum states corresponding to this classical configuration are distinctively different from those obtained from the collinear dynamics with electrons on different sides of the nucleus. The Rydberg series related to the classical $\Theta = 0$ dynamics are on the outermost rigth side in each N subspectrum in fig. 29.6, and contain the energetically highest states for given N, n quantum numbers, see also remark 29.5. A detailed account of the historical development as well as a modern interpretation of the spectrum can be found in ref. [29.1].

Remark 29.5 Beyond the unstable collinear helium subspace. The semiclassical quantization of the chaotic collinear helium subspace is

discussed in refs. [29.7, 29.8, 29.9]. Classical and semiclassical considerations beyond what has been discussed in sect. 29.2 follow several other directions, all outside the main of this book.

A classical study of the dynamics of collinear helium where both electrons are on the same side of the nucleus reveals that this configuration is fully stable both in the collinear plane and perpendicular to it. The corresponding quantum states can be obtained with the help of an approximate EBK-quantization which reveals helium resonances with extremely long lifetimes (quasi - bound states in the continuum). These states form the energetically highest Rydberg series for a given principal quantum number N, see fig. 29.6. Details can be found in refs. [29.10, 29.11].

In order to obtain the Rydberg series structure of the spectrum, that is the succession of states converging to various ionization thresholds, we need to take into account the dynamics of orbits which make large excursions along the r_1 or r_2 axis. In the chaotic collinear subspace these orbits are characterized by symbol sequences of form $(a0^n)$ where a stands for an arbitrary binary symbol sequence and 0^n is a succession of n 0's in a row. A summation of the form $\sum_{n=0}^{\infty} t_{a\,0^n}$, where t_p are the cycle weights in (29.19), and cycle expansion of indeed yield all Rydbergstates up the various ionization thresholds, see ref. [29.4].

For a comprehensive overview on spectra of two-electron atoms and semiclassical treatments ref. [29.1].

Résumé

We have covered a lot of ground starting with considerations of the classical properties of a three-body Coulomb problem, and ending with the semiclassical helium spectrum. We saw that the three-body problem restricted to the dynamics on a collinear appears to be fully chaotic; this implies that traditional semiclassical methods such as *WKB*quantization will not work and that we needed the full periodic orbit theory to obtain leads to the semiclassical spectrum of helium. As a piece of unexpected luck the symbolic dynamics is simple, and the semiclassical quantization of the collinear dynamics yields an important part of the helium spectrum, including the ground state, to a reasonable accuracy. A sceptic might say: "Why bother with all the semiclassical considerations? A straightforward numerical quantum calculation achieves the same goal with better precision." While this is true, the semiclassical analysis offers new insights into the *structure* of the spectrum. We discovered that the dynamics perpendicular to the collinear plane was stable, giving rise to an additional (approximate) quantum number ℓ. We thus understood the origin of the different Rydberg series depicted in fig. 29.6, a fact which is not at all obvious from a numerical solution of the quantum problem.

Having traversed the long road from the classical game of pinball all the way to a credible helium spectrum computation, we could declare victory and fold down this enterprise. Nevertheless, there is still much to think about - what about such quintessentially quantum effects as diffraction, tunnelling, ...? As we shall now see, the periodic orbit theory has still much of interest to offer.

References

[29.1] G. Tanner, J-M. Rost and K. Richter, Rev. Mod. Phys. **72**, 497 (2000).

[29.2] K. Richter, G. Tanner, and D. Wintgen, Phys. Rev. A **48**, 4182 (1993).

[29.3] Bürgers A., Wintgen D. and Rost J. M., J. Phys. B **28**, 3163 (1995).

[29.4] G. Tanner and D. Wintgen Phys. Rev. Lett. **75** 2928 (1995).

[29.5] P. Kustaanheimo and E. Stiefel, *J. Reine Angew. Math.* **218**, 204 (1965).

[29.6] E.L. Steifel and G. Scheifele, *Linear and regular celestial mechanics* (Springer, New York 1971).

[29.7] G.S. Ezra, K. Richter, G. Tanner and D. Wintgen, J. Phys. B **24**, L413 (1991).

[29.8] D. Wintgen, K. Richter and G. Tanner, CHAOS **2**, 19 (1992).

[29.9] R. Blümel and W. P. Reinhardt, *Directions in Chaos Vol 4*, eds. D. H. Feng and J.-M. Yuan (World Scientific, Hongkong), 245 (1992).

[29.10] K. Richter and D. Wintgen, J. Phys. B **24**, L565 (1991).

[29.11] D. Wintgen and K. Richter, Comments At. Mol. Phys. **29**, 261 (1994).

[29.12] P. Kustaanheimo, *Ann. Univ. Turku, Ser. AI.,* **73** (1964).

[29.13] T. Levi-Civita, *Opere mathematische* **2** (1956).

[29.14] H. Hopf, *Math. Ann.* **104** (1931).

Exercises

Exercise 29.1 **Kustaanheimo–Stiefel transformation.** *Check the Kustaanheimo–Stiefel regularization for collinear helium; derive the Hamiltonian (29.10) and the collinear helium equations of motion (29.11).*

Exercise 29.2 **Helium in the plane.** *Starting with the helium Hamiltonian in the infinite nucleus mass approximation $m_{he} = \infty$, and angular momentum $L = 0$, show that the three body problem can be written in terms of three independent coordinates only, the electron-nucleus distances r_1 and r_2 and the inter-electron angle Θ, see fig. 29.1.*

Exercise 29.3 **Helium trajectories.** *Do some trial integrations of the collinear helium equations of motion (29.11). Due to the energy conservation, only three of the phase space coordinates (Q_1, Q_2, P_1, P_2) are independent. Alternatively, you can integrate in 4 dimensions and use the energy conservation as a check on the quality of your integrator.*

The dynamics can be visualized as a motion in the original configuration space (r_1, r_2), $r_i \geq 0$ quadrant, or, better still, by an appropriately chosen 2-d Poincaré section, exercise 29.4. Most trajectories will run away, do not be surprised - the classical collinear helium is unbound. Try to guess approximately the shortest cycle of fig. 29.4.

Exercise 29.4 **A Poincaré section for collinear Helium.** *Construct a Poincaré section of fig. 29.3b that reduces the helium flow to a map. Try to delineate regions which correspond to finite symbol sequences, that is initial conditions that follow the same topological itinerary in the fig. 29.3a space for a finite number of bounces. Such rough partition can be used to initiate 2–dimensional Newton-Raphson method searches for helium cycles, exercise 29.5.*

Exercise 29.5 **Collinear helium cycles.** *The motion in the (r_1, r_2) plane is topologically similar to the pinball motion in a 3-disk system, except that the motion is in the Coulomb potential.*

Just as in the 3-disk system the dynamics is simplified if viewed in the fundamental domain, *in this case the region between r_1 axis and the $r_1 = r_2$ diagonal. Modify your integration routine so the trajectory bounces off the diagonal as off a mirror. Miraculously, the symbolic dynamics for the survivors again turns out to be binary, with 0 symbol signifying a bounce off the r_1 axis, and 1 symbol for a bounce off the diagonal. Just as in the 3-disk game of pinball, we thus know what cycles need to be computed for the cycle expansion (29.23).*

Guess some short cycles by requiring that topologically they correspond to sequences of bounces either returning to the same r_i axis or reflecting off the diagonal. Now either Use special symmetries of orbits such as self-retracing to find all orbits up to length 5 by a 1-dimensional Newton search.

Exercise 29.6 **Collinear helium cycle stabilities.** *Compute the eigenvalues for the cycles you found in exercise 29.5, as described in sect. 29.1.4. You may either integrate the reduced 2×2 matrix using equations (29.13) together with the generating function l given in local coordinates by (29.14) or integrate the full 4×4 Jacobian matrix, see sect. 17.1. Integration in 4 dimensions should give eigenvalues of the form $(1, 1, \Lambda_p, 1/\Lambda_p)$; The unit eigenvalues are due to the usual periodic orbit invariances; displacements along the orbit as well as perpendicular to the energy manifold are conserved; the latter one provides a check of the accuracy of your computation. Compare with table 29.1.4; you should get the actions and Lyapunov exponents right, but topological indices and stability angles we take on faith.*

Exercise 29.7 **Helium eigenenergies.** *Compute the lowest eigenenergies of singlet and triplet states of helium by substituting cycle data into the cycle expansion (29.23) for the symmetric and antisymmetric zeta functions (29.22). Probably the quickest way is to plot the magnitude of the zeta function as function of real energy and look for the minima. As the eigenenergies in general have a small imaginary part, a contour plot such as fig. 15.1, can yield informed guesses. Better way would be to find the zeros by Newton method, sect. 15.1.4. How close are you to the cycle expansion and quantum results listed in table 29.2? You can find more quantum data in ref. [29.3].*

Chapter 30

Diffraction distraction

(N. Whelan)

Diffraction effects characteristic to scattering off wedges are incorporated into the periodic orbit theory.

30.1 Quantum eavesdropping

As noted in chapter 29, the classical mechanics of the helium atom is undefined at the instant of a triple collision. This is a common phenomenon - there is often some singularity or discontinuity in the classical mechanics of physical systems. This discontinuity can even be helpful in classifying the dynamics. The points in phase space which have a past or future at the discontinuity form manifolds which divide the phase space and provide the symbolic dynamics. The general rule is that quantum mechanics smoothes over these discontinuities in a process we interpret as diffraction. We solve the local diffraction problem quantum mechanically and then incorporate this into our global solution. By doing so, we reconfirm the central leitmotif of this treatise: think locally - act globally.

While being a well-motivated physical example, the helium atom is somewhat involved. In fact, so involved that we do not have a clue how to do it. In its place we illustrate the concept of diffractive effects with a pinball game. There are various classes of discontinuities which a billiard can have. There may be a grazing condition such that some trajectories hit a smooth surface while others are unaffected - this leads to the creeping described in chapter 28. There may be a vertex such that trajectories to one side bounce differently from those to the other side. There may be a point scatterer or a magnetic flux line such that we do not know how to

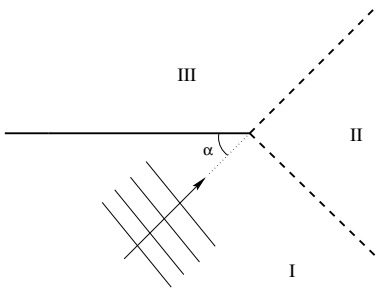

Figure 30.1: Scattering of a plane wave off a half line.

continue classical mechanics through the discontinuities. In what follows, we specialize the discussion to the second example - that of vertices or wedges. To further simplify the discussion, we consider the special case of a half line which can be thought of as a wedge of angle zero.

We start by solving the problem of the scattering of a plane wave off a half line (see fig. 30.1). This is the local problem whose solution we will use to construct a global solution of more complicated geometries. We define the vertex to be the origin and launch a plane wave at it from an angle α. What is the total field? This is a problem solved by Sommerfeld in 1896 and our discussion closely follows his.

The total field consists of three parts - the incident field, the reflected field and the diffractive field. Ignoring the third of these for the moment, we see that the space is divided into three regions. In region I there is both an incident and a reflected wave. In region II there is only an incident field. In region III there is nothing so we call this the shadowed region. However, because of diffraction the field does enter this region. This accounts for why you can overhear a conversation if you are on the opposite side of a thick wall but with a door a few meters away. Traditionally such effects have been ignored in semi-classical calculations because they are relatively weak. However, they can be significant.

To solve this problem Sommerfeld worked by analogy with the full line case, so let us briefly consider that much simpler problem. There we know that the problem can be solved by images. An incident wave of amplitude A is of the form

$$v(r,\psi) = Ae^{-ikr\cos\psi} \tag{30.1}$$

where $\psi = \phi - \alpha$ and ϕ is the angular coordinate. The total field is then given by the method of images as

$$v_{\rm tot} = v(r,\phi-\alpha) - v(r,\phi+\alpha), \tag{30.2}$$

where the negative sign ensures that the boundary condition of zero field on the line is satisfied.

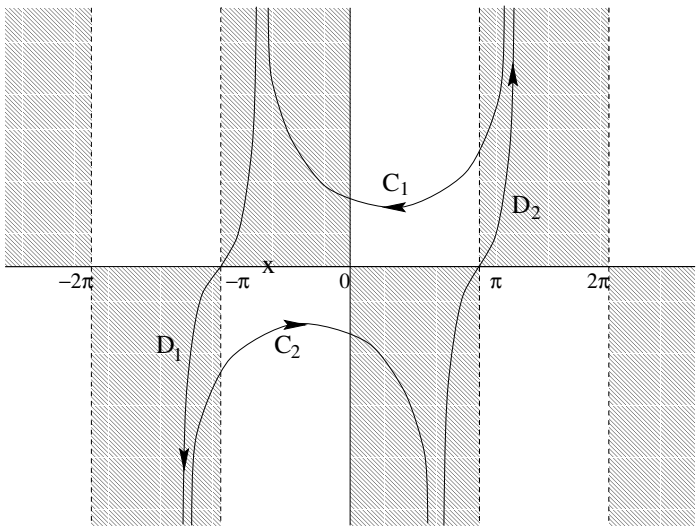

Figure 30.2: The contour in the complex β plane. The pole is at $\beta = -\psi$ (marked by $\times$ in the figure) and the integrand approaches zero in the shaded regions as the magnitude of the imaginary part of β approaches infinity.

Sommerfeld then argued that $v(r, \psi)$ can also be given a complex integral representation

$$v(r, \psi) = A \int_C d\beta f(\beta, \psi) e^{-ikr \cos \beta}. \tag{30.3}$$

This is certainly correct if the function $f(\beta, \psi)$ has a pole of residue $1/2\pi i$ at $\beta = -\psi$ and if the contour C encloses that pole. One choice is

$$f(\beta, \psi) = \frac{1}{2\pi} \frac{e^{i\beta}}{e^{i\beta} - e^{-i\psi}}. \tag{30.4}$$

(We choose the pole to be at $\beta = -\psi$ rather than $\beta = \psi$ for reasons discussed later.) One valid choice for the contour is shown in fig. 30.2. This encloses the pole and vanishes as $|\mathrm{Im}\, \beta| \to \infty$ (as denoted by the shading). The sections D_1 and D_2 are congruent because they are displaced by 2π. However, they are traversed in an opposite sense and cancel, so our contour consists of just the sections C_1 and C_2. The motivation for expressing the solution in this complicated manner should become clear soon.

What have we done? We extended the space under consideration by a factor of two and then constructed a solution by assuming that there is also a source in the unphysical space. We superimpose the solutions from the two sources and at the end only consider the solution in the physical space

to be meaningful. Furthermore, we expressed the solution as a contour integral which reflects the 2π periodicity of the problem. The half line scattering problem follows by analogy.

Whereas for the full line the field is periodic in 2π, for the half line it is periodic in 4π. This can be seen by the fact that the field can be expanded in a series of the form $\{\sin(\phi/2), \sin(\phi), \sin(3\phi/2), \cdots\}$. As above, we extend the space by thinking of it as two sheeted. The physical sheet is as shown in fig. 30.1 and the unphysical sheet is congruent to it. The sheets are glued together along the half line so that a curve in the physical space which intersects the half line is continued in the unphysical space and vice-versa. The boundary conditions are that the total field is zero on both faces of the half line (which are physically distinct boundary conditions) and that as $r \to \infty$ the field is composed solely of plane waves and outgoing circular waves of the form $g(\phi)\exp(ikr)/\sqrt{kr}$. This last condition is a result of Huygens' principle.

We assume that the complete solution is also given by the method of images as

$$v_{\text{tot}} = u(r, \phi - \alpha) - u(r, \phi + \alpha). \tag{30.5}$$

where $u(r, \psi)$ is a 4π-periodic function to be determined. The second term is interpreted as an incident field from the unphysical space and the negative sign guarantees that the solution vanishes on both faces of the half line. Sommerfeld then made the ansatz that u is as given in equation (30.3) with the same contour $C_1 + C_2$ but with the 4π periodicity accounted for by replacing equation (30.4) with

$$f(\beta, \psi) = \frac{1}{4\pi} \frac{e^{i\beta/2}}{e^{i\beta/2} - e^{-i\psi/2}}. \tag{30.6}$$

(We divide by 4π rather than 2π so that the residue is properly normalized.) The integral (30.3) can be thought of as a linear superposition of an infinity of plane waves each of which satisfies the Helmholtz equation $(\nabla^2 + k^2)v = 0$, and so their combination also satisfies the Helmholtz equation. We will see that the diffracted field is an outgoing circular wave; this being a result of choosing the pole at $\beta = -\psi$ rather than $\beta = \psi$ in equation (30.4). Therefore, this ansatz is a solution of the equation and satisfies all boundary conditions and therefore constitutes a valid solution. By uniqueness this is the only solution.

In order to further understand this solution, it is useful to massage the contour. Depending on ϕ there may or may not be a pole between

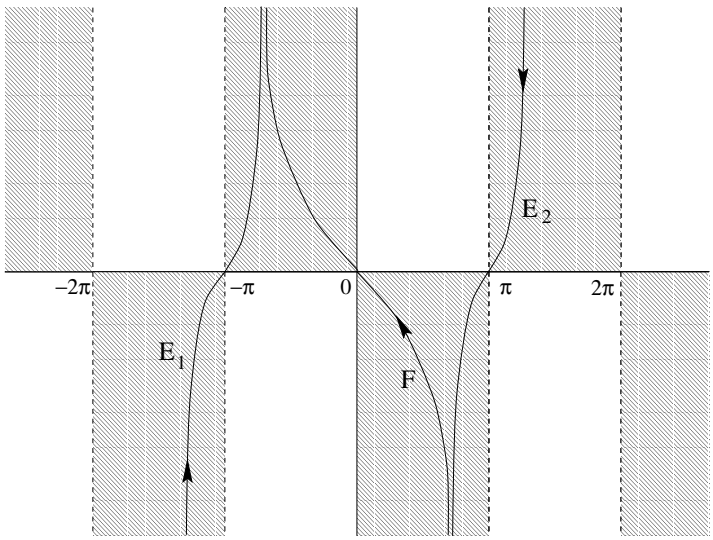

Figure 30.3: The contour used to evaluate the diffractive field after the contribution of possible poles has been explicitly evaluated. The curve F is traversed twice in opposite directions and has no net contribution.

$\beta = -\pi$ and $\beta = \pi$. In region I, both functions $u(r, \phi \pm \alpha)$ have poles which correspond to the incident and reflected waves. In region II, only $u(r, \phi - \alpha)$ has a pole corresponding to the incident wave. In region III there are no poles because of the shadow. Once we have accounted for the geometrical waves (i.e. the poles), we extract the diffracted waves by saddle point analysis at $\beta = \pm\pi$. We do this by deforming the contours C so that they go through the saddles as shown in fig. 30.2.

Contour C_1 becomes $E_2 + F$ while contour C_2 becomes $E_1 - F$ where the minus sign indicates that it is traversed in a negative sense. As a result, F has no net contribution and the contour consists of just E_1 and E_2.

As a result of these machinations, the curves E are simply the curves D of fig. 30.2 but with a reversed sense. Since the integrand is no longer 2π periodic, the contributions from these curves no longer cancel. We evaluate both stationary phase integrals to obtain

$$u(r, \psi) \approx -A \frac{e^{i\pi/4}}{\sqrt{8\pi}} \sec(\psi/2) \frac{e^{ikr}}{\sqrt{kr}} \tag{30.7}$$

so that the total diffracted field is

$$v_{\text{diff}} = -A \frac{e^{i\pi/4}}{\sqrt{8\pi}} \left(\sec\left(\frac{\phi - \alpha}{2}\right) - \sec\left(\frac{\phi + \alpha}{2}\right) \right) \frac{e^{ikr}}{\sqrt{kr}}. \tag{30.8}$$

Note that this expression breaks down when $\phi \pm \alpha = \pi$. These angles correspond to the borders among the three regions of fig. 30.1 and must be handled more carefully - we can not do a stationary phase integral in the vicinity of a pole. However, the integral representation (30.3) and (30.6) is uniformly valid.

30.1 page 582

We now turn to the simple task of translating this result into the language of semiclassical Green's functions. Instead of an incident plane wave, we assume a source at point x' and then compute the resulting field at the receiver position x. If x is in region I, there is both a direct term, and a reflected term, if x is in region II there is only a direct term and if x is in region III there is neither. In any event these contributions to the semiclassical Green's function are known since the free space Green's function between two points x_2 and x_1 is

$$G_{\rm f}(x_2, x_1, k) = -\frac{i}{4} H_0^{(+)}(kd) \approx -\frac{1}{\sqrt{8\pi kd}} \exp\{i(kd + \pi/4)\}, \qquad (30.9)$$

where d is the distance between the points. For a reflection, we need to multiply by -1 and the distance is the length of the path via the reflection point. Most interesting for us, there is also a diffractive contribution to the Green's function. In equation (30.8), we recognize that the coefficient A is simply the intensity at the origin if there were no scatterer. This is therefore replaced by the Green's function to go from the source to the vertex which we label x_V. Furthermore, we recognize that $\exp(ikr)/\sqrt{kr}$ is, within a proportionality constant, the semiclassical Green's function to go from the vertex to the receiver.

Collecting these facts, we say

$$G_{\rm diff}(x, x', k) = G_{\rm f}(x, x_V, k) d(\theta, \theta') G_{\rm f}(x_V, x', k), \qquad (30.10)$$

where, by comparison with equations (30.8) and (30.9), we have

$$d(\theta, \theta') = \sec\left(\frac{\theta - \theta'}{2}\right) - \sec\left(\frac{\theta + \theta'}{2}\right). \qquad (30.11)$$

Here θ' is the angle to the source as measured from the vertex and θ is the angle to the receiver. They were denoted as α and ϕ previously. Note that there is a symmetry between the source and receiver as we expect for a time-reversal invariant process. Also the diffraction coefficient d does not depend on which face of the half line we use to measure the angles. As we will see, a very important property of $G_{\rm diff}$ is that it is a simple multiplicative combination of other semiclassical Green's functions.

30.2 page 582

We now recover our classical perspective by realizing that we can still think of classical trajectories. In calculating the quantum Green's function, we sum over the contributions of various paths. These include the classical trajectories which connect the points and also paths which connect the points via the vertex. These have different weights as given by equations (30.9) and (30.10) but the concept of summing over classical paths is preserved.

For completeness, we remark that there is an exact integral representation for the Green's function in the presence of a wedge of arbitrary opening angle [30.15]. It can be written as

$$G(x,x',k) = g(r,r',k,\theta'-\theta) - g(r,r',k,\theta'+\theta) \tag{30.12}$$

where (r,θ) and (r',θ') are the polar coordinates of the points x and x' as measured from the vertex and the angles are measured from either face of the wedge. The function g is given by

$$g(r,r',k,\psi) = \frac{i}{8\pi\nu}\int_{C_1+C_2} d\beta \frac{H_0^+(k\sqrt{r^2+r'^2-2rr'\cos\beta})}{1-\exp\left(i\frac{\beta+\psi}{\nu}\right)} \tag{30.13}$$

where $\nu = \gamma/\pi$ and γ is the opening angle of the wedge. (ie $\gamma = 2\pi$ in the case of the half plane). The contour $C_1 + C_2$ is the same as shown in fig. 30.2.

The poles of this integral give contributions which can be identified with the geometric paths connecting x and x'. The saddle points at $\beta = \pm\pi$ give contributions which can be identified with the diffractive path connecting x and x'. The saddle point analysis allows us to identify the diffraction constant as

$$d(\theta,\theta') = -\frac{4\sin\frac{\pi}{\nu}}{\nu}\frac{\sin\frac{\theta}{\nu}\sin\frac{\theta'}{\nu}}{\left(\cos\frac{\pi}{\nu}-\cos\frac{\theta+\theta'}{\nu}\right)\left(\cos\frac{\pi}{\nu}-\cos\frac{\theta-\theta'}{\nu}\right)}, \tag{30.14}$$

which reduces to (30.11) when $\nu = 2$. Note that the diffraction coefficient vanishes identically if $\nu = 1/n$ where n is any integer. This corresponds to wedge angles of $\gamma = \pi/n$ (eg. n=1 corresponds to a full line and n=2 corresponds to a right angle). This demonstration is limited by the fact that it came from a leading order asymptotic expansion but the result is quite general. For such wedge angles, we can use the method of images (we will require $2n-1$ images in addition to the actual source point) to obtain the Green's function and there is no diffractive contribution to any

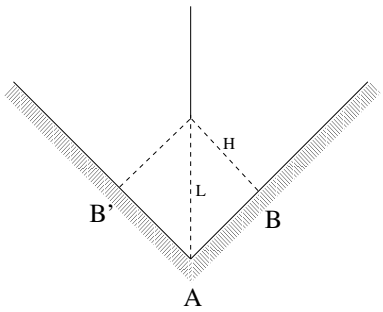

Figure 30.4: The billiard considered here. The dynamics consists of free motion followed by specular reflections off the faces. The top vertex induces diffraction while the bottom one is a right angle and induces two specular geometric reflections.

order. Classically this corresponds to the fact that for such angles, there is no discontinuity in the dynamics. Trajectories going into the vertex can be continued out of them unambiguously. This meshes with the discussion in the introduction where we argued that diffractive effects are intimately linked with classical discontinuities.

The integral representation is also useful because it allows us to consider geometries such that the angles are near the optical boundaries or the wedge angle is close to π/n. For these geometries the saddle point analysis leading to (30.14) is invalid due to the existence of a nearby pole. In that event, we require a more sophisticated asymptotic analysis of the full integral representation.

30.2 An application

Although we introduced diffraction as a correction to the purely classical effects; it is instructive to consider a system which can be quantized solely in terms of periodic diffractive orbits. Consider the geometry shown in fig. 30.4 The classical mechanics consists of free motion followed by specular reflections off faces. The upper vertex is a source of diffraction while the lower one is a right angle and induces no diffraction. This is an open system, there are no bound states - only scattering resonances. However, we can still test the effectiveness of the theory in predicting them. Formally, scattering resonances are the poles of the scattering S matrix and by an identity of Balian and Bloch are also poles of the quantum Green's function. We demonstrate this fact in chapter 28 for 2-dimensional scatterers. The poles have complex wave number k, as for the 3-disk problem.

Let us first consider how diffractive orbits arise in evaluating the trace of G which we call $g(k)$. Specifying the trace means that we must consider all paths which close on themselves in the configuration space while stationary phase arguments for large wavenumber k extract those which are periodic - just as for classical trajectories. In general, $g(k)$ is given by the sum over all diffractive and geometric orbits. The contribution of the simple diffractive

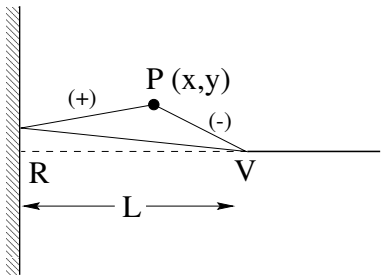

Figure 30.5: The dashed line shows a simple periodic diffractive orbit γ. Between the vertex V and a point P close to the orbit there are two geometric legs labeled $\pm$. The origin of the coordinate system is chosen to be at R.

orbit labeled γ shown in fig. 30.5 to $g(k)$ is determined as follows.

We consider a point P just a little off the path and determine the semiclassical Green's function to return to P via the vertex using (30.9) and (30.10). To leading order in y the lengths of the two geometric paths connecting P and V are $d_\pm = (L \pm x) + y^2/(L \pm x)^2/2$ so that the phase factor $ik(d_+ + d_-)$ equals $2ikL + iky^2/(L^2 - x^2)$. The trace integral involves integrating over all points P and is

$$g_\gamma(k) \approx -2d_\gamma \frac{e^{i(2kL+\pi/2)}}{8\pi k} \int_0^L \frac{dx}{\sqrt{L^2 - x^2}} \int_{-\infty}^{\infty} dy e^{\left(iky^2 \frac{L}{L^2-x^2}\right)}. \quad (30.15)$$

We introduced an overall negative sign to account for the reflection at the hard wall and multiplied by 2 to account for the two traversal senses, $VRPV$ and $VPRV$. In the spirit of stationary phase integrals, we have neglected the y dependence everywhere except in the exponential. The diffraction constant d_γ is the one corresponding to the diffractive periodic orbit. To evaluate the y integral, we use the identity

$$\int_{-\infty}^{\infty} d\xi e^{ia\xi^2} = e^{i\pi/4}\sqrt{\frac{\pi}{a}}, \quad (30.16)$$

and thus obtain a factor which precisely cancels the x dependence in the x integral. This leads to the rather simple result

$$g_\gamma \approx -\frac{il_\gamma}{2k} \left\{ \frac{d_\gamma}{\sqrt{8\pi k l_\gamma}} \right\} e^{i(kl_\gamma + \pi/4)} \quad (30.17)$$

where $l_\gamma = 2L$ is the length of the periodic diffractive orbit. A more sophisticated analysis of the trace integral has been done [30.6] using the integral representation (30.13). It is valid in the vicinity of an optical boundary and also for wedges with opening angles close to π/n.

Consider a periodic diffractive orbit with n_γ reflections off straight hard walls and μ_γ diffractions each with a diffraction constant $d_{\gamma,j}$. The total

length of the orbit $L_\gamma = \sum l_{\gamma,j}$ is the sum of the various diffractive legs and l_γ is the length of the corresponding prime orbit. For such an orbit, (30.17) generalizes to

$$g_\gamma(k) = -\frac{il_\gamma}{2k}\left\{\prod_{j=1}^{\mu_\gamma}\frac{d_{\gamma,j}}{\sqrt{8\pi k l_{\gamma,j}}}\right\}\exp\{i(kL_\gamma + n_\gamma\pi - 3\mu_\gamma\pi/4)\}. \quad (30.18)$$

30.3
page 582

Each diffraction introduces a factor of $1/\sqrt{k}$ and multi-diffractive orbits are thereby suppressed.

If the orbit γ is prime then $L_\gamma = l_\gamma$. If γ is the r'th repeat of a prime orbit β we have $L_\gamma = rl_\beta$, $n_\gamma = rp_\beta$ and $\mu_\gamma = r\sigma_\beta$, where l_β, p_β and σ_β all refer to the prime orbit. We can then write

$$g_\gamma = g_{\beta,r} = -\frac{il_\beta}{2k}t_\beta^r \quad (30.19)$$

where

$$t_\beta = \left\{\prod_{j=1}^{\sigma_\beta}\frac{d_{\beta,j}}{\sqrt{8\pi k l_{\beta,j}}}\right\}\exp\{i(kl_\beta + p_\beta\pi - 3\sigma_\beta\pi/4)\}. \quad (30.20)$$

It then makes sense to organize the sum over diffractive orbits as a sum over the prime diffractive orbits and a sum over the repetitions

$$g_{\rm diff}(k) = \sum_\beta\sum_{r=1}^{\infty} g_{\beta,r} = -\frac{i}{2k}\sum_\beta l_\beta\frac{t_\beta}{1-t_\beta}. \quad (30.21)$$

We cast this as a logarithmic derivative (12.7) by noting that $\frac{dt_\beta}{dk} = il_\beta t_\beta - \sigma_\beta t_\beta/2k$ and recognizing that the first term dominates in the semi-classical limit. It follows that

$$g_{\rm diff}(k) \approx \frac{1}{2k}\frac{d}{dk}\left\{\ln\prod_\beta(1-t_\beta)\right\}. \quad (30.22)$$

In the case that there are only diffractive periodic orbits - as in the geometry of fig. 30.4 - the poles of $g(k)$ are the zeros of a dynamical zeta function

$$1/\zeta(k) = \prod_\beta(1-t_\beta). \quad (30.23)$$

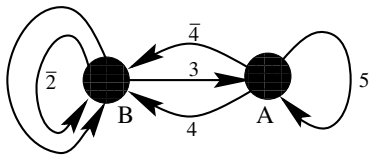

Figure 30.6: The two-node Markov graph with all the diffractive processes connecting the nodes.

For geometric orbits, this function would be evaluated with a cycle expansion as discussed in chapter 15. However, here we can use the multiplicative nature of the weights t_β to find a closed form representation of the function using a Markov graph, as in sect. 9.6.1. This multiplicative property of the weights follows from the fact that the diffractive Green's function (30.10) is multiplicative in segment semiclassical Green's functions, unlike the geometric case.

There is a reflection symmetry in the problem which means that all resonances can be classified as even or odd. Because of this, the dynamical zeta function factorizes as $1/\zeta = 1/\zeta_+\zeta_-$ (as explained in sects. 19.5 and 19.1.2) and we determine $1/\zeta_+$ and $1/\zeta_-$ separately using the ideas of symmetry decomposition of chapter 19.

In the Markov graph shown in fig. 30.6, we enumerate all processes. We start by identifying the fundamental domain as just the right half of fig. 30.4. There are two nodes which we call A and B. To get to another node from B, we can diffract (always via the vertex) in one of three directions. We can diffract back to B which we denote as process 1. We can diffract to B's image point B' and then follow this by a reflection. This process we denote as $\bar{2}$ where the bar indicates that it involves a reflection. Thirdly, we can diffract to node A. Starting at A we can also diffract to a node in three ways. We can diffract to B which we denote as 4. We can diffract to B' followed by a reflection which we denote as $\bar{4}$. Finally, we can diffract back to A which we denote as process 5. Each of these processes has its own weight which we can determine from the earlier discussion. First though, we construct the dynamical zeta functions.

The dynamical zeta functions are determined by enumerating all closed loops which do not intersect themselves in fig. 30.6. We do it first for $1/\zeta_+$ because that is simpler. In that case, the processes with bars are treated on an equal footing as the others. Appealing back to sect. 19.5 we find

$$\begin{aligned} 1/\zeta_+ &= 1 - t_1 - t_{\bar{2}} - t_5 - t_3t_4 - t_3t_{\bar{4}} + t_5t_1 + t_5t_{\bar{2}}\,, \\ &= 1 - (t_1 + t_{\bar{2}} + t_5) - 2t_3t_4 + t_5(t_1 + t_{\bar{2}}) \end{aligned} \tag{30.24}$$

where we have used the fact that $t_4 = t_{\bar{4}}$ by symmetry. The last term has a positive sign because it involves the product of shorter closed loops. To calculate $1/\zeta_-$, we note that the processes with bars have a relative

negative sign due to the group theoretic weight. Furthermore, process 5 is a boundary orbit (see sect. 19.3.1) and only affects the even resonances - the terms involving t_5 are absent from $1/\zeta_-$. The result is

$$\begin{aligned} 1/\zeta_- &= 1 - t_1 + t_{\bar{2}} - t_3 t_4 + t_3 t_{\bar{4}}\,, \\ &= 1 - (t_1 - t_{\bar{2}}). \end{aligned} \tag{30.25}$$

30.4 page 582

Note that these expressions have a finite number of terms and are not in the form of a curvature expansion, as for the 3-disk problem.

It now just remains to fix the weights. We use equation (30.20) but note that each weight involves just one diffraction constant. It is then convenient to define the quantities

$$u_A^2 = \frac{\exp\{i(2kL + 2\pi)\}}{\sqrt{16\pi kL}} \qquad u_B^2 = \frac{\exp\{i(2kH + \pi)\}}{\sqrt{16\pi kH}}. \tag{30.26}$$

The lengths L and $H = L/\sqrt{2}$ are defined in fig. 30.4; we set $L = 1$ throughout. Bouncing inside the right angle at A corresponds to two specular reflections so that $p = 2$. We therefore explicitly include the factor $\exp(i2\pi)$ in (30.26) although it is trivially equal to one. Similarly, there is one specular reflection at point B giving $p = 1$ and therefore a factor of $\exp(i\pi)$. We have defined u_A and u_B because, together with some diffraction constants, they can be used to construct all of the weights. Altogether we define four diffraction coefficients: d_{AB} is the constant corresponding to diffracting from B to A and is found from (30.11) with $\theta' = 3\pi/4$ and $\theta = \pi$ and equals $2\sec(\pi/8) \approx 2.165$. With analogous notation, we have d_{AA} and $d_{BB} = d_{B'B}$ which equal 2 and $1 + \sqrt{2}$ respectively. $d_{ij} = d_{ji}$ due to the Green's function symmetry between source and receiver referred to earlier. Finally, there is the diffractive phase factor $s = \exp(-i3\pi/4)$ each time there is a diffraction. The weights are then as follows:

$$\begin{aligned} t_1 = sd_{BB}u_B^2 \quad t_{\bar{2}} &= sd_{B'B}u_B^2 \quad t_3 = t_4 = t_{\bar{4}} = sd_{AB}u_A u_B \\ t_5 &= sd_{AA}u_A^2. \end{aligned} \tag{30.27}$$

Each weight involves two u's and one d. The u's represent the contribution to the weight from the paths connecting the nodes to the vertex and the d gives the diffraction constant connecting the two paths.

The equality of d_{BB} and $d_{B'B}$ implies that $t_1 = t_{\bar{2}}$. From (30.25) this means that there are no odd resonances because 1 can never equal 0. For the even resonances equation (30.24) is an implicit equation for k which has zeros shown in fig. 30.7.

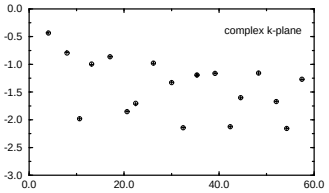

Figure 30.7: The even resonances of the wedge scatterer of fig. 30.4 plotted in the complex $k-$plane, with $L = 1$. The exact resonances are represented as circles and their semiclassical approximations as crosses.

For comparison we also show the result from an exact quantum calculation. The agreement is very good right down to the ground state - as is so often the case with semiclassical calculations. In addition we can use our dynamical zeta function to find arbitrarily high resonances and the results actually improve in that limit. In the same limit, the exact numerical solution becomes more difficult to find so the dynamical zeta function approximation is particularly useful in that case.

30.5
page 582

In general a system will consist of both geometric and diffractive orbits. In that case, the full dynamical zeta function is the product of the geometric zeta function and the diffractive one. The diffractive weights are typically smaller by order $O(1/\sqrt{k})$ but for small k they can be numerically competitive so that there is a significant diffractive effect on the low-lying spectrum. It might be expected that higher in the spectrum, the effect of diffraction is weaker due to the decreasing weights. However, it should be pointed out that an analysis of the situation for creeping diffraction [30.7] concluded that the diffraction is actually *more* important higher in the spectrum due to the fact that an ever greater fraction of the orbits need to be corrected for diffractive effects. The equivalent analysis has not been done for edge diffraction but a similar conclusion can probably be expected.

To conclude this chapter, we return to the opening paragraph and discuss the possibility of doing such an analysis for helium. The important point which allowed us to successfully analyze the geometry of fig. 30.4 is that when a trajectory is near the vertex, we can extract its diffraction constant without reference to the other facets of the problem. We say, therefore, that this is a "local" analysis for the purposes of which we have "turned off" the other aspects of the problem, namely sides AB and AB'. By analogy, for helium, we would look for some simpler description of the problem which applies near the three body collision. However, there is nothing to "turn off". The local problem is just as difficult as the global one since they are precisely the same problem, just related by scaling. Therefore, it is not at all clear that such an analysis is possible for helium.

Commentary

Remark 30.1 Classical discontinuities. Various classes of discontinuities for billiard and potential problems discussed in the literature:

- a grazing condition such that some trajectories hit a smooth surface while others are unaffected, refs. [30.1, 30.2, 30.3, 30.7]
- a vertex such that trajectories to one side bounce differently from those to the other side, refs. [30.2, 30.4, 30.5, 30.8, 30.9].
- a point scatterer [30.10, 30.11] or a magnetic flux line [30.12, 30.13] such that we do not know how to continue classical mechanics through the discontinuities.

Remark 30.2 Geometrical theory of diffraction. In the above discussion we borrowed heavily from the ideas of Keller who was interested in extending the geometrical ray picture of optics to cases where there is a discontinuity. He maintained that we could hang onto that ray-tracing picture by allowing rays to strike the vertex and then leave at any angle with amplitude (30.8). Both he and Sommerfeld were thinking of optics and not quantum mechanics and they did not phrase the results in terms of semiclassical Green's functions but the essential idea is the same.

Remark 30.3 Generalizations Consider the effect of replacing our half line by a wedge of angle γ_1 and the right angle by an arbitrary angle γ_2. If $\gamma_2 > \gamma_1$ and $\gamma_2 \geq \pi/2$ this is an open problem whose solution is given by equations (30.24) and (30.25) (there will then be odd resonances) but with modified weights reflecting the changed geometry [30.8]. (For $\gamma_2 < \pi/2$, more diffractive periodic orbits appear and the dynamical zeta functions are more complicated but can be calculated with the same machinery.) When $\gamma_2 = \gamma_1$, the problem in fact has bound states [30.21, 30.22]. This last case has been of interest in studying electron transport in mesoscopic devices and in microwave waveguides. However we can not use our formalism as it stands because the diffractive periodic orbits for this geometry lie right on the border between illuminated and shadowed regions so that equation (30.7) is invalid. Even the more uniform derivation of [30.6] fails for that particular geometry, the problem being that the diffractive orbit actually lives on the edge of a family of geometric orbits and this makes the analysis still more difficult.

Remark 30.4 Diffractive Green's functions. The result (30.17) is proportional to the length of the orbit times the semiclassical Green's

function (30.9) to go from the vertex back to itself along the classical path. The multi-diffractive formula (30.18) is proportional to the total length of the orbit times the product of the semiclassical Green's functions to go from one vertex to the next along classical paths. This result generalizes to any system — either a pinball or a potential — which contains point singularities such that we can define a diffraction constant as above. The contribution to the trace of the semiclassical Green's function coming from a diffractive orbit which hits the singularities is proportional to the total length (or period) of the orbit times the product of semiclassical Green's functions in going from one singularity to the next. This result first appeared in reference [30.2] and a derivation can be found in reference [30.9]. A similar structure also exists for creeping [30.2].

Remark 30.5 Diffractive orbits for hydrogenic atoms. An analysis in terms of diffractive orbits has been made in a different atomic physics system, the response of hydrogenic atoms to strong magnetic fields [30.23]. In these systems, a single electron is highly excited and takes long traversals far from the nucleus. Upon returning to a hydrogen nucleus, it is re-ejected with the reversed momentum as discussed in chapter 29. However, if the atom is not hydrogen but sodium or some other atom with one valence electron, the returning electron feels the charge distribution of the core electrons and not just the charge of the nucleus. This so-called quantum defect induces scattering in addition to the classical re-ejection present in the hydrogen atom. (In this case the local analysis consists of neglecting the magnetic field when the trajectory is near the nucleus.) This is formally similar to the vertex which causes both specular reflection and diffraction. There is then additional structure in the Fourier transform of the quantum spectrum corresponding to the induced diffractive orbits, and this has been observed experimentally [30.24].

Résumé

In this chapter we have discovered new types of periodic orbits contributing to the semiclassical traces and determinants. Unlike the periodic orbits we had seen so far, these are not true classical orbits. They are generated by singularities of the scattering potential. In these singular points the classical dynamics has no unique definition, and the classical orbits hitting the singularities can be continued in many different directions. While the classical mechanics does not know which way to go, quantum mechanics solves the dilemma by allowing us to continue in all possible directions. The likelihoods of different paths are given by the quantum mechanical weights

called diffraction constants. The total contribution to a trace from such orbit is given by the product of transmission amplitudes between singularities and diffraction constants of singularities. The weights of diffractive periodic orbits are at least of order $1/\sqrt{k}$ weaker than the weights associated with classically realizable orbits, and their contribution at large energies is therefore negligible. Nevertheless, they can strongly influence the low lying resonances or energy levels. In some systems, such as the N disk scattering the diffraction effects do not only perturb semiclassical resonances, but can also create new low energy resonances. Therefore it is always important to include the contributions of diffractive periodic orbits when semiclassical methods are applied at low energies.

References

[30.1] A. Wirzba, CHAOS **2**, 77 (1992);

[30.2] G. Vattay, A. Wirzba and P. E. Rosenqvist, Phys. Rev. Lett. **73**, 2304 (1994); G. Vattay, A. Wirzba and P. E. Rosenqvist in *Proceedings of the International Conference on Dynamical Systems and Chaos: vol. 2*, edited by Y.Aizawa, S.Saito and K.Shiraiwa (World Scientific, Singapore, 1994).

[30.3] H. Primack, H. Schanz, U. Smilansky and I. Ussishkin, Phys. Rev. Lett. **76**, 1615 (1996).

[30.4] N. D. Whelan, Phys. Rev. E **51**, 3778 (1995).

[30.5] N. Pavloff and C. Schmit, Phys. Rev. Lett. **75**, 61 (1995).

[30.6] M. Sieber, N. Pavloff, C. Schmit, Phys. Rev. E **55**, 2279 (1997).

[30.7] H. Primack et. al., J. Phys. A **30**, 6693 (1997).

[30.8] N. D. Whelan, Phys. Rev. Lett. **76**, 2605 (1996).

[30.9] H. Bruus and N. D. Whelan, Nonlinearity, **9**, 1 (1996).

[30.10] P. Seba, Phys. Rev. Lett. **64**, 1855 (1990).

[30.11] P. E. Rosenqvist, N. D. Whelan and A. Wirzba, J. Phys. A **29**, 5441 (1996).

[30.12] M. Brack et. al., Chaos **5**, 317 (1995).

[30.13] S. M. Reimann et. al., Phys. Rev. A **53**, 39 (1996).

[30.14] A. Sommerfeld, Mathem. Ann. **47**, 317 (1896); *Optics* (Academic Press, New York 1954).

[30.15] H. S. Carslaw, Proc. London Math. Soc. (Ser. 1) **30**, 121 (1989); H. S. Carslaw, Proc. London Math. Soc. (Ser. 2) **18**, 291 (1920).

[30.16] J. B. Keller, J. Appl. Phys. **28**, 426 (1957).

[30.17] A. Voros, J. Phys. A **21**. 685 (1988).

[30.18] see for example, D. Ruelle, *Statistical Mechanics, Thermodynamic Formalism* (Addison-Wesley, Reading MA, 1978).

[30.19] see for example, P. Grassberger, Z. Naturforsch. **43a**, 671 (1988).

[30.20] P. Cvitanović and B. Eckhardt, Nonlinearity **6**, 277 (1993).

[30.21] P. Exner, P. Seba and P. Stovicek, Czech J. Phys **B39**, 1181 (1989).

[30.22] Hua Wu and D. W. L. Sprung, J. Appl. Phys. **72**, 151 (1992).

[30.23] P. A. Dando, T. S. Monteiro, D. Delande and K. T. Taylor, Phys. Rev. Lett. **74**, 1099 (1995). P. A. Dando, T. S. Monteiro and S. M. Owen, preprint (1997).

[30.24] D. Delande et. al., J. Phys. B **27**, 2771 (1994); G. Raithel et. al., J. Phys. B **27**, 2849 (1994); M. Courtney et. al., Phys. Rev. Lett., **73**, 1340 (1994).

Exercises

(N. Whelan)

Exercise 30.1 Stationary phase integral. *Evaluate the two stationary phase integrals corresponding to contours E_1 and E_2 of fig. 30.3 and thereby verify (30.7).*

Exercise 30.2 Scattering from a small disk *Imagine that instead of a wedge, we have a disk whose radius a is much smaller than the typical wavelengths we are considering. In that limit, solve the quantum scattering problem - find the scattered wave which result from an incident plane wave. You can do this by the method of partial waves - the analogous three dimensional problem is discussed in most quantum textbooks. You should find that only the $m = 0$ partial wave contributes for small a. Following the discussion above, show that the diffraction constant is*

$$d = \frac{2\pi}{\log\left(\frac{2}{ka}\right) - \gamma_e + i\frac{\pi}{2}} \tag{30.28}$$

where $\gamma_e = 0.577\cdots$ is Euler's constant. Note that in this limit d depends weakly on k but not on the scattering angle.

Exercise 30.3 Several diffractive legs. *Derive equation (30.18). The calculation involves considering slight variations of the diffractive orbit as in the simple case discussed above. Here it is more complicated because there are more diffractive arcs - however you should convince yourself that a slight variation of the diffractive orbit only affects one leg at a time.*

Exercise 30.4 Unsymmetrized dynamical zeta function. *Assume you know nothing about symmetry decomposition. Construct the three node Markov diagram for fig. 30.1 by considering A, B and B' to be physically distinct. Write down the corresponding dynamical zeta function and check explicitly that for $B = B'$ it factorizes into the product of the the even and odd dynamical zeta functions. Why is there no term $t_{\bar{2}}$ in the full dynamical zeta function?*

Exercise 30.5 Three point scatterers. *Consider the limiting case of the three disk game of pinball of fig. 1.1 where the disks are very much smaller than their spacing R. Use the results of exercise 30.2 to construct the desymmetrized dynamical zeta functions, as in sect. 19.6. You should find $1/\zeta_{A_1} = 1 - 2t$ where $t = de^{i(kR-3\pi/4)}/\sqrt{8\pi kR}$. Compare this formula with that from chapter 9. By assuming that the real part of k is much greater than the imaginary part show that the positions of the resonances are $k_nR = \alpha_n - i\beta_n$ where $\alpha_n = 2\pi n + 3\pi/4$, $\beta_n = \log\left(\sqrt{2\pi\alpha_n}/d\right)$ and n is a non-negative integer. (See also reference [30.11].)*

Epilogue

> Nowadays, whatever the truth of the matter may be (and we will probably never know), the simplest solution is no longer emotionally satisfying. Everything we know about the world militates against it. The concepts of indeterminacy and chaos have filtered down to us from the higher sciences to confirm our nagging suspicions.
> L. Sante, "Review of 'American Tabloid' by James Ellroy", *New York Review of Books* (May 11, 1995)

A motion on a strange attractor can be approximated by shadowing long orbits by sequences of nearby shorter periodic orbits. This notion has here been made precise by approximating orbits by prime cycles, and evaluating associated curvatures. A curvature measures the deviation of a long cycle from its approximation by shorter cycles; the smoothness of the dynamical system implies exponential fall-off for (almost) all curvatures. We propose that the theoretical and experimental non–wandering sets be expressed in terms of the symbol sequences of short cycles (a topological characterization of the spatial layout of the non–wandering set) and their eigenvalues (metric structure)

Cycles as the skeleton of chaos

> Étant données des équations ... et une solution particuliére quelconque de ces équations, on peut toujours trouver une solution périodique (dont la période peut, il est vrai, étre trés longue), telle que la différence entre les deux solutions soit aussi petite qu'on le veut, pendant un temps aussi long qu'on le veut. D'ailleurs, ce qui nous rend ces solutions périodiques si précieuses, c'est qu'elles sont, pour ansi dire, la seule bréche par où nous puissions esseyer de pénétrer dans une place jusqu'ici réputée inabordable.
> H. Poincaré, *Les méthodes nouvelles de la méchanique céleste*

We wind down this chatty chapter by asking: why cycle?

We tend to think of a dynamical system as a smooth system whose evolution can be followed by integrating a set of differential equations. Traditionally one used integrable motions as zeroth-order approximations to physical systems, and accounted for weak nonlinearities perturbatively. However, when the evolution is actually followed through to asymptotic times, one discovers that the strongly nonlinear systems show an amazingly rich structure which is not at all apparent in their formulation in terms of differential equations. In particular, the periodic orbits are important because they form the *skeleton* onto which all trajectories trapped for long times cling. This was already appreciated century ago by H. Poincaré, who, describing in *Les méthodes nouvelles de la méchanique céleste* his discovery of homoclinic tangles, mused that "the complexity of this figure will be striking, and I shall not even try to draw it". Today such drawings are cheap and plentiful; but Poincaré went a step further and, noting that hidden in this apparent chaos is a rigid skeleton, a tree of *cycles* (periodic orbits) of increasing lengths and self-similar structure, suggested that the cycles should be the key to chaotic dynamics.

The zeroth-order approximations to harshly chaotic dynamics are very different from those for the nearly integrable systems: a good starting approximation here is the stretching and kneading of a baker's map, rather than the winding of a harmonic oscillator.

For low dimensional deterministic dynamical systems description in terms of cycles has many virtues:

1. cycle symbol sequences are *topological* invariants: they give the spatial layout of a non–wandering set

2. cycle eigenvalues are *metric* invariants: they give the scale of each piece of a non–wandering set

3. cycles are *dense* on the asymptotic non–wandering set

4. cycles are ordered *hierarchically*: short cycles give good approximations to a non–wandering set, longer cycles only refinements. Errors due to neglecting long cycles can be bounded, and typically fall off exponentially or super-exponentially with the cutoff cycle length

5. cycles are *structurally robust*: for smooth flows eigenvalues of short cycles vary slowly with smooth parameter changes

6. asymptotic averages (such as correlations, escape rates, quantum mechanical eigenstates and other "thermodynamic" averages) can be efficiently computed from short cycles by means of *cycle expansions*

Points 1, 2: That the cycle topology and eigenvalues are invariant properties of dynamical systems follows from elementary considerations. If the same dynamics is given by a map f in one set of coordinates, and a map g in the next, then f and g (or any other good representation) are related by a reparametrization and a coordinate transformation $f = h^{-1} \circ g \circ h$. As both f and g are arbitrary representations of the dynamical system, the explicit form of the conjugacy h is of no interest, only the properties invariant under any transformation h are of general import. The most obvious invariant properties are topological; a fixed point must be a fixed point in any representation, a trajectory which exactly returns to the initial point (a cycle) must do so in any representation. Furthermore, a good representation should not mutilate the data; h must be a smooth transformation which maps nearby cycle points of f into nearby cycle points of g. This smoothness guarantees that the cycles are not only topological invariants, but that their linearized neighborhoods are also metrically invariant. In particular, the cycle eigenvalues (eigenvalues of the Jacobian matrixs $df^n(x)/dx$ of periodic orbits $f^n(x) = x$) are invariant.

Point 5: An important virtue of cycles is their *structural robustness*. Many quantities customarily associated with dynamical systems depend on the notion of "structural stability", that is robustness of non–wandering set to small parameter variations.

Still, the sufficiently short unstable cycles are structurally robust in the sense that they are only slightly distorted by such parameter changes, and averages computed using them as a skeleton are insensitive to small deformations of the non–wandering set. In contrast, lack of structural stability wreaks havoc with long time averages such as Lyapunov exponents, for which there is no guarantee that they converge to the correct asymptotic value in any finite time numerical computation.

The main recent theoretical advance is **point 4:** we now know how to control the errors due to neglecting longer cycles. As we seen above, even though the number of invariants is infinite (unlike, for example, the number of Casimir invariants for a compact Lie group) the dynamics can be well approximated to any finite accuracy by a small finite set of invariants. The origin of this convergence is geometrical, as we shall see in appendix J.1.2, and for smooth flows the convergence of cycle expansions can even be superexponential.

The cycle expansions such as (15.5) outperform the pedestrian methods such as extrapolations from the finite cover sums (16.2) for a number of reasons. The cycle expansion is a better averaging procedure than the naive box counting algorithms because the strange attractor is here pieced together in a topologically invariant way from neighborhoods ("space average") rather than explored by a long ergodic trajectory ("time average").

The cycle expansion is co-ordinate and reparametrization invariant - a finite nth level sum (16.2) is not. Cycles are of finite period but infinite duration, so the cycle eigenvalues are already evaluated in the $n \to \infty$ limit, but for the sum (16.2) the limit has to be estimated by numerical extrapolations. And, crucially, the higher terms in the cycle expansion (15.5) are deviations of longer prime cycles from their approximations by shorter cycles. Such combinations vanish exactly in piecewise linear approximations and fall off exponentially for smooth dynamical flows.

In the above we have reviewed the general properties of the cycle expansions; those have been applied to a series of examples of low-dimensional chaos: 1-d strange attractors, the period-doubling repeller, the Hénon-type maps and the mode locking intervals for circle maps. The cycle expansions have also been applied to the irrational windings set of critical circle maps, to the Hamiltonian period-doubling repeller, to a Hamiltonian three-disk game of pinball, to the three-disk quantum scattering resonances and to the extraction of correlation exponents, Feasibility of analysis of experimental non–wandering set in terms of cycles is discussed in ref. [15.1].

Homework assignment

> "Lo! thy dread empire Chaos is restor'd, Light dies before thy uncreating word; Thy hand, great Anarch, lets the curtain fall, And universal darkness buries all."
> Alexander Pope, *The Dunciad*

We conclude cautiously with a homework assignment posed May 22, 1990 (the original due date was May 22, 2000, but alas...):

1. **Topology** Develop optimal sequences ("continued fraction approximants") of finite subshift approximations to generic dynamical systems. Apply to (a) the Hénon map, (b) the Lorenz flow and (c) the Hamiltonian standard map.

2. **Non-hyperbolicity** Incorporate power–law (marginal stability orbits,"intermittency") corrections into cycle expansions. Apply to long-time tails in the Hamiltonian diffusion problem.

3. **Phenomenology** Carry through a convincing analysis of a genuine experimentally extracted data set in terms of periodic orbits.

4. **Invariants** Prove that the scaling functions, or the cycles, or the spectrum of a transfer operator are the maximal set of invariants of an (physically interesting) dynamically generated non–wandering set.

5. **Field theory** Develop a periodic orbit theory of systems with many unstable degrees of freedom. Apply to (a) coupled lattices, (b) cellular automata, (c) neural networks.

6. **Tunneling** Add complex time orbits to quantum mechanical cycle expansions (WKB theory for chaotic systems).

7. **Unitarity** Evaluate corrections to the Gutzwiller semiclassical periodic orbit sums. (a) Show that the zeros (energy eigenvalues) of the appropriate Selberg products are real. (b) Find physically realistic systems for which the "semiclassical" periodic orbit expansions yield the exact quantization.

8. **Atomic spectra** Compute the helium spectrum from periodic orbit expansions (already accomplished by Wintgen and Tanner!).

9. **Symmetries** Include fermions, gauge fields into the periodic orbit theory.

10. **Quantum field theory** Develop quantum theory of systems with infinitely many classically unstable degrees of freedom. Apply to (a) quark confinement (b) early universe (c) the brain.

Conclusion

> Good-bye. I am leaving because I am bored.
> George Saunders' dying words
>
> Nadie puede escribir un libro. Para Que un libro sea verdaderamente, Se requieren la aurora y el poniente Siglos, armas y el mar que une y separa.
> Jorge Luis Borges El Hacedor, *Ariosto y los arabes*

The buttler did it.

Index

abscissa
  absolute conv., 296
  conditional conv., 296
accelerator mode, 395
action, 486, 497
  helium, 540
  relation to period, 551
admissible
  periodic points, 175
  trajectories, number of, 171
Airy
  equation, 454
  function, 454
Airy function, 459, 461
  at a bifurcation, 461
alphabet, 146
analyticity
  domain, 215
anomalous diffusion, 404
antiharmonic extension, 642
arc, 165
area
  preserving map, 686
Artin-Mazur zeta function, 181
attractor, 36
  basin, 36
  Hénon, 61
  strange, 36, 40, 134
Aubry-Mather theory, 477
autonomous flow, 39, 269
average
  space, 112
  time, 112
averages
  chaotic, 348
averaging, 29
  space, 128
  time, 126
Axiom A
  systems, 249

baker's map, 91
Balmer spectrum, 442
basin of attraction, 36, 75
Bernoulli
  polynomials, 243
  shift, 242, 358
bi-infinite itinerary, 163
bifurcation
  Airy function approximation, 461
  bizarre, 642
  generic, 91
  Hopf, 415
  saddle-node, 59
billiard
  map, 87
  stadium, 86
billiards, 86, 91
  stability, 88
binary
  symbolic dynamics
    collinear helium, 545
Birkhoff
  ergodic theorem, 112
Birkhoff coordinates, 12
block
  finite sequence, 163
block, pruning, 165
Bohr
  – de Broglie picture, 442
  -Sommerfeld quantization, 442, 516, 614
  helium, 537, 552
  Uetli Schwur, 613
Bohr, N., 761
Boltzmann
  equation, 410
Boltzmann, L, 24
boredom, 323, 587
Borges, J.L., 587
boundary orbits, 377
bounded operators, 701
Bowen, 26
brain, rat, 3, 27
branch cut, 342

singularity, 343
Bunimovich
billiard, *see* stadium
Burnett coefficient, 400

C_{3v} symmetry, 382
canonical
transformation, 85
canonical transformations, 622
Cartwright M.L., 608
Cauchy criterion, 700
caustic, 489
ceiling function, 51, 210, 256
center, 69
center manifold, 45
center of mass, 278
chain rule, 73
matrix, 697
change
of coordinates, 95
chaos, 5–7
caveats, 9
diagnostics, 46
skeleton of, 11, 12
successes, 9
character
orthonormalitity, 678
representation, 674
characteristic
function, 106
polynomial, 178
chicken heart palpitations, 6
circle map
critical, 418
coarse graining, 166
coarse-graining, 106
coding, *see* symbolic dynamics
collinear helium, 444
symbolic dynamics, 545
combinatorics
teaching, 157
complete
N-ary dynamics, 147
complexity
algorithmic, 192
confession
C.N. Yang, 111
Kepler, 604
St. Augustine, 105
conjugacy, 96, 97
invariant, 101
smooth, 96, 101, 104, 767
topological, 159
connection formulas, 454
conservation
equation, 627
phase space volume, 85, 114, 628
continuity
equation, 116
continuity equation, 114, 487, 628
contour integral, 220
contracting
flow, 36, 40, 78
map, 81, 169
stability eigenvalues, 74, 203
convergence
abscissa of, 296
mediocre, 692
radius, 215
super-exponential, 237, 463
convexity, 140
coordinate
change, 95, 97
longitudinal, 498
transformations, 104
Copenhagen School, xi, 613
correlation
decay
power law, 336
function, 253
spectrum, 253
time, 310
cost function, 464
covering
symbolic dynamics, 163
critical
point, 156
value, 156, 398
critical point, 76
cumulant
expansion, 176, 181, 284
Plemelj-Smithies, 706
curvature
correction, 281
expansion, 29, 281
cycle, 11
expansion, 19, 281, 515
3-disk, 301
finite subshift, 291
stability ordered, 292
fundamental, 178, 281
limit, 134
Lyapunov exponent, 75

point, 164
prime, 164, 195, 204, 261
3-disk, 473
Hénon map, 468
pruning, 185
stability, 74, 273
stable, 76
superstable, 76
unstable, 12
weigth, 218
cycle expansion
Lyapunov exponent, 290
cycles
fundamental, 690
Rössler system, 263
cyclic
invariance, 262
symmetry, 174

D'Alambert's wave equation, 617
damped Newton method, 266
de Broglie wavelength, 481
decay
rate, 226
degree of freedom, 9
delta function
Dirac, 108, 449
density, 106, 627
evolution, 24
density of states
average, 511
Green's function, 450
quantum, 450
desymmetrization
3-disk, 388
determinant
Fredholm, 709
graph, 191
Hadamard, 216
spectral, 23, 176, 216
for flows, 217
trace relation, 176
trace-class operator, 702
deterministic
dynamics, 34
deterministic dynamics, 6
deterministic flow, 113
differential equations
ordinary
almost, 48
diffraction
Green's function, 570
Keller, 578
Sommerfeld, 578
diffusion
partial differential equations, 618
anomalous, 404
constant, 130
dimension
box counting, 326
fractal, 325
generalized, 3
information, 326
intrisic, 9
Dirac delta function, 108
Dirichlet series, 295
dissipative
map, 81, 169
distribution, 619
divergence rate
local, 137
divergence ultraviolet, 512
doubling map, 247
Duffing oscillator, 38
Duffing system, 45
dynamical
system, 33, 34
deterministic, 34
gradient, 48
smooth, 34
systems
equivalent, 102
transitivity, 173
zeta function, 18, 219
Euler product rep., 219
dynamical system
infinite, 50
smooth, 19, 20, 29, 189, 608, 730, 733, 735
dynamics
deterministic, 6
hyperbolic, 149
irreversible, 37
reversible, 38
stochastic, 6
symbolic, 10, 146, 162, 313
symmetry, 677
topological, 146, 162, 164

edge, 165
eigen
directions, 65
eigenfunction
energy, 447

eigenfunctions
Perron-Frobenius, 236
eigenstate, *see* eigenfunction
eigenvalue
exponential spacing, 217
spectral determinant, 237
zero, 459, 496
eigenvalues, 226
elastic
scattering, 523
elliptic
partial differential equations, 618
stability, 85
enemy
thy, 337
English
plain, 163
ensemble
microcanonical, 141
entropy
barrier, 298
topological, 7, 172, 186, 191
equation
of variations, 64
equilibrium
measure, *see* natural measure
point, 39, 70, 110
equilibrium point, 468
equivalence
of dynamical systems, 102
ergodic
average, 112
theorem
multiplicative, 141
theory, 112
escape
intermittency, 346
rate, 14, 308
3-disk, 289, 302
escape rate, 109
3-disk, 305
essential
spectral radius, 242
essential spectral radius, 239
Euler
formula, 237, 771
limit, 71
product, 223
product rep.
dynamical zeta function, 219
totient function, 420
Euler-MacLaurin
formula, 254
Eulerian
coordinates, 35, 64, 69
evolution
group, 48, 765
kernel
probabilistic, 113
operator, 21, 133
quantum, 449
semigroup, 134
expanding
stability eigenvalues, 74, 203
expectation value, 129, 143
exponent
stability, 75
exponential
convergence, 215, 237
of a matrix, 67
exponential proliferation, 22, 192
extremal point, 455

false zeros, 223
Farey
map, 335, 360
mediant, 421
series, 420
tree, 421
Feynman path integral, 494
Feynman, R.P., 761
finite subshift
cycle expansion, 291
first return function, 51
first return time, 357
fixed point, 262
maps, 62
marginally stable, 335
Floquet multipliers, 202
flow, 35, 37
autonomous, 39, 269
contracting, 36, 40, 78
deterministic, 113
generator of, 114, 630
Hamiltonian, 83, 686
hyperbolic, 75, 85, 226
incompressible, 78, 114, 628
infinite-dimensional, 41, 53, 617
inverse hyperbolic, 85
linear, 66
linearized, 64
nonhyperbolic, 75
spectral determinant, 217

stability, 69
stationary, 39
stochastic, 113
stretch&fold, 156
form
normal, 99
Fourier
mode, 618
spatial, 43
truncation, 44
fractal, 324
aggregates, 3, 313
dimension, 325
geometry of nature, 3
probabilistic, 3
science, 2
Fredholm
determinant, 709
integral equations, 240
integral operator, 240
Fredholm theory, 240
Frenkel-Kontorova model, 477
frequency analysis, 46
Fresnel integral, 456, 460
function
space
piecewise constant, 205
functional, 618
Lyapunov, 36
functions
L^2 square integrable, 239
analytic, 238
fundamental
cycle, 178
cycles, 690
domain, 151
collinear helium, 544
matrix, 73
fundamental matrix, *see* Jacobian matrix

Galerkin truncation, 44
Gatto Nero
professor, 762
Gauss shift, 421
gaussian
integral, d-dimensional, 491
generating function, 477
generating partition, 164
generator
of flow, 114, 630
golden mean
pruning, 178
gradient
system, 48
gradient algorithm, 465
grammar
symbolic dynamics, 165
grandmother
of fractals, 328
graph, 165
irreducible, 166
Markov, 165
Green's function
analogue of, 634
density of states, 450
diffraction, 570
energy dependent, 449
regularized, 513
scattering, 529
semiclassical, 502, 505
short distance, 500
trace, 450
long orbits, 499
group, 673
dynamical, 38
evolution, 48, 765
finite, 673
integration, 677
matrix, 674
order of, 673
representation, 674
semi-, 114, 629
Gutzwiller
trace formula, 510

Hénon
map
transient, 468
Hadamard determinant, 216
Hadamard product, 514
Hamilton
-Jacobi equation, 482
equations, 482
principal function, 485
Hamiltonian, 447, 483
flow, 686
spectral determinant, 224
stability, 624
flows, stability, 84, 621
repeller, periodic orbits, 277
Hankel function, 500
Heaviside function, 451
Heisenberg, 614

picture, 699
Heisenberg, W, 629
Helfand moments, 400
helium, 537, 613
collinear, 49, 61, 83, 444, 563
cycles, 277, 563
eigenenergies, 564
fundamental domain, 544
Poincar/'e section, 563
stabilities, 564
stability, 277
Hénon
-Heiles
symbolic dynamics, 385
attractor, 61, 112
map, 57, 58, 465, 479
fixed points, 61
prime cycles, 468, 479
stability, 73
symmetries, 686
Hénon, M., 59
heroes
unsung, xi, xv
Hessian matrix, 85
Hilbert
-Schmidt condition, 240
-Schmidt operators, 701
space, 448
Hopf bifurcation, 415
hydrodynamical
interpretation of QM, 501
hyperbolic
partial differential equations, 618
flow, 75, 226
flows, 85
non-, 25
hyperbolicity assumption, 16, 203

in/out nodes, 69
inadmissible symbol sequence, 164
incompressible flow, 78
indecomposability, 173
metric, 146
index
Maslov, *see* topological index
indifferent
stability, 65
induced map, 351
inertial manifold, 43, 45, 618
infinite-dimensional flows, 41, 53, 617
inflection point, 416
information
dimension, 326
initial
conditions
sensitivity to, 6
point x_0, 15, 35, 64
state x_0, 15, 35
integrable system, 95
integrated observable, 126
integration
group, 677
Runge-Kutta, 49
intermittency, 91, 334
escape rate, 346
piecewise linear model, 337
resummation, 353
stability ordering, 294
invariance
cyclic, 262
of flows, 77
symplectic, 84, 621
invariant
measure, 110
metric, 74, 101
topological, 74
inverse
hyperbolic flows, 85
inverse iteration, 264
Hamiltonian repeller, 277
inward/outward spirals, 69
irreducible
graph, 166
segment, 366
irreversibility, 24, 166
irreversible
dynamics, 37
iteration, 35
inverse, 264
Hamiltonian repeller, 277
itinerary, 10, 12, 146
bi-infinite, 148, 163
future, 157, 162
past, 163

Jacobian, 78, 107
Jacobian matrix, 15, 64, 634
mapping, 73
Jonquière function, 339, 404, 410

KAM
tori, 335
Keller
diffraction, 578

Keplerian orbit, 442
kernel
  resolving, 241
Koopman operator, 315, 629, 634
Kramers, 614
Krein-Friedel-Lloyd formula, 530
KS, *see* Kustaanheimo-Stiefel
Kuramoto, Y., 45
Kuramoto-Sivashinsky system, 42, 70, 617
kurtosis, 144, 400
Kustaanheimo-Stiefel transformation, 540

L^2 function space, 239
Lagrangian, 485
  coordinates, 35, 64, 69
  manifold, 486
laminar states, 334
Laplace
  transform, 23, 115, 182, 208, 213, 449, 502, 630
  transform, discrete, 176, 204, 358
Laplacian, 617
Lautrup, 761
least action principle, 473
Legendre transform, 486
Leibniz, 5
libration orbit, 546, *see* self–retracing
lifetime, 14
limit
  cycle, 134
linear
  flows, 66
  stability, 63
linearized
  flow, 64
link, 165
Liouville
  equation, 117
  operator, 117
  theorem, 85, 114, 628
Littlewood J.E., 608
local
  divergence rate, 137
  stability, 63
logistic map, *see* unimodal
longitudinal
  coordinate, 498
loop
  intersecting, 178
Lorentz gas, 334, 360
Lorenz, E.N., 59
loxodromic, 85, 624
Lozi map, 57, 59
Lyapunov exponent, 6, 78, 135
  cycle, 75
  cycle expansion, 290
  natural measure, 137
  numerical, 141
  numerically, 136
Lyapunov functional, 36
Lyapunov time, 7, 9, 38

$\mathcal{M}$ phase space volume, 131
Mandelbrot set, 313
manifold
  stable, 154
map, 35
  area preserving, 686
  contracting, 81, 169
  dissipative, 81, 169
  expanding, 148
  fixed point, 62
  Hénon, 57, 465, 686
    prime cycles, 468
  logistic, *see* unimodal
  Lozi, 57, 59
  order preserving, 159
  orientation preserving, 686
  orientation reversing, 686
  quadratic, 58, 156
  return, 12, 16, 51
  sawtooth, 367
  stability, 72
  tent, 156
  Ulam, 301
  unimodal, 156
marginal
  stability, 16, 74, 335
    fixed point, 335
  stability eigenvalues, 203
Markov
  graph, 165
    infinite, 181
  partition, 401
    finite, 148, 149
    not unique, 150
Maslov index, *see* topological index
material invariant, 627
Mather, *see* Aubry-Mather theory
matrix
  exponential, 67, 632
  group, 674

of variations, 64
Maupertuis, P.L.M. de, 473
measure, 106
cylinder, 313
equipartition, 313
invariant, 110
natural, 111, 129
smooth, 127
mechanics
quantum, 447
statistical, 24
mediocre
convergence, 692
memory
finite, 161
metric
indecomposability, 146, 694
invariant, 74, 101
stability eigenvalues, 101
transitivity, 694
microcanonical ensemble, 141
Mira, C., 59
Misiurewicz, M., 59
mixing, 7, 16, 112
mode
Fourier, 43
Moebius inversion, 184
monodromy matrix, 202, 623
Morse index, *see* topological index
mother
of fractals, 328
multifractals, 328, 726
multiplicative ergodic theorem, 141
multipoint shooting method, 266

natural measure, 111, 129, 137, 274
nature
geometry of, 3
Navier-Stokes equation, 41
neighborhood, 79
Nero, G, 762
neutral, *see* marginal
stability, 65
Newton method
damped, 266
Newton's method, 265
convergence, 265
flows, 269
optimal surface of section, 272
node, 165
non-wandering set, 36
nonequilibrium, 391
nonhyperbolic
flow, 75, 77
norm, 700
normal form, 99

obscure
foundations, 613
jargon, 146
topology, 45, 53
observable, 111, 126
ODE, *see* ordinary differential equations
open systems, 14, 131
operator
evolution, 133
Hilbert-Schmidt, 701
Koopman, 315, 629, 634
Liouville, 117
norm, 699
Perron-Frobenius, 108, 140
positive, 701
regularization, 708
resolvent, 115, 631
semigroup
bounded, 115, 630
shift, 163
trace-class, 700
orbit, 35
Keplerian, 442
periodic, 163, 508, 510
returning, 508
order preserving map, 159
ordinary differential equations
almost, 48
orientation
preserving map, 686
reversing map, 686
Oseledec multiplicative ergodic theorem, 141

palpitations, chicken heart, 6
parabolic
partial differential equations, 618
paradise
this side of, 305
partial differential equations, 41, 617
partition, 146, 164
generating, 164
infinite, 188, 191
Markov, 148
phase space, 106
partition function, 140

PDE, *see* partial differential equations
period
  doubling
    repeller, 313
  relation to action, 551
periodic
  orbit, 163, 508, 510
  orbit condition, 261, 274, 463
  orbit extraction, 261–275, 463–473
    Hamiltonian repeller, 277
    inverse iteration, 264
    multipoint shooting, 266
    Newton's method, 265
    relaxation algorithm, 465
  point, 11, 22, 163
    admissible, 175
    count, 183
    unstable, 12
Perron-Frobenius
  matrix, 173
  operator, 108, 140, 236
  theorem, 252, 256, 730
phase space, 34
  3-disk, 694
  partition, 106
  volume $\mathcal{M}$, 131
piecewise constant function, 205
piecewise linear map, 359
  intermittency, 337
  repeller, 109
pinball, *see* 3-disk
plain English, 163
Plemelj-Smithies cumulants, 706
Poincaré
  return map, 51
    polynomial, 56
  section, 12, 51, 87
    3-disk, 87
    Hénon trick, 58
Poincaré section, 11
point
  non-wandering, 36
  periodic, 11, 163
  scatterer, 582
  wandering, 36
Poisson
  bracket, 116, 117
  resummation, 23
  summation, 354
Pollicott, M, 140, 357
polylogarithm, 339
polynomial
  characteristic, 178
  topological, 181
Pomeau, Y., 59
positive operators, 701
potential
  partial differential equations, 618
power law
  correlation decay, 336
pressure, 140
  thermodynamic, 140
prime cycle, 164, 195, 204, 261
  3-disk, 148, 195, 473
  count, 184
  Hénon map, 468
primitive cycle, *see* prime cycle
probabilistic zeta function, 357
propagator, 449
  semiclassical, 490
  short time, 492, 500
  Van Vleck, 493
pruning, 10, 335
  block, 165
  golden mean, 178
  individual cycles, 185
  rules, 149
  symbolic dynamics, 164
pseudocycle, 280

quadratic map, 58
quantization
  Bohr-Sommerfeld, 442
  semiclassical, 507
  WKB, 453, 456
quantum
  chaology, 446, 513
  chaos, 445, 446
  evolution, 449
  interference, 481
  mechanics, 447
  potential, 501
  propagator, 449
  resonances, 442
  theory, old, 613

radius
  of convergence, 215
random matrix theory, 446
recoding, 150, 165
rectification
  flows, 97

maps, 98
recurrence, 36, 146
time, *see* return time
regularization, 514, 540
Green's function, 513
operator, 708
relaxation algorithm, 465
renormalization, 91
repeller, 14, 37, 131, 444
piecewise-linear, 109
single fixed point, 236
representation
character, 674
equivalent, 675
faithful, 675
matrix, 674
regular, 675
representative point, 34
residue
stability, 85
resolvent
kernel, 241
operator, 115, 631
resonance
Ruelle-Pollicott, 357
resonances
complex, 444
quantum, 442
Ruelle-Pollicott, 140
resummation
intermittency, 353
return map, 12, 16
return time, 357
distribution, 358
returning orbit, 508
reversible
dynamics, 38
Riemann zeta function, 295, 360
Rössler system, 40, 155
cycles, 263
Ruelle, 26
-Pollicott resonances, 140, 357
zeta function, *see* dynamical zeta function
Ruelle, D, 140, 357
Runge-Kutta integration, 49
running orbits
Lorentz gas, 395
Rutherford, 537
Rydberg series, 552

saddle, 69
saddle point, *see* stationary phase
saddle-node
bifurcation, 59
sawtooth map, 367
SBR measure, *see* natural measure
scattering
3-dimensional spheres, 92
elastic, 523
Green's function, 529
matrix, 524
phase shift, 532
point, 582
Schrödinger
equation, 447
time independent, 447
picture, 699
Schrödinger, E, 629
Schwartz, 619
section
Poincaré, 12, 51, 87
Selberg
product
eigenvalue index, 237
self-retracing cycle, 546
self-similar, 22
semiclassical
spectral determinant
collinear helium, 554
approximation, 482
Green's function, 502, 505
propagator, 490
quantization, 507
wave function, 488
semiclassical zeta function, 515
semiclassical resonances
3-disk, 757
semigroup, 114, 629
dynamical, 38
evolution, 134
operator, 115, 630
sensitivity to initial conditions, 6, 134
shadowing, 19, 189
3-disk, 289
shift, 163
Bernoulli, 242, 358
finite type, 165
full, 163
map, 416
operator, 163
sub-, 164
Sinai, 26

Sinai-Bowen-Ruelle measure, *see* natural measure
single fixed point
repeller, 236
spectral determinant, 237
singular value decomposition, 69
singularity
branch cut, 343
Sivashinsky, G.I., 45
skeleton of chaos, 11, 12
Smale, 26, 228
wild idea, 217, 227
Smale S., 191, 608
Smale, S, 9
S-matrix, 524
smooth
conjugacy, 96, 101, 104, 767
dynamical system, 50
dynamics, 19, 20, 29, 34, 189, 608, 730, 733, 735
approximated, 689
Spectral determinant, 256
interaction, 737
measure, 127
potential, 91
Sommerfeld
diffraction, 578
space
analytic functions, 238
average, 112
averaging, 128
density functions, 205
spectral
determinant, 23, 176, 216
1-d maps, 223
2-d hyperbolic Hamiltonian flow, 224
entire, 217, 237
for flows, 217
infinite product rep., 218
single fixed point, 237
weighted, 224
spectral determinant
1-dimensional, 516
2-dimensional, 517
radius, 242
essential, 239
staircase, 450
spectral stability, 404
spectrum
Balmer, 442
specular reflection, 86
SRB measure, 59
St. Augustine, 105
stability
billiards, 88
cycle, 273
eigenvalues, 69, 74, 203
eigenvalues, metric invariants, 101
exponents, 75
flow, 69
Hamiltonian flow, 624
Hamiltonian flows, 84, 621
indifferent, 65
linear, 63
maps, 72
neutral, 65, *see* marginal
ordering
cycle expansions, 292
intermittent flows, 294
residue, 85
spectral, 404
structural, 190, 403
window, 75
stable
cycle, 76
manifold, 16, 154
flow, 154
map, 154
stadium billiard, 86
stagnation point, 39, *see* equilibrium point
staircase
mean eigenvalue density, 555
spectral, 450
standard map, 334
standing orbit
Lorentz gas, 395
state, 146, 165
set, 146
state space, 34, *see* phase space
stationary
flow, 39
phase approximation, 455, 460, 461, 494, 509, 569, 582, 783
point, 39, *see* equilibrium point
state, 110
statistical mechanics, 24
Sterling formula, 461
stochastic dynamics, 6
stochastic flow, 113
Stokes theorem, 487

stosszahlansatz, 24, 410
strange
  attractor, 36, 40
strange attractor, 134
stretch & fold dynamics, 57
stretch&fold flow, 156
strobe method, 51
strongly connected graph, 166
structural stability, 190, 403
subshift, 164
  finite type, 149, 165
super-exponential
  convergence, 463
super-stable fixed point, 463
superstable cycle, 76
surface of section
  optimal, 272
survival probability, 14, *see* escape rate
symbol
  sequence
    inadmissible, 164
symbolic
  dynamics, 313
    at a bifurcation, 91
    complete N-ary, 147
    covering, 163
symbolic dynamics, 10, 146, 162
  3-disk, 32, 148, 169
  binary
    collinear helium, 545
  coding, 165
    Markov graph, 291
  complete, 156
  grammar, 165
  Hénon-Heiles, 385
  pruned, 164
  recoding, 150, 165
  unimodal, 156
symmetry
  C_{3v}, 382
  3-disk, 151, 366, 382, 388
  cyclic, 174
  discrete, 150
  dynamical system, 677
  Hénon map, 686
symplectic
  form, 84
  group $Sp(2D)$, 622
  integrator, 633
  invariance, 84, 621
  transformation, 85, 117
systems
  open, 131

tangent
  bundle, 38, 64
  space, 64
Tauberian theorem, 360
teaching
  combinatorics, 157
template, 264
tessalation
  smooth dynamics, 689
thermodynamical
  pressure, 140
3-body problem, 444, 507, 537, 603, 614
3-dimensional sphere
  scattering, 92
3-disk
  boundary orbits, 377
  convergence, 245, 689
  cycle
    analytically, 94
    count, 386, 653
    expansion, 301
  escape rate, 234, 289, 302, 305
  fractal dimension, 324
  geometry, 87
  hyperbolicity, 203
  phase space, 12, 324, 694
  pinball, 5, 88, 91
  point scatterer, 582
  prime cycles, 17, 148, 195, 473
  semiclassical resonances, 757
  shadowing, 289
  simulator, 93, 94
  symbolic dynamics, 11, 32, 148, 169
  symmetry, 151, 366, 382, 388
  transition matrix, 147
time
  arrow of, 24
  as parametrization, 96
  average, 112, 136
  averaging, 126
  ceiling function, *see* ceiling function
  ordered integration, 72, 79
time delay
  Wigner, 532
topological

conjugacy, 159
dynamics, 146, 162, 164, 165
entropy, 7, 172, 186
equivalence, 69
future coordinate, 159
index, 490
invariant, 74
polynomial, 181
trace formula, 175
transitivity, 173
zeta function, 181, 182
topological index, 511, 614
totient function, 420
t_p
cycle weigth, 218
trace
formula
classical, 23
flows, 208
Gutzwiller, 510
maps, 205
topological, 175, 182
local, 174
trace-class operator, 700
determinant, 702
trajectory, 35, 66
discrete, 56
transfer
matrix, 109
transfer operator, 227
spectrum, 216
transformation
coordinate, 104
transient, 36, 147
transition matrix, 147, 172, 174
3-disk, 147
transverse
stability, 499
Trotter product formula, 699
truncation
Galerkin, 44
truncations
Fourier, 44
turbulence
problem of, 41

Ulam map, 276, 301
ultraviolet divergence, 512
unimodal map, 156
symbolic dynamics, 156
unstable
cycle, 12, 76
manifold, 16, 154
map, 154
manifold, flow, 154
periodic point, 12
unsung
heroes, xi, xv

Van Vleck
propagator, 493
vector field, 38
vector fields
singularities, 97
vertex, 165
visitation sequence, *see* itinerary
Viswanath, 761
volume preservation, 90
von Neumann
ergodicity, 634

wandering point, 36
wave
partial differential equations, 618
wave function
semiclassical, 488
WKB, 490
weight
multiplicative, 29
Wentzel-Kramers-Brillouin, 453, *see* WKB
Wentzel-Kramers-Brillouin, 482
Weyl rule, 511
Wigner delay time, 532
winding number, 416, 418
WKB, 482, 619
function, 454
quantization, 453, 456
wave function, 490

Yang, C.N., 111
Young, L.-S., 59

zero eigenvalue, 459, 496
zeros
false, 223
zeta function
Artin-Mazur, 181
dynamical, 18, 219
probabilistic , 357
Ruelle, *see* dynamical
topological, 181, 182